2018

Water Dynamics and the Effect of Static and Alternating Electric Fields

Mohammadmahdi Shafiei Alavijeh

Water Dynamics and the Effect of Static and Alternating Electric Fields

A dissertation submitted in partial fulfillment of the requirements for the degree

of

Doctor of Philosophy at Virginia Commonwealth University

by

MohammadMahdi Shafiei Alavijeh

M. Sc, University of Zanjan

Director: Dr. Alenka Luzar

Professor, Department of Chemistry

Virginia Commonwealth University

Richmond, Virginia

October 2018

Acknowledgement

This work is dedicated to my family who have made me more tenacious, more delighted and more fulfilled than I could have ever imagined. My sincere thanks must also go to my supervisor, Professors Alenka Luzar, you have been a tremendous mentor for me. I must express my gratitude to Professors Dusan Bratko for the patient guidance, encouragement, and advice he has provided throughout my time in the lab.

I wish to thank the members of my dissertation committee Professor Sarah Rutan and Professor Puru Jena. They kindly gave their time to provide me valued remarks toward improving my work. I sincerely thank Michael von Domaros for lending me his skills and intuition to my scientific presentation. These brilliant friends and colleagues inspired me over the many years: Serban Zamfir, Jyoti Roy Choudhuri, and Shadrak Jabes. Also, Virginia Commonwealth University and National science Foundation are appreciated for their support during my graduate school years.

Finally, I thank with love to Neda, my wife. Thank you for supporting me for everything. Some special words of gratitude go to our friends in Richmond who have been like our family and inspired us over the many years.

Glossary

$\vec{p}$	Molecular dipole moment
ω	Angular velocity
δ	The differencefrom the average
ϵ	Dielectric constant
β	Thermodynamic beta
α	Angle with of one dipole moment with an adjacent one
θ	Angle with the z direction in the aboratory frame, which is the direction of application of the electric fields
ρ	Density
κ	Transmission coefficient
τ_0	Jump time, the time between successful large amplitude jumps
τ_D	Specific diffusion time in Luzar's model
τ_n	Orientational relaxation time
<>	Ensemble average
AC	Alternating Electric Field
C_{PR}	Stable state cross correlation function.

D	Translational diffusion
D_R	Rotational Diffusion
DC	Static Electric Field
D_0	Size independent diffusion
D_{PBC}	Size dependent translational diffusion
$H(t)$	Restriction function
ILT	Inverse Laplace transform
MSR	Mean Square Rotation
P	Overall dipole moment
P_n	nth Legendre polynomial
V	Volume
a	The radiusof a water molecule
c(t)	Hydrogen bond time correlation function
g(r)	Radial distribution function
h	Hydrogen bond population operator
$k,$	The rateconstant of hydrogen bond breaking
k'	The rate constant of hydrogen bond reforming
k(t)	Relaxation rate of hydrogen bonding
$k_{in}(t)$	Restrictive reactive flux function
$n(t)$	The probabilityhat a hydrogen bond forms at t = 0, and at t the bond is broken but the two molecules are in the first coordination shell of each other
n_{HB}	Number of hydrogen bonds
n_c	Coordination number

ps	Picosecond
q	Order parameter
GHz	Giga Hertz
k_s	Rate constant of H-bond switching when the previous pair separate
k_d	Rate constant of H-bond switching when the previous pair do not separate
τ_r	Residence time after switching the bond:$\frac{1}{k_s} - 1/k_d$
k_o	The rate constant of other way bonding

Table of Contents

Acknowledgement iii

Glossary iv

Table of Contents i

Abstract xiv

Chapter 1. Introduction 1

1.1. Water under an external electric field 1

1.2. Hydrogen Bond Dynamics 7

1.2.1. Luzar and Chandler Model 7

1.2.2. The re-orientational extended jump model 12

1.3. How this thesis is arranged 16

Chapter 2. Models and Methods 18

2.1. Molecular force field 18

2.2. Simulation 22

Chapter 3. A Unified Framework for Hydrogen Bond Dynamics in Water 25

3.1. H-bond switching 27

3.2. Diffusion 35

3.3. Reconciliations with other descriptions 46

3.4. Conclusions 49

Chapter 4. Water under Static Electric Fields 50

4.1. Structure 51

4.1.1. The radial distribution function 54

4.1.2. Tetrahedral order parameter 58

4.1.3. Triplet angle distribution 59

4.1.4. Average Orientational Correlations 61

4.1.5. Spatial Distribution Function 62

4.1.6. Number of H-bonds 64

4.1.1. Structure of polarizable models 66

4.2. Thermodynamics 68

4.3. Dynamics 71

4.3.1. H-bonds dynamics 71

4.3.2. Extended jump model 78

4.3.3. Switching correlation function 81

4.3.4. Diffusion 83

4.3.5. Roto-translational coupling 85

4.4. Conclusion and Remarks 88

Chapter 5. Water under Alternating Electric Field 90

5.1. Results and Discussion 92

5.1.1. Structure 92

5.1.2. Number of hydrogen bonds 96

5.1.3. Radial distribution functions and tetrahedral order parameters 98

5.1.4. Average Orientational Correlations 100

5.1.5. Re-orientation of water molecules and Extended Jump model under AC E-fields 102

5.1.6. Hydrogen Bonding kinetics 105

5.1.7. Diffusion 111

5.2. Conclusion 115

Chapter 6. Summary and Outlook 117

Bibliography 119

Appendices 137

Appendix 1. Tetrahedral order parameters 137

Appendix 2. The effect of thermostat 138

Appendix 3. Large jump trajectories 140

Appendix 4. The other-way bonding probability 144

Appendix 5. Accessing the validity of eq. 9 145

Appendix 6. The polarizable Water models..... 147

Appendix 7. Buckingham and Lennard Jones potential..... 149

List of Figures

Figure 1. The scheme that Luzar suggested for H-bond switching of allegiances[55] which is almost the same as the picture introduced by Laage and Hynes. Molecule (1) and (3) are initially H-bonded, then molecule (1) switches H-bond to molecule (2). The Luzar model does not consider which hydrogen is donated, and the Laage and Hynes model does not measure the diffusion of the primary acceptor out of the first shell. The transition state is the bifurcation of a H-bond in frame (b), and by each switch the previous acceptor leaves the first shell. 26

Figure 2. The $Ct(t)$ function, eq. 6 (left), $ns(t)$, eq. 25 (middle) and $ktt = -dct(t)/dt$ for SPC/E, BK3, and SWM4-NDP water models. 29

Figure 3.The correlation of equation 23 for SPC/E water in $300\ K$ in the absence of external E-fields. 30

Figure 4. The value of the correlation function: n(t) (equation 7), $nsd(t)$ (equation 21), $ns(t)$ (equation 24) and $nd(t)$ (equation 25) for SPC/E water..... 32

Figure 5. Comparing the first passage time probability density of H-bonds, P(t), and the probability distribution of OFF times, Q(t), if a broken bond reforms, in two situations: if the donated hydrogen experiences another switching before switching back to the originally bonded partner, and if not. The second condition is only met when the breaking is a

librational breaking, and because of that it, relaxes extremely fast. This plot shows that almost all the "OFF times" are the times that $H*$ is switched to another acceptor. 35

Figure 6. The displacement distribution of a water molecule during sequential H-bond switching. A single jump can be one flip which is reversed by a flop or can be a switch to a new H-bond acceptor, which is a big jump. For performing a big jump, the water molecule must displace more. 37

Figure 7. A schematic of the diffusion of water molecules via a random walk process based on intra- and inter-basin translational jumps. Each color represents on "basin", thick lines symbolize large translational inter-basin jumps, and thin lines show intra-basin jumps. ... 39

Figure 8. Comparing the distribution of average $O* \dots Oa$ distance during the time when the $O* - Ob$ bond exists in two different situations: when $H*$ will return to Oa or when $H*$ switches to a new acceptor. There is a clear difference between these distributions, and the pairs that are going to re-form again, do not separate more than 5 Å when the bond between them is OFF. 43

Figure 9. The correlation between the diffusion coefficient and the different H-bond breaking and reforming rate constants. The Paesani results are calculations using the MB-pol[185] water model using the trajectories that Paesani group shared with us. The fitted line can pass through (0,0) or can have a Y-intercept. Having a Y-intercept means that when the translational diffusion is zero, the molecules can still re-orient a little bit. 44

Figure 10. Reconciliation of the Laage and Hynes model and our suggested step time, eq. 27, for SPC/E, BK3, SWM4-NDP, and MB-pol water models. 48

Figure 11. The average of the angle of the water dipoles and water molecule bisector vectors with the E-field direction. Below $E = 0.05\ V/\text{Å}$, the increase in the alignment is significant. The rate of the alignment of water with the field is almost negligible beyond $E = 0.1\ V/\text{Å}$. 52

Figure 12. (Left) The distribution of the angle of water dipole moments with the E-field direction. Like the average alignment of dipole moment that increases dramatically bellow $0.05\ V/\text{Å}$, the position of the distribution shifts to the higher angles. (Right) the intramolecular OH bond angle distribution with the E-field direction. After $0.05\ V/\text{Å}$, the maximum of the probability distribution does not shift, but the distribution gets narrower..... 54

Figure 13. The radial distribution function of water: $g\text{OO}(r)$ (top), $gOH(r)$(middle) and $gHH(r)$ (bottom). 56

Figure 14. gl ‖ and gl ⊥ cylindrical distribution functions under zero field and $E = 0.2\ V/\text{Å}$ for SPC/E(top), BK3 (middle), and SWM4-NDP (bottom)..... 56

Figure 15. The distribution of the $Oa - Oa$ distance in the x and z directions. This plot shows that with increasing the static E-field, the z component of the $Oa - Oa$ distance goes toward shorter distances, meaning that acceptors are almost in the same plane. In such a plane, the H-bond acceptors of the same molecule keep the distance of $\sim 4\ \text{Å}$. 57

Figure 16. Triplet angle distribution function OOO in the presence of three water models under static electric fields. 60

Figure 17. (Left) Distance-dependent orientational correlations in SPC/E water (solid lines), BK3 (dashed lines), and SWM4-NDP (dotted lines) under no field and under $E = 0.1\ V\text{Å} - 1$. All models behave qualitatively similar, although BK3 water molecules are stronger correlated

than in other models. (Right): A schematic illustration of a possible configuration of H-bonded (2, 3) and non-H-bonded (4) water molecules. Molecule 4 is located at the boundary of the second coordination shell, lacking angular preferences due to H-bonding, which makes it relatively free to rotate. 60

Figure 18. The spatial distribution function of SPC/E water in the first(left) and the second (right) shell for no field (blue) and $E = 0.2V/\text{Å}$ (red). Both plots for the first shell have an average iso-value density of 1.3 and for the second shell, the density iso-value is 1.8. The central molecules is added to show the relative positions of the lobes to a water molecule. In the first shell, the strong E-field does not change the probable position of the H-bond accepting molecules, but the positions of the H-bond donor molecules are more restricted. In the second shell, however, the shape of the density profile is more different under the strong static E-field..... 62

Figure 19. The Relation of the average number of H-bonds to the angular hydrogen bond criterion. The E-fields do not make any significant difference, so we stay with our traditional H-bond criteria when we study for SPC/E, BK3, and SWM4-NDP water models under static E-fields..... 65

Figure 20. (left) number of H-bonds and (middle) coordination number which is the total number of neighboring molecules within the first coordination shell of a molecules, 3.5Å. Despite the trend, the overall change of both values under DC fields is negligible: less than 1%. (right) The percentage of the water molecules that have a specific number of H-bonds. There is a very slight increase and decrease in the percent of the molecules with a higher and lower

number of bonds respectively under the E-field of $0.2\ V/\text{Å}$, but the overall change in the number of H-bonds is negligible. 66

Figure 21. The change in the dipole moment of BK3, and SWM4-NDP water molecules under static electric fields. The dashed, red line shows how the dipole moment of BK3 water molecules deviates from a linear trend. 67

Figure 22. The change in the energy of the system under static E-fields. We see that the main change in the energy of the system is due to the change of the interaction of the field with water molecules. The change in water-water energy (cohesive energy, black line) is less than 2%. 69

Figure 23. Changes in average cohesive and electric field energy of the system, $\Delta Ecoh$ and $Efield$, with and electric field for various water models. For $E = 0$, $EcohSPC/E = -46.6\ kJ\ mol - 1$, $EcohBK3 = -43.4\ kJ\ mol - 1$, and $EcohSWM4 - NDP = -43.3\ kJ\ mol - 1$ 71

Figure 24. Hydrogen bond kinetics correlation plots. For classic model, red lines, showing the best fit between $k(t)$ (y-axis) and $k\ ct - k'n(t)$ (x-axis) to find the rate constantst k and k'. For the new model, the blue lines shows the best fit between kst (y-axis) and $ks\ ct - ks'ns(t)$ (x-axis) to find the a pair of rate constants ks and ks'.in SPC/E (left), BK3 (middle) and SWM4-NDP (right) for zero field (top) and $E = 0.1\ V/\text{Å}$ (bottom). 72

Figure 25. k(t) (left) and $kint$ (right) functions (black line) along with the analytic line (red line) calculated from eq. 10 and eq. 11 using the rate constants k and k' calculated from the correlation plots, Figure 24, and fitted the best value of τD. The qualitative agreement does

exist between the model and the. The results for BK3 and SWM4-NDP water are in Appendix 6. 74

Figure 26. The rate constants of hydrogen bond breaking k and switching ks (top, left), as well as the rates of H-bond reforming, k' and switching back ks' (top, right) for three water models under electric fields ranging from 0 to $0.2\ V\text{Å} - 1$. Bottom panels: The percentual change of the same quantities. Lines are meant to guide the eye. 75

Figure 27. (Top) The transient time behavior of $k(t)$ under the different static E-fields. This plot shows that the librations of water molecules do not change under static E-fields. (Bottom left) the numeric value of $\tau contHB = 1/kTST$ versus E-fields. We still see minimum at around $0.05\ V/\text{Å}$, but the overall change is less than 4% between 0 to $0.2\ V/\text{Å}$. On the other hand, the transmission coefficient of breaking and switching a H-bond (Bottom right) decreases over 8% and 17% , respectively, in the same range of E-fields. 76

Figure 28. The hydrogen bond time correlation functions (from left to right) ct, $n(t)$, and $kt = -dc/dt$ for various water models $E = 0.1\ V/\text{Å}$. 77

Figure 29. (Top)Field-dependence of jump time, $\tau 0$, the second order re-orientation time from jump model, $\tau 2JM$, the second order re-orientational jump model from the extendend jump model, $\tau 2EJM$ along with the re-orientation time calculated directly form molecular dynamic of p and q vector under E-fields for three water models . (Bottom) and a scheme defining the molecular vectors p and q for a water molecule. 80

Figure 30. Isotropic diffusion coefficients D as well as the parallel $D\parallel$ and perpendicular components $D\perp$ of the diffusion tensor in SPC/E water (top) BK3 water (middle) and SWM4-NDP water(bottom). The left panels are semi-log plots to show the increase in $D\perp$

in weak E-fields and right panels show the overall trend. The black line is the best fit of the overall diffusion using the H-bond switching as the random walk waiting time, eq. 26. Brown line is the same, but using the breaking rate constant, k to fit eq. 26. 84

Figure 31. (top-left) The rotational diffusion is calculated using eq. 41. The difference in the trend of the rotational diffusion of the p, q, and r axes is due to the different effects of hydrogen bonding under the E-fields on those axes. (top-right) The percentage change of two different rotations of a water molecule. (bottom) The roto-translational coupling of water molecules under static E-fields. The correlation of Rq and Rr remains mostly unchanged with the alignment of water, since when the molecules are aligned with the field, the q and r vectors are parallel to the x-y plane, so their rotation and translation is less affected under the static E-fields..... 87

Figure 32. The average alignment of water molecules $< cos\alpha >$ where α is the angle of the water dipole moment with the field direction in a range of $E0$ strengths and two frequencies: 100GHz (left) and 200GHz (right). When the E-field is strong enough, on average, water molecules follow the field, even at the increased frequencies..... 92

Figure 33. The distribution of the angle of water molecule with the E-field direction, z, per each moment of the period time. The time is normalized by T, the period time, and $x = time/T$. The solid lines are just $sin(t/T)$ indicating the phase of the E-field. The distribution is apparently narrower under $200\ GHz$. We use the different colors for the solid lines to show it better. The retardation of the maximum alignment, shown as the brightest point, relative to the E-field maximum at $x = 0.25$ is observable in both figures..... 94

Figure 34. The average of the distribution of the molecular alignment (left) $200GHz$ and (right) 500GHz, in every moment of the phase, $time/T$ where T is the period of the AC field. Increasing the E-field strength and the frequency increases and decreases the maximum alignment respectively. 95

Figure 35. (left) the maximum of the average alignment of water molecules in Figure 33 The maximum alignment increases with $E0$ and decreases with frequency. (right) The maximum alignment happens with a delay time after the maximum E-field at (T/4). In this figure we have plotted the $\delta = tmaxT - 0.25$ where t_max is the time of maximum alignment in Figure 34. There is almost no trend in the retardation phase under AC E-fields. The lines are eye guides. 95

Figure 36. The number of H-bonds per water molecules (filled circles-left axis) and the coordination number, means the number of neighboring molecules within $3.5\ \text{Å}$ of the central molecule (hollow circles-right axis) under the different AC E-fields for SPC/E water. For both sets, blue is 100GHz, red is 200GHz, and black is 500GHz. Application of the AC E-fields decreases the number of H-bonds, but the percentage of the change under such high intensity and fast reversing alternating E-fields is less than 6%..... 97

Figure 37. The radial distribution function of water under different AC field frequencies with a very strong E-field strength of $0.2\ V/\text{Å}$ for SPC/E (top left), BK3 (top right), and SWM4-NDP water models (bottom). The difference between the height and the position of the peaks for the different frequencies is small..... 99

Figure 38. (left) The relative alignment of water molecules, $gdd(r)$ under $E0 = 0.2\ V\text{Å}$ for different frequencies. Application of the E-field aligns the adjacent molecules, but increasing

the frequency, decreases this alignment since the nearby molecules cannot rotate with the same rate, because they have different H-bonding states. (right) The ultimate value of the $gdd(r)$ at a long enough distance (10 Å). Like many other plots, we see a sharp decrease in the relative alignment of water molecules, indicating that despite maintaining the structure, at a long distance, there is more chaos in bulk water under the fast reversing AC E-fields. 101

Figure 39. The jump and extended jump model for the reorientation time of water molecules under the different $E0$ strengths and frequencies.[61] 103

Figure 40. The jump angle, which is the average re-orientation angle of water molecules during a H-bond stable to stable switching. Increasing the E-field strength and frequency increases the jump angle. 104

Figure 41. The change in the JM and EJM re-orientation time, $\tau 2$, under AC E-fields, and comparing them with the MD results. There is a minimum in all of them at around $200GHz$. We will show in the next sections that these minimums are related to the response of the H-bond dynamics of the molecules to the E-field induced re-orientation..... 105

Figure 42. The correlation between the left and the right side of eq. 8, and the best pair of k and k'. We chose our highest $E0$ to show that the phenomenological relation does not break even under such a strong E-field and when the field direction is changing so fast. 106

Figure 43. The different rates constants of hydrogen bonding from the methods that we presented in this report for two different $E0$ strengths versus frequencies. All the rates constants are calculated from the correlation plots, the application of the AC field may interrupt the first order kinetics and make the correlation plots non-linear only in a few cases

of ks which we explain later. We have eliminated those numbers from data set before plotting them in this figure. Still almost all the rates constants show a maximum in the $200\ GHz$..... 107

Figure 44. The relation of Δt, which is the time difference between AC field half period time, $T2$, and H-bond switching time, $1/ks$, or H-bond breaking time $1/k$, and the E-field frequency. When the hydrogen bond breaking time is smaller than the half period, means $\Delta\ t < 0$, the higher E-field frequency results in a higher H-bond breaking rate, and we have faster dynamics. But when the half period is shorter than $1/k$, the water dynamics cannot follow the E-field reversal, and the breaking of hydrogen bond slows down with frequency, see Figure 43. 109

Figure 45. Translational diffusion for two $E0$ strengths for a range of frequencies for SPC/E (top left) BK3 (top right) and SWM4-NDP water model (bottom). The filled circles and lines are for overall 3D diffusion coefficient, and the thin lines and hollow circle are for Dz. Diffusion has the same trend as the H-bond rates constants has, and we showed in section 4.3.4 the diffusion is highly correlated to the H-bonding. The diffusion in z direction follows the same trend..... 112

Figure 46. Rotational diffusion of the water dipole moment for two $E0$ strengths in a range of frequencies. The maximum difference between the p_z component and p_x component happens when the H-bond rate, and translational and rotational diffusion is maximum. 114

Figure 47. The Oxygen-Oxygen potential of Buckingham (with BK3 parameters), and Lennard Jones potential with SPC/E and SWM4-NDP parameters. 149

Abstract

Having a net dipole moment, water molecules tend to align with an external electric field. The re-orientation of water molecules to align with the field direction can result in structural and dynamic changes in liquid water. Studying these changes can help us to understand the role of an E-field in many biological systems, chemical reactions, and many technology advancements.

In short, the application of static electric fields causes molecules to stay aligned with the field, so, fewer hydrogen bonds break, and molecules have slower dynamics. This type of field can be used when the mobility of water molecules needs to be reduced, like in electroporation. Alternating electric fields, on the other hand, cause continuous re-orientation of dipole moments, which results in more H bond breaking, water is less structured, and molecules have faster motion.

Water under static and alternating electric fields have several applications in science and technology. Although many of the interesting usages of the application of electric fields to water happen at surfaces, the response of hydrogen bonding of water molecules to an E-field is still not fully understood even in bulk. For instance, the rate of hydrogen bond breaking, the re-orientation of water molecules, and the random walk of water molecules under the restrictions of the static electric field have not been thoroughly assessed. The static electric field limits the re-orientation of water molecules, but the translation reduces at the same time, this is clear

evidence of roto-translational coupling, and the static electric field is a great groundwork for studying this coupling which is generated by the hydrogen bonds.

For studying the effects of an E-field on H-bonding dynamics in depth, we need a model of hydrogen bonding. There are a few models for dynamics of H-bonding and reorientation of water molecules, including Luzar and Chandler model, published in 1996, and the Laage and Hynes jump model, published in 2006, which are described in the introduction chapter. The two models are related but have different perspectives, so it would be very interesting to look for a more general framework of hydrogen bonding by combining these two models, with the help of the influence of external electric fields. We also explain the relation of the random walk diffusion of water molecules and the hydrogen bonding.

Since the external electric field can change the dipole moment of water molecules, for a more realistic picture, we need do the simulations with sophisticated polarizable water models to obtain a better estimate of the behavior of experimental water in an electric field.

In this thesis, we introduce our generalized hydrogen bond framework; then we assess this framework, as well as other static and dynamic properties of water under static and alternating electric fields.

Chapter 1. **Introduction**

1.1. **Water under an external electric field**

Water molecules have a large electric dipole and quadrupole moments due to the partial charges and the $\widehat{H\text{-}O\text{-}H}$ angle.[1] This results in a strong interaction of water molecules with an external electric field. In liquid water, the structure and dynamics of water molecules under electric fields is complicated because of the competition between the effect of the external E-field and hydrogen bonding.[2] The interactions of water molecules with a surface makes these dynamics even more complicated.[3–5]

Investigation of the change of the properties of liquid water in the presence of an electric field is very interesting because of vast applications in science and technology.[4,6,7] Joseph and Aluru[8] reported the enhancement of water flux in a single file nanotube when a static electric field is applied parallel to the tube axis. Application of an electric field can change the hydrophobicity of a surface, resulting in an enhancement of micro- and nano-flows.[3,9–11] Applying electric fields can alternate the permeability of the solutions, a process that is called electroporation and has found many applications in biochemistry.[12–14] English and Waldron have published a comprehensive review of the scientific and the technological applications of applying electric fields to water systems.[15]

If the system has charged particles of opposite signs, these particles will be separated under E-fields.[16,17] On the other hand, if the molecules are electrically neutral, but have partial opposite

charges, like water, application of an external electric field can change the orientation of the molecules.[18]

Molecular simulations can help in understanding the behavior of water molecules under an E-field.[19] For doing molecular simulations, we need to choose a water model, which exhibits similar responses to the E-field as real water.[20,21] Also, we need to carefully choose an appropriate thermostat and a proper set of electric boundary conditions.

Simulation of water molecules can be done in conjunction with[21] or without controlling the temperature,[20] but a more realistic simulation will be with a thermostat because the interactions of the AC E-field and molecules increases the energy of the system and a realistic system cannot be heated continuously.[21] Because the application of an alternating E-field, as an external force, controls the dynamics of water, it results in non-equilibrium systems.[16,22]

For controlling the temperature in a static E-field, the Nosé-Hoover[23,24] thermostat works well because it produces a correct canonical ensemble, the system is reversible, and the total energy of the system plus thermostat remains constant. Under E-fields, however, because energy is pumped to the system, none of the above advantages exist, and the extra energy is stored in the thermostat to keep the kinetic energy constant. Avena *et al.*[25] believe that the most realistic thermostat for simulation of the systems in an external electric field is the Bussi-Donandio-Parrinello Canonical Sampling Velocity Rescaling (CSVR) thermostat.[26] We have examined Nosé-Hoover, Berendsen, and CSVR thermostat and we show in Appendix 2 that the effect of the different thermostats lead to equivalent results.

Our group in 2007 reported a powerful influence of the direction of an external electric field on the surface wetting.[4] In 2008, they studied the effect of static E-fields on the water in confinements in NTP and μPT ensembles.[27] They observed completely different results for a fixed number of molecules and for an open system. In an open system, the density in a planar confinement increases under a static E-field. When the number of particles is fixed, the attractions among the molecules are relaxed, so at constant pressure, molecules move more freely, and the density decreases. In an open system, on the other hand, the application of an electric field helps in filling the hydrophobic surfaces with more molecules, and this increases the density. In agreement with the previous reports,[28,29] they show that the average number of hydrogen bonds, see section 4.1.6, does not change significantly under a static electric field. Besides, the radial distribution function, g(r), and the triple oxygen angle distribution function $P(\cos(\theta_{OOO}))$, see section 4.1.2, does not change significantly.

Vanzo, Bratko, and Luzar in our lab applied an external E-field in between of two disk-like confinements and observed a net attraction of water molecules from the surrounding area into the confined area.[30] In another work, they used an electric field to completely wet and de-wet a hydrophobic nano-confinment.[31]

Saitta *et al.*[32] have performed an ab initio simulation on the effect of a static E-field on bulk water. They consider the change in the intramolecular distance distribution as a change in the structure. It is shown in Figure 1 of their paper, that the enhancement of structure between $0 - 0.2\ V\text{Å}^{-1}$ is only 2%. Sutmann[28] have reported that water molecules completely line up at $0.1V\text{Å}^{-1}$, and under a very strong hypothetical E-field of $3.0\ V\text{Å}^{-1}$ the system converts to a highly ordered ice.

Vegiri[29,33] sees a change in the radial distribution function (RDF) of water at $250\ K$ under an unrealistic field of $3.0\ V\text{Å}^{-1}$.

Regarding the thermodynamic calculations, Amadei *et al.* have developed a quasi-Gaussian entropy (QGE) theory for the thermodynamics of dielectric fluids as a function of temperature and the strength of the E-field.[34] Aragones *et al.*[35] have calculated the effect of the strength of the static E-field on the phase diagram of water. Vaitheeswaran *et al.*[36] have assessed the effect of an E-field on water dynamics in a narrow carbon nanotube and calculated the change in the free energy of filling a nano-tube with a chain of H-bonded water molecules. They have also computed the entropy from the free energy of filling the nanotube by measuring the probability of finding a nanotube filled with water. Hernandez-Rojas and Gonzalez[37] focus on a water octamer and calculate many structural and thermodynamic properties of water, including the heat capacity, and an order parameter, Q_4, for a cluster of water molecules. Choi *et al.* have performed ab-initio simulations on water clusters under E-fields, and concluded that increasing the strength of the applied E-field reduces the probability of having a ring of water molecules, and increases the probability of forming a chain of molecules instead.[38]

At a surface, water molecules tend to have an orientation correlated with the hydrogen bonding, but an external E-field tries to align the dipole moments with the field direction. If we apply an E-field perpendicular to two hydrophobic interfaces while water is inside, these two propensities compete on the E-field incoming surface and collaborate on the E-field outgoing surface.[3] The incoming field surface then will remain hydrophobic, and the other surface will become hydrophilic; this is an E-field induced Janus interface.[39] von Domaros *et al.* observed that the

alignment of water molecules in E-field-induced Janus interfaces produces a huge difference between the orientation dynamics in incoming and the outgoing fields. This difference decreases with the E-field since the stronger E-field finally dominates the effect of the surface, but there is a point at near $0.03\ V\text{Å}^{-1}$ where the two effects cancel each other, and the molecules are freer to re-orient.

Under an alternating E-field, water molecules re-orient all the time.[40] If the system contains ions, the temperature goes up because of two reasons: firstly the heat will be generated from the friction of moving ions among the water molecules. Besides, more H-bond will break, and molecules with fewer H-bonds move faster and have higher kinetic energy.[41]

English *et al.* have used Non-Equilibrium Molecular Dynamics, NEMD, for water under square-wave electric fields.[42] They observe that the oscillations in the translational and rotational cross-correlation functions increase with the field frequency, and the translational diffusion decreases at frequencies higher than $200\ GHz$. They say that this is because water molecules re-orient very fast and the molecules return to their original orientation, and this is like the water molecules have not rotated at all, so molecules do not move, and the translational dynamics slow down. They guess that the reduction in the molecular mobility is related to the H-bonding, but they do not do any measurement.[43] They also observe that under alternating E-fields, increasing the E-field intensity, increases the roto-translational coupling.

In their 2014 paper,[44] again a square-wave alternating E-field is applied. This time their theory for the reduction of the translational diffusion with the E-field frequency is that beyond certerin frequency the molecules cannot follow the E-field reversion. So, the water alignment does not

change dramatically, and this is the reason for having a maximum in the diffusion versus frequency plot.[20]

The well-accepted machinery for calculating the re-orientation of water molecules is the large orientational jump model introduced by Laage and Hynes,[45] and we will describe this model in section 1.2.2. English *et al.*[44] on a basic interpretation of this model have calculated the probability that a water molecule has five H-bonds, which means that at least one of the bonds is bifurcated. They have used this interpretation since during a re-orientational jump; a hydrogen bond can be unstably bifurcated. As it is expected, the faster the E-field alternates, the higher is the number of bifurcated H-bonds. This makes sense since when the E-field frequency is higher, at any moment, more hydrogens are in the H-bond switching process.

Recently[40] the English group has done ab-initio molecular dynamics simulations of water under static and alternating electric fields, and they have calculated static properties, as well as hydrogen bond dynamics of water,[45] and they, show that the dynamics slows down under static E-field and accelerates under alternating E-field. We will discuss these conclusions in chapter 5.

In spite of publishing several papers,[15,18,25,43,46–48] the interpretation of English group of the effects of external electric fields on H-bond dynamic and roto-translational coupling is still not clear, and a precise link between hydrogen bond kinetics and the roto-translational coupling is still missing. We will talk about that in the future work section.

Suresh *et al.* introduced a theoretical method for calculating the effects of a static E-field on the H-bond network of water.[49,50] In their approach, they assume that before a water molecule

reorients, all the H bonds should break. Based on this assumption, they calculate the probability that a water molecule has zero H-bonds, i. e., no accepted and no donated bonds. They conclude that the static E-fields enhance the H-bond network since increasing the strength of the external E-field reduces the probability that a water molecule has zero H-bonds.

1.2. Hydrogen Bond Dynamics

Currently, the two most important models for explaining the dynamics of water hydrogen bonding are the model that Luzar and Chandler proposed in 1996[51] and the model that Laage and Hynes proposed in 2006.[45] Here we explain the models briefly and explain their similarities and differences.

To the best of our knowledge, these models have not been thoroughly studied for water under external E-fields. The current reports are limited to the calculation of the H-bond breaking time by English *et al.*[44] and studying the large jumps during one switch of the field direction by Takae *et al.*[52] We analyzed these models extensively in chapters 4 and 5 under static and alternating E-fields, but first, we need to have an overview of the two models:

1.2.1. Luzar and Chandler Model

Luzar and Chandler introduced their model to characterize H-bond dynamics between a pair of water molecules.[51] They define the state of hydrogen bonding by a dynamical variable $h(t)$, which is equal to 1 when a pair of molecules are H-bonded and zero otherwise. A hydrogen bond is defined with geometric criteria: the bond is ON when the oxygen-oxygen distance is less than

3.5 Å, the angle between $O-H$ and oxygen-oxygen axes is less than $30°$, and the distance of the donated hydrogen and the acceptor oxygen $O\ldots H$ is less than 2.45 Å. We will talk about these criteria later in chapters 3 and 4. To study the dynamics of bond forming and breaking we can define a H-bond time correlation function:

$$c(t)=\frac{<\delta h(t)\delta h(0)>}{<\delta\, h>}=\frac{<h(t)h(0)>}{<h>} \qquad 1$$

which is the probability that a pair of molecules are bonded at time t if the bond was ON at time $t=0$, regardless of breakings of H-bonds between these two times. In other words, $c(t)$ is an intermittent H-bond correlation function. If we expand the middle expression of the above equation with $\delta h(t)=h(t)-<h>$ we get the right-hand side because $<h^2>=<h>$, and $<h(0)>=<h(t)>$ for a long enough simulation, and $\frac{<h>}{<h>^2}\sim 0$ for a big system, with $n_{mol}\gg 1$. The H-bond relaxation function is:

$$k(t)=-\frac{dc(t)}{dt}=\frac{<\dot{h}(0)h(t)>}{<h>} \qquad 2$$

and the process of H-bond forming and breaking can be described as a phenomenological process:

$$A \underset{k'}{\overset{k}{\rightleftharpoons}} B \qquad 3$$

which A means H-bond "ON", and B means H-bond “OFF”, and k and k' are the rate constants of H bond forming and breaking. If this is a simple first order reaction, we can write the time evaluation of $c(t)$ as:

$$c_A(t)=c_A(0)e^{-\frac{t}{\tau}} \qquad 4$$

where $\tau = k + k'$.

The short time behavior of $k(t)$ at the time < 0.3 ps is a transient behavior which is related to the fast H-bond breaking generated by molecular librations.[53] If the bond breaks and never re-forms, i. e., the reaction passes the transient period only one time, the reaction rate would be a transition state theory (TST) rate, that is: $k \sim k(0^+) = k_{TST}$, but if the pair come back to H-bonding, the rate of relaxation is reduced. We can define the reduction of the relaxation rate because of re-crossings by a dynamical transmission coefficient: $\kappa(t) = \frac{k(t)}{k(0^+)}$. Since the number of these re-crossings depends highly on the position of the dividing surface, $\kappa(t)$ highly depends on the choice of H-bond criteria. It can be proved in the reactive flux method[54] that by multiplying the two parameters that are inversely related to the H-bond criteria, the function $k(t) = \kappa(t) \times k(0^+)$ is independent of the choice of H bond criteria after the transient time. The relaxation of the H-bonding then is supposed to be exponential:

$$k(t) \sim ke^{-kt}, \qquad t > t_{trans} \qquad 5$$

For water, however, the relaxation is not exponential, and relaxes much slower, see the semi-log plot of k(t) in section 4.3.1. Luzar and Chandler proposed that the non-exponential relaxation of H-bond dynamics is related to the diffusion of water molecules out of the first shell:

$$A \underset{k'}{\overset{k}{\rightleftharpoons}} B \overset{\tau_D}{\rightarrow} Separated\ pairs \qquad 6$$

This time state B means the probability that the bond is broken but the pair are still in the first coordination shell of each other. We replace the state B by $n(t) = \int_0^t dt' \ k_{in}(t')$, and k_{in} is the restrictive reactive flux function: $k_{in}(t) = \frac{<\dot{h}[1-h(t)]H(t)>}{<h>}$. H(t) is the limiting function that is 1

if the pair are still in the first coordination shell, bonded or not bonded, and zero otherwise. $n(t)$ is the probability that the bond is ON at time 0 and OFF at time t , but the pair are still in the first coordination shell of each other:

$$n(t) = \frac{< h(0)[1 - h(t)]H(t) >}{< h >} \qquad 7$$

we can find the rate constants of H-bond breaking and re-forming by assuming that the reaction is the first order: $-\frac{d[A]}{dt} = k[A] - k'[B]$. So, in terms of hydrogen bond dynamics:

$$k(t) = kc(t) - k'n(t) \qquad 8$$

we can find a pair of k and k' that match the left side versus the right side of the above equation.

There are two sources of relaxation of $n(t)$: the population may decrease because of the pair re-bonds, or because molecules diffuse away from the first shell. Luzar and Chandler modeled diffusion with source and sink dynamics:

$$\frac{\partial}{\partial t}\rho(\boldsymbol{r}, t) = \boldsymbol{D}\,\nabla^2\rho(\boldsymbol{r}, t) + \delta kc(t) - \delta(\boldsymbol{r})k'n(t) \qquad 9$$

where D is the diffusion coefficient, $\rho(\boldsymbol{r})$ is the density in the first shell equal to $\frac{n(t)}{a^3}$ where a is the water molecule radius. By solving the above equation using a Laplace transform, they came up with the following analytic equation for $k(t)$:

$$k(t) = ILT\{\frac{k}{s + k + k'sf(s)}\},$$
$$f(s) = 3\,\tau_d\left[1 - \sqrt{s\,\tau}_d \arctan\left(\frac{1}{\sqrt{s\tau_d}}\right)\right] \qquad 10$$

and

$$k_{in}(t) = ILT\{sf(s)LT(k(t))\} \qquad 11$$

where ILT means the Inverse Laplace Transform and $\tau_d = (6\pi^2)^{-\frac{2}{3}} \frac{a^2}{D}$ is the diffusion time. When diffusion is small, the above equation leads to a single exponential kinetics:

$$k(t) = ke^{-(k+k')t} \qquad 12$$

which is exactly eq. 4 and it means that in the absence of any diffusion, the bonding, and non-bonding states just interchange. In water, however, the diffusion is not small, and the relaxation of H-bonding is non-exponential. The quantity τ_D is the average time that a non-H-bonded pair of water molecules need to leave the bonding area, $a \sim 1.5\text{Å}$.

Luzar and Chandler's model describe the H-bond dynamics for a pair of water molecules, but Luzar[55] also explained how $n(t)$ changes when there are 3 water molecules. They show that the free energy of bonded and non-bonded states does not differ significantly. They concluded that this is because a breaking of a bond, is accompanied with the formation of a new H-bond with a neighboring molecule, and the process of breaking the bond, re-bonding, and diffusion are parts of a *switching of allegiances* process.[56] In this picture, the 3 molecules that have formed a tetrahedral structure, switch their partners and form another tetrahedral structure, but the previous H-bonded pair, are not in the first shell anymore.

However, they have never calculated the rate of H-bond switching to prove their point. In this research, we suggest a method for calculating the rate of H-bond switching using a reactive flux method, and we discuss Luzar's theory.

Csajka and Chandler[57] used transition path sampling[58] for studying the hydrogen bonding. The transition path sampling examines a series of states in a many-body system: starting from region A, passing an energy barrier, and ending to region B. They have used this method for a tagged pair of water molecules that remain in the first coordination shell, for going from bonding state, A, to non-bonding state, B. Although bond forming-breaking is not a rare event, they have used this problem for testing the transition path sampling method, because having many of H-bond breakings, makes a comparison of this method with direct simulations easier.

Their results show a large jump of the hydrogen atom during the breaking of an H-bond, while no jump in the $O-O$ distance occurs. At the moment of breaking the H-bond, the potential energy increases up to $10\ KJ/mol$ (decreases in absolute value), and both the donor and the acceptor molecules experience a sudden reduction in the number of H bonds. They mention that in about 40% of the trajectories, this sudden changes is accompanied with finding a new acceptor and removal of neighboring molecules from the perfect tetrahedral structure, which is again consistent with what Stillinger calls[56] *"switching allegiances"* .

1.2.2. The re-orientational extended jump model

Laage and Hynes introduced their model for water reorientation in 2006.[45] In short; they state that the switching of the H-bond acceptors of hydrogen is by a large rotational jump of the donor molecule so that the donated hydrogen jumps from the first H-bond cone to the second H-bond cone.

They say that the diffusive model, which explains the reorientation of molecules by small angular Brownian steps, cannot correctly describe the reorientation of water molecules. The orientational correlation function is:

$$\mathrm{C_n(t)} = < \mathrm{P_n}[\mathbf{u}(0).\mathbf{u}(\mathrm{t})] > \qquad 13$$

where P_n is the n'th-rank Legendre polynomial and $\boldsymbol{u}(t)$ is a unit vector attached to the water molecule's dipole moment. This function relaxes exponentially, and the relaxation time of $c_n(t)$ is τ_n. If the re-orientation of water molecules is with diffusive re-orientations, time follows the below relation:[59]

$$\tau_n = \frac{1}{n(n+1)D_R} \qquad 14$$

where D_R is the rotational diffusion coefficient.[60] It has been shown that the ratio of $\tau_1/\tau_2 = 3$ and $\tau_1/\tau_3 = 6$ differs significantly from simulation results.[61]

In their model, the donor oxygen is O^*, the donated hydrogen is H^*, the first acceptor is O_a and the second acceptor is O_b. Their proposed mechanism can be summarized in the following steps:

- At the beginning, H^* has been donated to O_a.
- With a large re-orientation of the donor molecule H^* jumps from the H-bond cone of O_a to the H-bond cone of O_b. This re-orientation happens in a plane formed by the donor molecule, the first, and the next acceptors.
- After the jump, O_a gradually separates from O^*.

The essential explanation of the model lies in the heart of figure 1 of their Science paper[45] where the average oxygen-oxygen distances and the $H^*\widehat{O^*O_a}$ and $H^*\widehat{O^*O_b}$ exhibit a big and fast change during a H-bond acceptor switching.

The jump time can be calculated from the Ivanov model[61]

$$\tau_n^{jump} = \tau_0 \left\{ 1 - \frac{1}{2n+1} \frac{\sin[\left(n+\frac{1}{2}\right)\Delta\theta]}{\sin(\frac{\Delta\theta}{2})} \right\} \qquad 15$$

where τ_0 is the jump time calculated from the relaxation of the stable state cross correlation function:

$$C_{RP} =< n_R(0) n_p(t) > \qquad 16$$

where n_R and n_P are the probabilities that H^* is in the stable reactant and stable product states respectively, and τ_0 can be calculated from $(1 - c_{RP}) = e^{-t/\tau_0}$. In other words, τ_0 is the time that H^* travels from stably H-bonded to O_a to stably H-bonded to O_b.

For a better description of the jump process, Laage and Hynes have taken the reorientation of the frame of the jump into account, and they call their model the Extended Jump Model, EJM. The total re-orientation time is calculated from:

$$\frac{1}{\tau_n} = \frac{1}{\tau_n^{Jump}} + \frac{1}{\tau_n^{frame}} \qquad 17$$

Using the above model, they calculate $\tau_1/\tau_2 = 2.4$ which is much closer to the simulation result. That transition happens when the central molecule has any number of HBs, but only when $n_{HB} = 5$ we can be sure that we have at least one of the bonds in the transition and the bond is bifurcated.[62,63] Kyohei and Onuki[52] remarked that when $n_{HB} = 3$ the probability of having a

molecule in the transition state is higher than when $n_{HB} = 5$. It seems interesting to observe the effect of an external E-field on the large jumps, which is how fast the molecules re-orient, how large are the jumps.[52] We have studied this model extensively under the E-fields, see chapters 4 and 5.

The Laage and Hynes re-orientation model and Luzar H-bond switching model are very similar, see Appendix 3. The difference is that Laage and Hynes do not talk about the H-bond kinetics, and instead they focus on the reorientation of the intra-molecular O-H bond. The main objection to this model is that the large jump mechanism is only about a few percents of the trajectories: 15% based on ref. [64] in quantum simulations and 40% according to ref. [57] using transition path sampling method. What happens to the rest? We will show in section 3.3 that the rest of the trajectories simply do not end up in a stable state. In the 2008 paper of Laage and Hynes,[61] they mention that not all the jumps result in the stable product state, and the transmission coefficient is near 0.5; we will talk about this discrepancy in section 3.3.

Chowdhary and Ladanyi[65] were the first group who tried to find the connection of the Luzar's and Laage's model. Their first picture is that the hydrogen bonds break and reform according to Luzar's model, and the H-bond partners exchange according to Laage's mechanism. They find that the jump time in Laage model is close to the average H bond lifetime in Luzar's model. We will expand this theory in chapter 3.

Qvist *et al.* have performed quasi-elastic neutron scattering experiments and MD simulations on water to provide a detailed analysis of H-bonding. They propose a model of re-orientational and translational jumps which differs from Laage's jump model. They observe that a little change in

the energy of vaporization and consequently the H-bond network makes a significant difference in the re-orientational dynamics of molecules. They suggest a continuous random walk (CTRW) model, for the translational diffusion of water molecules. They divide the translational jumps into intra- and inter-basin jumps and they calculate the diffusion coefficient using their model which is in a good agreement with the diffusion coefficient calculated from the mean square displacement of molecules. We show in chapter 3 that the basins that Qvist and Halle are referring to, are cages[66] that are formed by hydrogen bonding, and the inter-basin jumps are H-bond switching of allegiances.

Recently, Kawasaki and Kim[67] have calculated the lifetime of a hydrogen bond from the relaxation time of the total number of H-bonds in the system. They show that the diffusion coefficient and H-bond breakage time are correlated. In this research, however, we calculate the dynamics of H-bonding more rigorously, and we show that the random walk diffusion of water molecules happens in between H-bond breakings.

1.3. How this thesis is arranged

In this thesis we first introduce our generalized framework of hydrogen bond breaking, reforming and switching, and then we bring our results for water under the static and alternating electric field, and we explain them using our generalized framework.

Chapter 2 is about model and methods where we explain the details of our simulations. In Chapter 3 we explain our generalized framework for hydrogen bond dynamics. We will introduce a new set of correlation functions, and we will try to modify the current model[51] for the relation

of H-bonding and diffusion of water molecules. In Chapter 4 we bring our results for water under static E-fields, where molecules align with the E-field but keep their dynamics mostly in the direction perpendicular to the E-field. We show that the roto-translation coupling still exists even when the E-field only limits the the re-orientation of water molecules.

Finally, in Chapter 5, we study water under alternating E-fields. Specifically, we explain why the hydrogen bond lifetime and diffusion coefficient are maximum when the E-field frequency is around $200GHz$.

Chapter 2. **Models and Methods**

Our observation method is molecular dynamic simulations, as it is one of the most prominent, if not the most prominent, theoretical method of exploring the properties of liquid water. Here we explain the methods and challenges in our simulations.

2.1. **Molecular force field**

A popular potential for MD simulation with a directional attraction of molecules such as the case of hydrogen bonds combines the Lennard-Jones potential[24,68] with an electric force between partially charged atoms, to form the force field of the simulation.

Quantum simulation methods are not studied for this research for two reasons: Firstly, this is because they are very time-consuming and have size limitations. For instance, when doing Car-Parrinello molecular dynamics simulation,[69] we need to take dispersion forces into account. Dispersion forces include forces between a permanent dipole moment and a corresponding induced dipole (Debye force) and two instantaneously induced dipoles (London dispersion force). Calculation of these forces limits simulation time and system size to under 20 ps and below 100 molecules, respectively. The second reason is that hydrogen bonds are predominantly electrostatic and only $\sim 10\%$ covalent bonds.[70] We are exploring the physical phenomenon resulting from the electrostatic interaction of molecules, which happen in picosecond timescale, while quantum effects are mostly considerable in studying the covalent characteristics of bonds and happen in sub-picosecond timescales. For example in Luzar's model,[51] the relaxation

dynamics is studied after the transient time, near $300\ fs$, where the physics of the coupling between translational diffusion and H-bond kinetics would not be affected by quantum interactions. In the case of re-orientational dynamics and the jump model of Laage, the classical description of nuclear motion has been criticized in the literature.[64] However, its validity is supported by the very small isotope effects that have been measured experimentally for the water reorientation time[71]. This experimental finding is consistent with the computed jump mechanism that does not involve tunneling.[72] A recent semi-classic MD simulation study of water HB dynamics confirmed that the jump mechanism is unchanged when the hydrogens nuclear motion is explicitly quantized.[73]

In Table 1 we have summarized the most important properties of the most important water models. As explained before, a proper model needs to show similar behavior to experimental water, having a developed force field, and be doable with a fast-paralleled simulation package.

Table 1. A list of major water models and the important properties compared to the experimental values.

	Model	D_{PBC}[1]	D_0[2]	Dielectric Constant (ϵ)	Dipole Moment[3]	Shear Viscosity[4]	Surface Tension[5]
Non-polarizable	SPC/E	2.30[74]	2.97 ±	70.7 ± 0.8[74]	2.35[76]	0.729[77]	63.6[78]
	TIP5P	2.62 ±		81.5 ± 1.6[79]	2.29[80]	0.699[77]	
	TIP4Q	2.08[81]	2.55[6]	93.2[82]	2.44[82]		69[77]
	TIP4P/2005	2.17[75]	2.49[75]	58[83]	2.30[84]	0.855[77]	69.3[78]
	SPC	4.18[85]		65[86]	2.27		65.1[78]
polarizable	SWM4-NDP[7]	2.30[87]		79 ± 0.5[87]	2.456[87]	0.62[88]	65[89]
	TIP4P-FQ	1.9[90]		79 ± 8[90]	2.62[90]		
	iAmoeba		2.54[91]	80.7[92]	1.864[93]	0.85[91]	68.3[91]
	Amoeba14	1.99[91]	2.36[91]	79.14[91]	2.20	0.9[91]	69.21
	uAmoeba	2.41[93]		78.41 ± 1[93]	1.80[93]	0.72 ± 0.05[93]	
	BK3	2.08[94]	2.37[94]	79[94]	2.66[94]	0.951[94]	
Experimental			2.3[95]	78.4[95]	2.95[96]	0.896[97]	71.99[98]

[1] *Diffusion in the units of* $10^{-9}m^2/s$

[2] D_0 *is size independent diffusion calculated by extrapolating diffusion for infinite size of the simulation box*

[3] *Dipole moment in unit of Debye*

[4] *Shear viscosity in unit of* $mPa.s$

[5] *Surface tension in unit of* mN/m

[6] *A prediction based on equation 22 using viscosity*

[7] *WM4-NDP is TIP4P with a Drude oscillator*

We simulate one non-polarizable water model, SPC/E,[76] and two polarizable water models, BK3,[99] and SWM4-NDP.[100] The extended simple point charge model, SPC/E, is a successful three site successful water model. The oxygen atom has a partial charge of $-0.8476\ q_e$ and the two hydrogens have $+0.4238\ q_e$ where q_e is the electron charge $q_e = 1.602 \times 10^{-19}$. The intra-molecular oxygen hydrogen distance is 1.0Å and the, hydrogen-oxygen-hydrogen angle is $109.47°$. The oxygen site has Lennard-Jones parameters of $\epsilon_O = 0.6502\ kJ/mol$, and $\sigma = 3.166\ \text{Å}$.

The two polarizable water models that we use also show similar properties to experimental water. SWM4-NDP is a five site water model, where each hydrogen has a charge of $q_H = 0.5573\ q_e$, the oxygen atom has a charge of $q_O = -1.7162\ q_e$ and a Drude particle with the charge of $q_D = 1.7162\ q_e$ with a spring constant of $k_D = 4184.0\ kJ/mol\text{Å}^2$ is attached to the oxygen atom. A massless charge of $q = -1.1146\ q_e$ is also attached to the oxygen in a distance of $d_{OM} = 0.24\ \text{Å}$. The oxygen-hydrogen distance is $d_{OH} = 0.95\ \text{Å}$ and the hydrogen-oxygen-hydrogen angle is $104.52°$. The Lennard Jones parameters of oxygen atoms are $\epsilon_O = 0.88\ kJ/mol$ and $\sigma = 3.184\ \text{Å}$.

The BK3 water model has 3 Gaussian charges on spring: two $q_H = 0.584\ q_e$ charge with a characteristic distance of $\sigma = 0.72\ \text{Å}$ connected to the hydrogen atom, and one $q_H = -1.168\ q_e$ with a characteristic distance of $\sigma = 0.4\text{Å}$ connected to a massless and chargless particle M at distance of $d_{OM} = 0.2661\ \text{Å}$ to the oxygen atom. The oxygen-hydrogen distance is $d_{OH} = 0.975\ \text{Å}$ and the hydrogen-oxygen-hydrogen angle is $104.52\ \text{Å}$. The overall polarizibility is $1.44\ \text{Å}^3$ and the equilibrium dipole moment of water is $\mu_0 = 2.95\ D$. The Buckingham potential

for the short range $O-O$ intractions is used with the parameters: $A = 326600\ kJ\ mol^{-1}$, $B = 3.59\ \text{Å}^{-1}$ and $C = 2970\ kJ\ \text{Å}^6$. The force field potentials are plotted in Appendix 7.

2.2. Simulation

Simulation packages:

The SPC/E and SWM4-NDP simulations have been done using Large-Scale Atomic/ Molecular Massively Parallel Simulator (LAMMPS).[101,102] The BK3 simulations have been done using a modified GROningen MAchine for Chemical Simulations (GROMACS)[103] modified by Marcello-Sega[104] where they added the capability of calculating the dynamics of Gaussian charges. Despite limitations, these well parallelized packages make the simulation process much faster than developing our own codes.[105,106] Our simulation of 512 and 1000 water molecules is performed in cubic boxes of size $24.85\ \text{Å}$ and $29.89\ \text{Å}$ respectively both with density $1\ g/cm^3$ with periodic boundary condition in all three directions. The simulation step time is $1fs$, and we use this time step also to calculate the H-bond correlation functions.

Electrostatic

We calculate long range electrostatic interactions using the particle−particle−particle−mesh (PPPM) solver with 10^{-5} accuracy for SPC/E and 10^{-3} for BK3 and SWM4-NDP. We use the periodic boundary conditions in all three directions. Electrostatic forces are truncated after $12\ \text{Å}$. It is necessary to remove the extra charges that are accumulated at the boundaries because of the polarization of the system. When we apply an electric field, the water molecules will be aligned, and there would be a separation of charges at the two boundaries of the simulation box.

These charges produce an electric field with the opposite direction to the external electric field, and the water molecules experience an E-field that is weaker than the applied field. We remove these charges by using an electrical boundary condition named tin foil[107] to make sure that the water molecules feel the same E-field as is applied. The default electric boundary conditions in Lammp and Gromacs are conducting boundary conditions.

By applying an alternating external electric field, we continuously pump energy into the system, so the system is never in equilibrium. The molecular dynamics simulation of this situation is called non-equilibrium molecular dynamics (NEMD).[21] We need to keep controlling the temperature by doing NVT simulations as NEMD. This is because the dynamic variables in this report depend highly on the temperature, and to compare results under different E-field strengths, we need to have the same temperature for all systems. We implement Nosé-Hoover thermostat[23] at $T = 300\ K$ with a relaxation time of $0.03\ ps$. We have also tested the velocity rescaling thermostat Canonical Sampling through Velocity Rescaling (CSVR) thermostat[26] which is similar to Berendsen thermostat[108] but rescales randomly using a Gaussian probability. The relaxation time for CSVR thermostat is also $0.03ps$ and we confirm that there is no difference in the results by using either of the two thermostats. We equilibrate the system for $300\ ps$, and the results are averaged over 500 to $1000\ ps$ of the simulation.

The Spatial Distribution Function plots are calculated using TRAVIS[109] and are plotted with VMD[110] using *iso-surfaces* style.

Diffusion coefficient

We calculate the diffusion coefficient from the mean square displacement:

$$< |r(t) - r(0)|^2 > = 2dDt \qquad 18$$

where $r(t)$ is the position of a molecule at time t, d is the dimension of the system, $<>$ means the ensemble and time averages, and D is the diffusion coefficient. We have calculated the diffusion from the slope of the Mean Squar Displacement (MSD) function in the time range of $50 - 70\ ps$. Our calculated diffusion of bulk water under zero field is $2.55 \times 10^{-9}\ m^2/s$ for SPC/E, $2.02 \times 10^{-9}\ m^2/s$ for BK3, and $2.64 \times 10^{-9}\ m^2/s$ for SWM4-NDP which agrees with the previous results[75] and close to the experimental value. [95]

Yeh and Hummer remarked that the calculated diffusion in periodic boundary conditions is highly size-dependent and for calculating a size independent self-diffusion, we need to use the following equation:[111]

$$D_0 = D_{PBC} + 2.8372\ \frac{k_{BT}}{6\pi\eta L} \qquad 19$$

where D_0 is the size independent diffusion, D_{PBC} is the size dependent diffusion, and η is the shear viscosity that can be calculated with a NVT simulation. We have not used this correction since the long-range interactions that influence the diffusion coefficient, will also influence other dynamical variables, especially hydrogen bond dynamics. As we study the relation of the hydrogen bond dynamics and diffusion of molecules in the next chapters, doing this correction is

not necessary. In other words, we believe that the theories that we develop in this thesis, will be size independent.

Chapter 3. **A Unified Framework for Hydrogen Bond Dynamics in Water**

A relatively large number of hydrogen bonds per molecule, a strong network of H-bonds and a short lifetime of H-bonds are three characteristics that make water the most special liquid in the world.[53] Explaining the behavior of water molecules helps us to understand the properties of more complex systems in science and technology.[112–115] To perceive the physics of hydrogen bonding in depth, we need a comprehensive model of hydrogen bond dynamics, translation, and rotation of water molecules. Today, the existing models for studying these dynamical variables are the Luzar and Chandler model[51] and Laage and Hynes model.[45,61] We have explained these two models in section 1.2.

Both models have been successful in explaining many computer simulations[116,117] and experiments.[71,118,119] These models describe the hydrogen bond breaking and switching from the different perspectives. The purpose of both models is measuring the different aspects of water dynamics: H-bond lifetime, rotation, and translation of water molecules. Hence, our search for a unified framework narrows down to understanding how these dynamical processes happen in time and distance. In this chapter, we provide a generalized framework by incorporating and reconciling the current interpretations.

The Luzar and Chandler model[51] is based on a population operator $h(t)$ which is one if a pair of

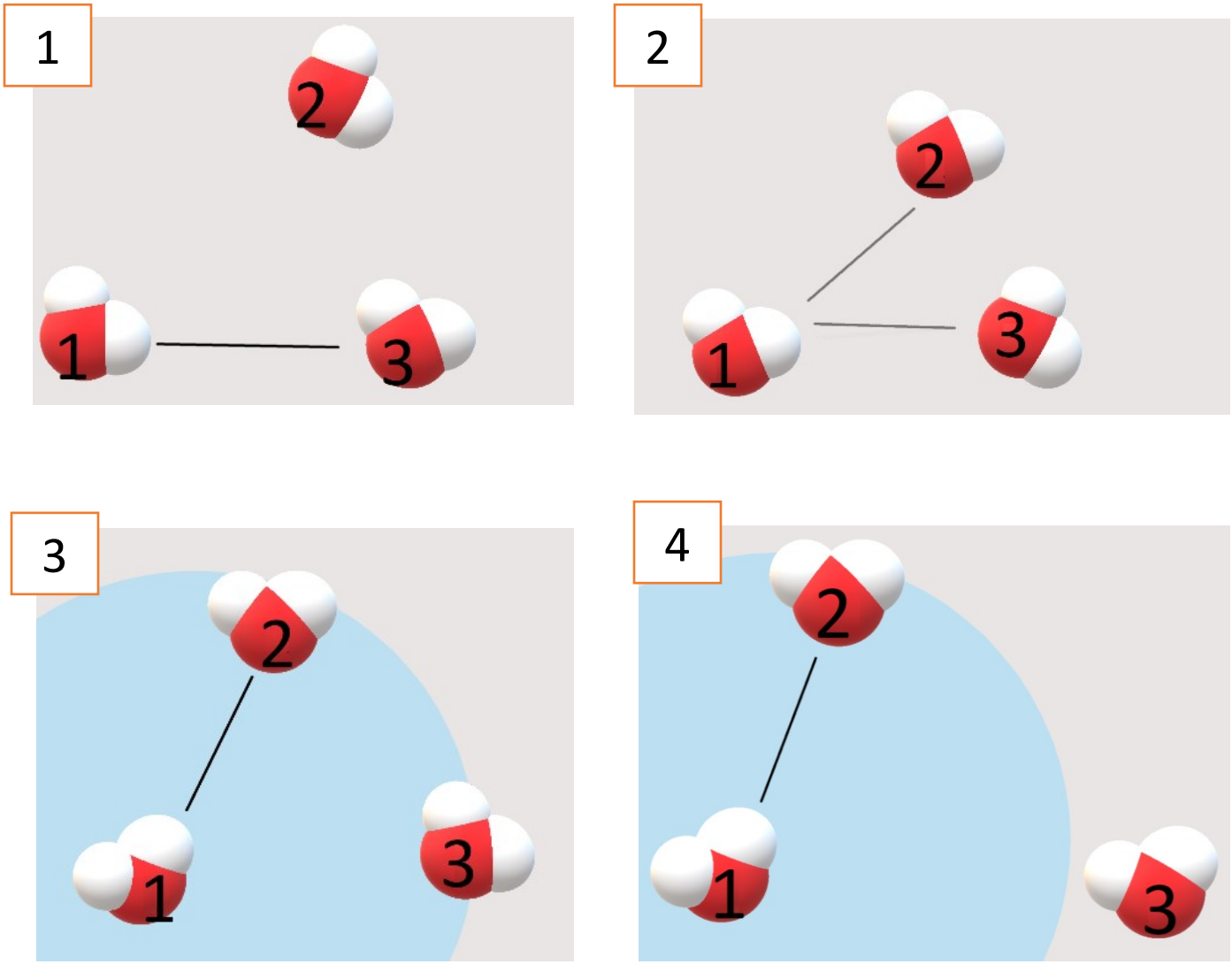

Figure 1. The scheme that Luzar suggested for H-bond switching of allegiances[55] which is almost the same as the picture introduced by Laage and Hynes. Molecule (1) and (3) are initially H-bonded, then molecule (1) switches H-bond to molecule (2). The Luzar model does not consider which hydrogen is donated, and the Laage and Hynes model does not measure the diffusion of the primary acceptor out of the first shell. The transition state is the bifurcation of a H-bond in frame (b), and by each switch the previous acceptor leaves the first shell.

water molecules are H-bonded, and zero otherwise. In this model, the donor and the acceptor molecules are not distinguished.[120]

3.1. H-bond switching

The H-bond network of water is preserved in liquid water when near 10% of all possible hydrogen bonds are broken, see ref [118]. Luzar,[55] by comparing the free energy of bonded and un-bonded states suggested that the existence of a new allegiance facilitates bond breaking. A simple three molecule scheme, depicted in Figure 1 indicates that the switching of allegiance happens with the same rate of H-bond breaking and re-forming. Below, we introduce a method for calculating the switching rate constants, and we show that the rate of switching of H-bonds, is close but not necessarily equal to the rate of H-bond breaking.

We hypothesize that during the time that a bond between a pair of water molecules is broken in the Luzar model, the donated hydrogen has switched to another acceptor. After any H-bond breaking in the Luzar and Chandler model, which is due to the re-orientation of the donor molecule, re-forming falls into one of these three categories: (i) If the break is because of the small amplitude librations of the intra-molecular O-H bond, the bond will reform instantly. (ii) If the hydrogen switches its acceptor through a hindered rotation in an angular jump-like process, there is still a chance that the switch reverses. These re-formings take a longer time, and we will talk about them shortly. (iii) It is possible that the hydrogen never switches back, but the pair of water molecules re-associate in another way, either by donating the other hydrogen of the donor molecule to the acceptor or by swapping of the donor-acceptor roles. In Luzar model, the first type of re-formings are seen in the transient time of $k(t)$ function, and the second and the third possibilities are not distinguished.

As a side note, when H^* switches its acceptor, it passes through a potential barrier.[61,63] This is the reason that the H-bond switching happens with the large angular jump of the donor water molecule. Describing the transition state as a *"bifurcated state"* depends on the H-bond criteria: with angularly wide H-bond criterion, all the switches pass through the bifurcated states, and with more restricted criteria, fewer switches happen through the H-bond bifurcation. What is clear from our simulations and many previous studies,[61,121] is that the presence of the next acceptor is the reason for breaking the bond with a large jump.

We need a criteria independent method to calculate the overall switching time, but without omitting the librations, so we use a reactive flux method, see section 1.2.1. The goal of both reactive flux method and the stable state picture, SSP, used by Laage and Hynes,[45] is the same: calculating the overall time of the transformation from the initial state, in which H^* is donated to O_a to the final step, in which H^* is donated to O_b. We show that the switching time that is calculated with the reactive flux method is almost the same as the switching time that is calculated using the stable state picture, but the reactive flux results depend less on the H-bond criteria. To do this, we write Luzar and Chandler's H-bond correlation functions[51] for a tagged hydrogen.

We define the two states of the hydrogen bonding of H^*: first, H^* is bonded to the first acceptor, O_a , and second, H^* is donated to O_b. The tagged hydrogen bond correlation function is:

$$c_t(t) = \frac{< h_t(t) h_t(0) >}{< h_t >} \qquad 20$$

where $h_t = 1$ if H^* is donated to O_a and zero otherwise. We also introduce the second state as the switching correlation function of a H-bond:

$$n_{sd}(t) = \frac{< h_t(0) h_{t2}\,(t) >}{< h_t >} \qquad 21$$

where $h_{t2} = 1$ if H^* is donated to O_b and zero otherwise. We can split $n_{sd}(t)$ based on the position of the previous pair has left the first coordination of the donor molecule or not (see eq. 24 and eq. 25). The switching of H-bond allegiances is then:

$$c_t(t) \underset{k'_{sd}}{\overset{k_{sd}}{\leftrightarrows}} n_s(t) \qquad 22$$

and the rate constants of switching and switching back, k_{sd} and k'_{sd}, can be calculated by finding the best pair of k_{sd} and k'_{sd} that makes the following equation true, see section 1.2.1 and ref. 120:

$$-\frac{dc_t(t)}{dt} = k_{sd} c_t(t) - k'_{sd} n_s(t) \qquad 23$$

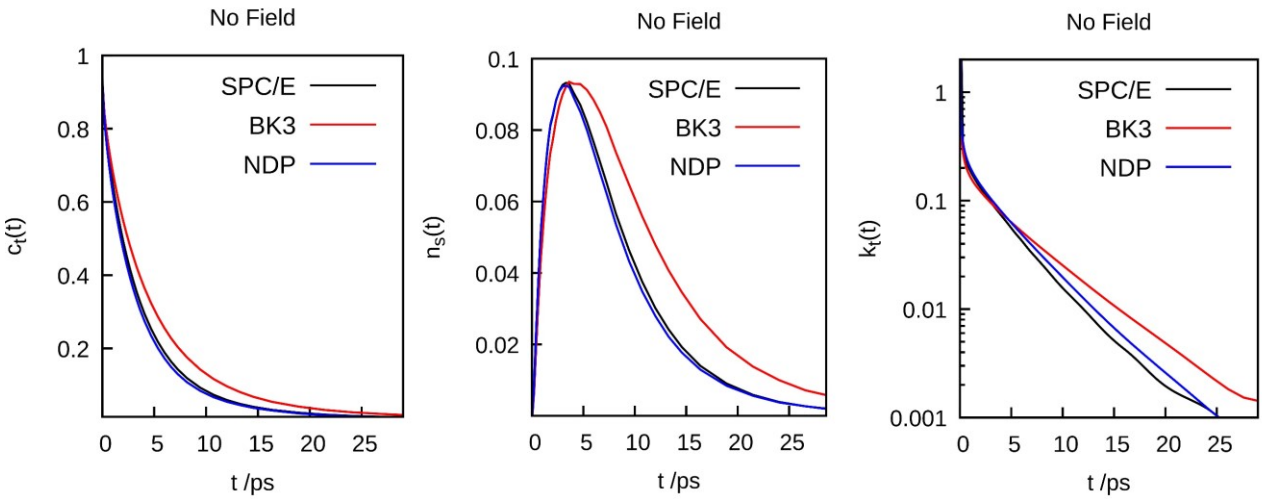

Figure 2. The $C_t(t)$ function, eq. 6 (left), $n_s(t)$, eq. 25 (middle) and $k_t(t) = -dc_t(t)/dt$ for SPC/E, BK3, and SWM4-NDP water models.

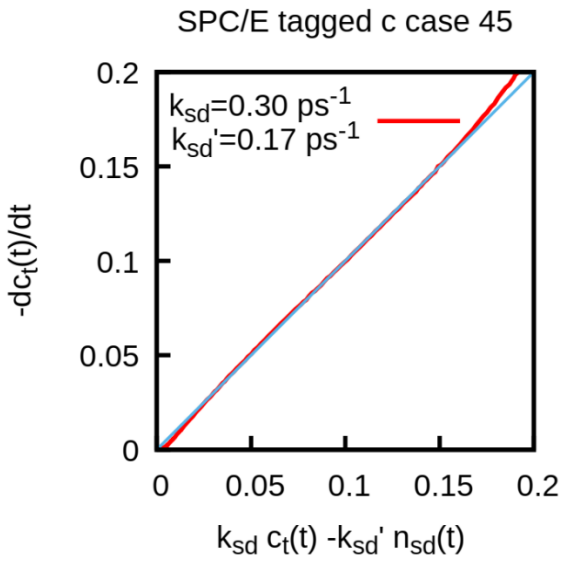

Figure 3.The correlation of equation 23 for SPC/E water in $300\ K$ *in the absence of external E-fields.*

In Figure 3 we have plotted the above correlation function, with the best pair of k_{sd} and k'_{sd} for bulk water at $T = 300\ K$. This correlation continues to hold, with the different rates, for water under E-fields and water in different temperatures. The time that it takes for a proton to switch from state A: H^* is donated to O_a to state B: H^* is donated to O_b for SPC/E water is $\frac{1}{k_{sd}} = 3.33\ ps$. In the following table, we see that the values calculated from SSP, using restricted criteria and the reactive flux, using regular criteria for H-bond definition, are close, but our suggested reactive flux value depends less on the H-bond criteria.

We pause here to talk about the diffusion of a water molecule after breaking the bond, that is the subject of the second part of Luzar and Chandler's model. According to the Laage and Hynes

Table 2. The characteristic switching time using a Stable State Picture, τ_0, and the reactive flux method, $\frac{1}{k_s}$, for SPC/E system at $300\ K$. The SSP results for restricted criteria first calculated by Laage and Hynes[61] as $\tau_0 = 3.3\ ps$ and near 5% difference can be related to the simulation details. Regular criteria are: $H\text{-}\widehat{O^*\text{-}O_a} = 30^\circ, d_{O^*-Oa} < 3.5$Å and $d_{H-O_a} < 2.4$ Å and the restricted criteria are : $H\text{-}\widehat{O^*\text{-}O_a} = 30^\circ, d_{O^*-Oa} < 3.1$ Å and $d_{H-O_a} < 2.0$ Å.

Characteristic times	H-bond Reg. Criteria (ps)	H-bond Res. Criteria (ps)
$\frac{1}{k_{sd}}$	3.33	3.44
$\frac{1}{k_s}$	3.38	3.45
τ_0	2.37	3.13

model[61] when the new H-bond forms, the previous pair gradually separates. This separation is observable in switching trajectories, see Appendix 3 and ref. 61. Let us distinguish between the two states: the previous acceptor has or has not left the first shell of the donor molecule. We re-write equation 21 to calculate the probability of switching a H-bond acceptor, before O_a leaves the first shell of O^*:

$$n_d(t) = \frac{< h_t(0) H(t)\big(1 - h_t(t)\big) h_{t2}\,(t) >}{< h_t >} \qquad 24$$

or after O_a leaves the first shell of O^*:

$$n_s(t) = \frac{< h_t(0)(1 - H(t))\big(1 - h_t(t)\big)h_{t2}\,(t) >}{< h_t >} \qquad 25$$

and $H(t) = 1$ if the O_a is still in the first coordination shell of O^* and zero otherwise. The different switching correlation functions are plotted in Figure 4.

As the new bond stabilizes, the previous pair gradually leaves the first shell of the donor molecules. The transition between $n_{sd}(t)$ to n_s(t) is fast, and the values of k_{sd} and k_s are close, so the better choice for the rate of H-bond switching is k_s not k_{sd}. Please note that after breaking the second bond, there is a good chance that the first pair reform a bond in a way other than donating H^* to O_a. The breaking of this latest bond contributes in $n(t)$ function, so the relaxation of a non-tagged hydrogen correlation function $n(t)$ is slower than the relaxation of $n_s(t)$ which is about a tagged hydrogen.

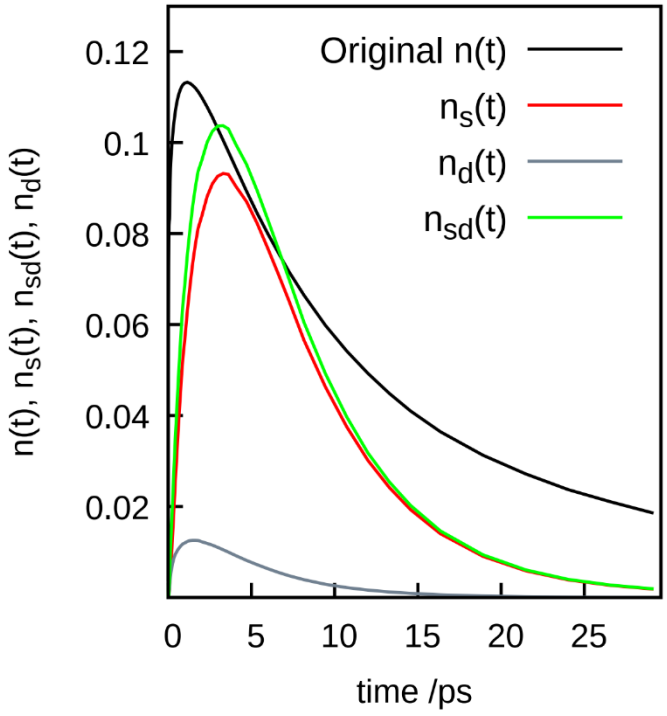

Figure 4. The value of the correlation function: n(t) (equation 7), $n_{sd}(t)$ (equation 21), $n_s(t)$ (equation 24) and $n_d(t)$ (equation 25) for SPC/E water.

Let us restate the Luzar and Chandler model in our framework: They rate of H-bond breaking and re-forming inside the first coordination shell and the diffusion time after breaking the bond is calculated. We suggest that the breaking in Luzar model coincides with the switching of the donated hydrogen to another acceptor, and the re-formings, correspond to switching back. How can we prove this?

In the Luzar model, the non-exponential relaxation of the hydrogen bonds is associated with the reforming events that happen with the diffusion of the separated pairs back to the original bond. Luzar introduces two functions:[120] $P(t)$, which is the probability distribution of continuous lifetimes of the hydrogen bonds that are formed at $t = 0$, and Q(t) is the probability distribution of OFF times between the same pair when the bond is broken for the last time at $t = 0$. The history of a hydrogen bond between a pair consists of a series of p(t)….P(t)…Q(t)…P(t)….Q(t)…. where p(t) is exactly like P(t), except that we relax the condition that the bond has formed at $t = 0$. Luzar shows that the relaxation of the H-bonds is made of $P(t)$ and $Q(t)$ functions: $k(t) = ILT\left[\frac{\tilde{p}(s)(1-\tilde{Q}(s))}{1-\tilde{P}(s)\tilde{Q}(s)}\right]$, where ILT means inverse Laplace transform. These three functions have been plotted in Figure 5, clearly showing that $P(t)$ is exponential and $Q(t)$ is not. Luzar concludes that the source of non-exponentiality $k(t)$ is $Q(t)$ and Q(t) is not exponential because after a bond breaks, the molecules diffuse out of the first coordination shell, and for a re-forming, the molecule diffuses back to the first shell; a process which is not first order anymore.

We go one step farther and show that a bond re-forming that happens with diffusing back of the separated molecules is a switch-back of H^*. As we mentioned before, Q(t), is the probability distribution of the time between the last break, until the next bond formation. We divide the

$Q(t)$ function into two different possibilities based on whether H^* has formed an H-bond during time $0-t$ with another acceptor or not. Figure 5 shows the non-exponential behavior of the reforming when there *is* a switch in between time 0 to t. So, the source of non-exponentiality of $Q(t)$ and hence $k(t)$, is switching of the H-bond acceptor during the OFF times of bond between O^* and O_a. In other words, the non-exponentiality of $Q(t)$ is because the donated hydrogen has performed a *flip-flop* between time 0 to t.

So, a complete switching of the H-bond acceptor can be regarded as the outcome of a series of switches and switches back, like a *"flip-flop"* of H^* between the two acceptors. A flip is a switch of H^* from O_a to O_b, and a flop is the reverse. We have calculated the time of one *"flip"* directly from the distribution of $\tau_{flip} = t^0_{O_a} - t^0_{O_b}$ where $t^0_{O_a}$ and $t^0_{O_b}$ are the first moment that H^* is H-bonded to O_a and O_b respectively. On the average, escaping from the first H-bond cone to the next one takes around $\tau_{flip} = 1.1\ ps$.

The total switching time, $\frac{1}{k_s}$ is near 3 times longer than the average flip time: $\frac{1}{k_s} \approx 3 \times \tau_{flip}$. The difference exists because after one switch there could be a switch back, or two switches back after two switches forward and so on. Let us stress on the difference here: a single switch of the H-bond acceptor is a *"flip"* that happens on average every $1.1\ ps$, but this flip can be reversed by a *"flop"*. Using a stable state picture, we do not see many of these flip-flops, while in the reactive flux method we calculate the switching time after all the *flip-flops*. We do not want to neglect those flip-flops, because they have an important role in the diffusion of the water molecules, see section 4.3. Please see the Table 3. for the difference of the H-bond process time definitions.

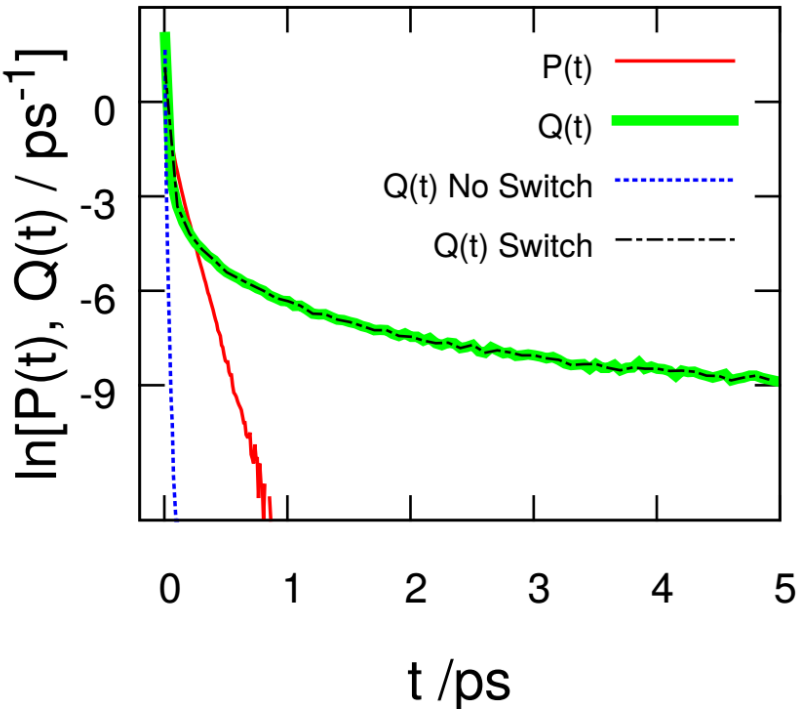

Figure 5. Comparing the first passage time probability density of H-bonds, P(t), and the probability distribution of OFF times, Q(t), if a broken bond reforms, in two situations: if the donated hydrogen experiences another switching before switching back to the originally bonded partner, and if not. The second condition is only met when the breaking is a librational breaking, and because of that it, relaxes extremely fast. This plot shows that almost all the "OFF times" are the times that H^* is switched to another acceptor.

3.2. **Diffusion**

The immediate effect of the H-bond switching of allegiances is the rotation of the central water molecule, the diffusion of the previous acceptor from the first coordination shell of the donor molecule, and infiltration of the new H-bond acceptors into the first coordination shell of the donor molecule. As we explained above, the rotational part is clearly explained by Laage and

Hynes[45] using Ivanov model. Here we explain the role of hydrogen bond switching in the random walk diffusion of water molecules.

When a H-bond breaks, the previous acceptor goes directly away from the donor molecule. We can see that from the average H-bond trajectories, figure 3 of ref.[61] and in Appendix 3 where $\phi = \widehat{O_a O^* O_b}$ remains constant before and after switching the acceptors and the $O_a - O_b$ distance reaches a minimum at the switching moment. Here we are interested in the translation of the donor molecule in a flip-flop process.

In Figure 6 we have plotted the directly calculated distribution of the displacement of a water molecule during a flip: $l_{flip} = r_{O^*}(t^0_{O_a}) - r_{O^*}(t^0_{O_a})$ where $r_{O^*}(t^0_{O_a})$ and $r_{O^*}(t^0_{O_a})$ are the positions of the donor molecule at the first moment that it is H-bonded to O_a and O_b in the laboratory frame, respectively. We can distinguish between the switches to an *"old"* or to a *"new"* acceptor: an old acceptor is a molecule that has been among the last 10 acceptors of H^*. The average distances are: $l^{new}_{flip} = 1.49$ Å , $l^{old}_{flip} = 1.04$ Å and times: $\tau^{new}_{flip} = 1.9\, ps$ and $\tau^{old}_{flip} = 1.1\, ps$ and the τ_{flip} introduced in the previous section is the average of τ^{new}_{flip} and τ^{old}_{flip}. So, we can divide the translation of a water molecule into intra- and inter-basin diffusion, where jumping to a new acceptor is an inter-basin and jumping to an old one is an intra-basin jump, see Figure 7. The intra-basin jumps consist of: (i) half-switch-jumps related to the failed jump and (ii) the switches back, or "flops". The total time that a water molecule stays in a basin is the total switching time, τ_{step}. We will show the relation of τ_{step} to $\frac{1}{k_s}$ and $\frac{1}{k}$ shortly.

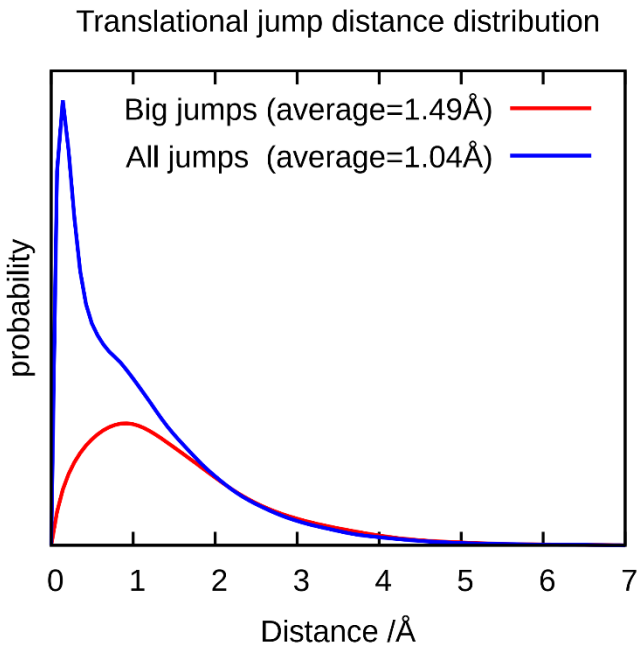

Figure 6. The displacement distribution of a water molecule during sequential H-bond switching. A single jump can be one flip which is reversed by a flop or can be a switch to a new H-bond acceptor, which is a big jump. For performing a big jump, the water molecule must displace more.

Table 3. A list of the different timescales of the hydrogen bond breaking and switching, and the diffusion of the molecules.

Description	Symbol	Time
Continuous H-bond lifetime	$\frac{1}{k_{TST}}$	$\sim 300\ fs$
One flip of a hydrogen	τ_{flip}	$\sim 1.1\ ps$
The overall flip-flop time when the previous pair has left.	$\frac{1}{k_s}$	$3.3\ ps$
The overall flip-flop time when the previous pair has *not* left.	$\frac{1}{k_d}$	$2.78\ ps$
Total time of breaking a hydrogen bond	$1/k$	$2.8\ ps$
Residence time[55]	τ_{res}	$3.2\ ps$
the complete *switch of allegiances* time. (See below)	$\tau_{step} = \max\left(\tau_{res}, \frac{1}{k_s}\right)$	$3.3\ ps$
The jump time from a stable state picture	τ_0	$3.1\ ps$
Time to other way bonding	$\frac{1}{k_o}$	$3.6\ ps$

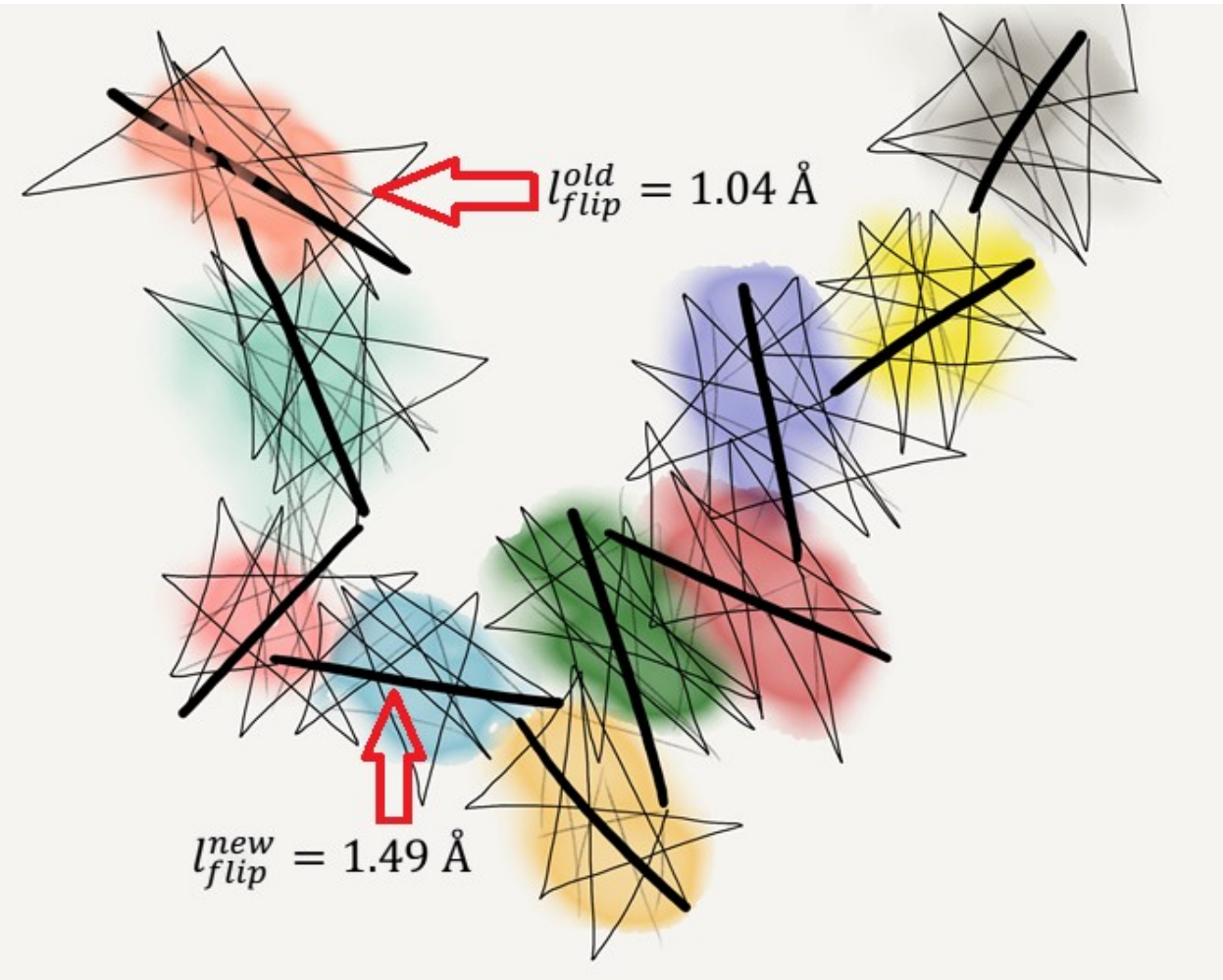

Figure 7. A schematic of the diffusion of water molecules via a random walk process based on intra- and inter-basin translational jumps. Each color represents on "basin", thick lines symbolize large translational inter-basin jumps, and thin lines show intra-basin jumps.

We hypothesize that the hydrogen bonding governs the translation, as well as the rotation of the water molecules. In other words, the translational diffusion of a water molecule is the result of a random walk process of a molecule, where the waiting time and the translational jump distance are H-bond characteristics.[122–124]

$$D = \frac{s_D^2}{6\tau_{step}} \qquad 26$$

We have listed several H-bond dynamic processing times, but which one is τ_{step}? When a water molecule performs one diffusional step, two conditions should be met: (1) The donated hydrogen of the molecule switches its bond acceptor, and (2) the previous pair break all possible ways of H-bonding and none of them reforms again. When both conditions are met, one translational step is done. The time that meeting condition (1) takes is $\frac{1}{k_s}$, and it includes all the flip-flops. To meet condition (2), all kinds of H-bonds between a pair of water molecules should break, which takes $\frac{1}{k}$, and the water molecules must go out of the first shell and never return, which takes an addition time of τ_D in Luzar model. We emphasize on the breaking of all ways of bonding since after breaking the $H^*..O_a$ bond, the $O^* - O_a$ pair may re-bond by donating another hydrogen to the acceptor or swapping the donor-acceptor roles.

Simply, the first condition is about forming a new H-bond, that is explained by Laage and Hynes and we reformulated it here, and the second condition is about breaking the previous bond and leaving the bonding domain, explained by Luzar and Chandler.[55] Based on the system, either of the conditions can be met faster than the other one. Obviously, the rate limiting step event is the slowest one. So, the step time is:

$$\tau_{step} = \max\left(\tau_{res}, \frac{1}{k_s}\right) \qquad 27$$

where $\tau_{res} = \frac{1}{k} + \tau_D$ is the residence time.[55] To assess the validity of using τ_{step} in eq. 27 in the diffusion expression in eq. 26, we have plotted the diffusion coefficient versus $\frac{1}{\tau_{step}}$ for different water models including SPC/E, BK3, and a semi-classic water model called MB-POL[64] under

different temperatures or different electric fields in Figure 9. For the details of simulations see section 2.2, and the details of water dynamics under external E-fields are explained in chapters 4 and 5. All the results follow the linear correlation between the diffusion coefficient and $\frac{1}{\tau_{step}}$, which shows two things: first, the suggested τ_{step} is truly the random walk step time, irrespective of the water model and the system, second, the translational jump distance is quite the same for all the systems that we have observed. From the slope of the linear fit, we can calculate the jump distance of $s_D = 2.4$ Å.

The dynamics would be a combination of intra- and inter-basin movements and the jump distance, s_D, is a combination of all of them. In the extended jump model for re-orientation of water molecules,[61] the frame is like the basin: The large jumps are the intra-basin dynamics, the rotation of the frame is the dynamics of the basin, and there is no need to see the inter-basin dynamics since after each switch, the rotational frame changes.

The translation of a water molecule in the structural dynamics model introduced and shown experimentally by Qvist, Schober, and Halle[125] is based on the inter- and intra- basin moves. There is no need to see the dynamics of the basin, since our frame of observation is attached to the moving molecule, and the movement of the basin is the same as the movement of the particle. Our explanation is like the structural dynamics: the intra-basin jumps length is $l_{flip}^{old} = 1.04$ Å and the inter-basin jump length is $l_{flip}^{new} = 1.49$ Å. Our intra- and inter-basin jump lengths, are very close to the intra- and inter- basin jumps reported by Qvist et al. [125], but the difference here is that we calculated these values from the H-bond switching. We showed that each flip of flop is a straight translational jump, but jumps can happen in a different angle. The overall

displacement of a molecule after all the flip flops, is around $s_D = 2.4\ \text{Å}$ and it takes $\tau_{step} = 3.3ps$ for ambient water at $300K$.

When a switch or a *"flip"* happens, there is always a probability that the flip is followed by a *"flop"*. But why flops happen and when do the flip-flops end? To find the answer, we have plotted the probability distribution of the $O^* - O_a$ distance, during the time that the $O^* - O_a$ bond is OFF and the $H^* - O_b$ in ON, in two situations: (i) if after the $H^* - O_b$ bond breaks, $H^* - O_a$ re-forms again, i. e. a flop happens, or (ii) if H^* finds a new acceptor, say O_c. The distribution of $O^* - O_a$ distance in the two situations has been plotted in Figure 8, showing that for a flop to happen, the average distance of $O^* - O_a$ cannot exceed $5.0\ \text{Å}$, which happens to be close to the border of the second coordination shell of a water structure.[126] Our conclusion is that, as long as a pair of water molecules are in the second coordination shell of each other[127] there is still a chance for them to re-bond, but if they move beyond the border of the second shell, the bond reforming is statistically rare.

The average hydrogen bond distance, from the first peak of the radial distribution function is near 2.7Å,[128] and the jump distance during one switch is $s_D = 2.4\text{Å}$, so if a pair, after all the flip-flops, reaches to the distance of $2.4 + 2.7 = 5.3\ \text{Å}$ from the previous acceptor, the bond will not re-form. In other words, the inter-basin translations are those that take a water molecule beyond the second coordination shell of its previous H-bond partner.

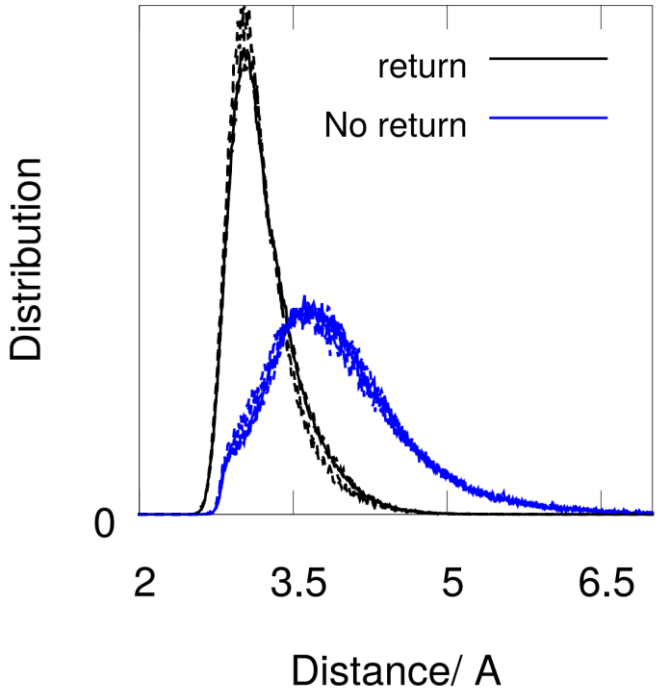

Figure 8. Comparing the distribution of average $O^* \dots O_a$ *distance during the time when the* $O^* - O_b$ *bond exists in two different situations: when* H^* *will return to* O_a *or when* H^* *switches to a new acceptor. There is a clear difference between these distributions, and the pairs that are going to re-form again, do not separate more than* 5 Å *when the bond between them is OFF.*

We have also plotted the Laage and Hynes rotational waiting time, τ_0, and H-bond dynamic time, $1/k$ versus diffusion in Figure 10. As we explained before, the waiting time that is calculated from a stable state picture, is a summation of the flip-flops and jump times. For a wide range of simulations, including polarizable, non-polarizable, and semi-classic water models and water at different temperatures or under different external electric fields, we have observed that $\tau_0 \approx \tau_{step}$. As we explained before, the major drawback of using the stable state approach, is that we neglect the details of H-bond flip-flops, which can play an important role in specific systems.[129] In the chapters 5 and 6 we bring two examples: For water molecules under static E-field, H-bond switching is more time consuming because of the re-orientation restrictions

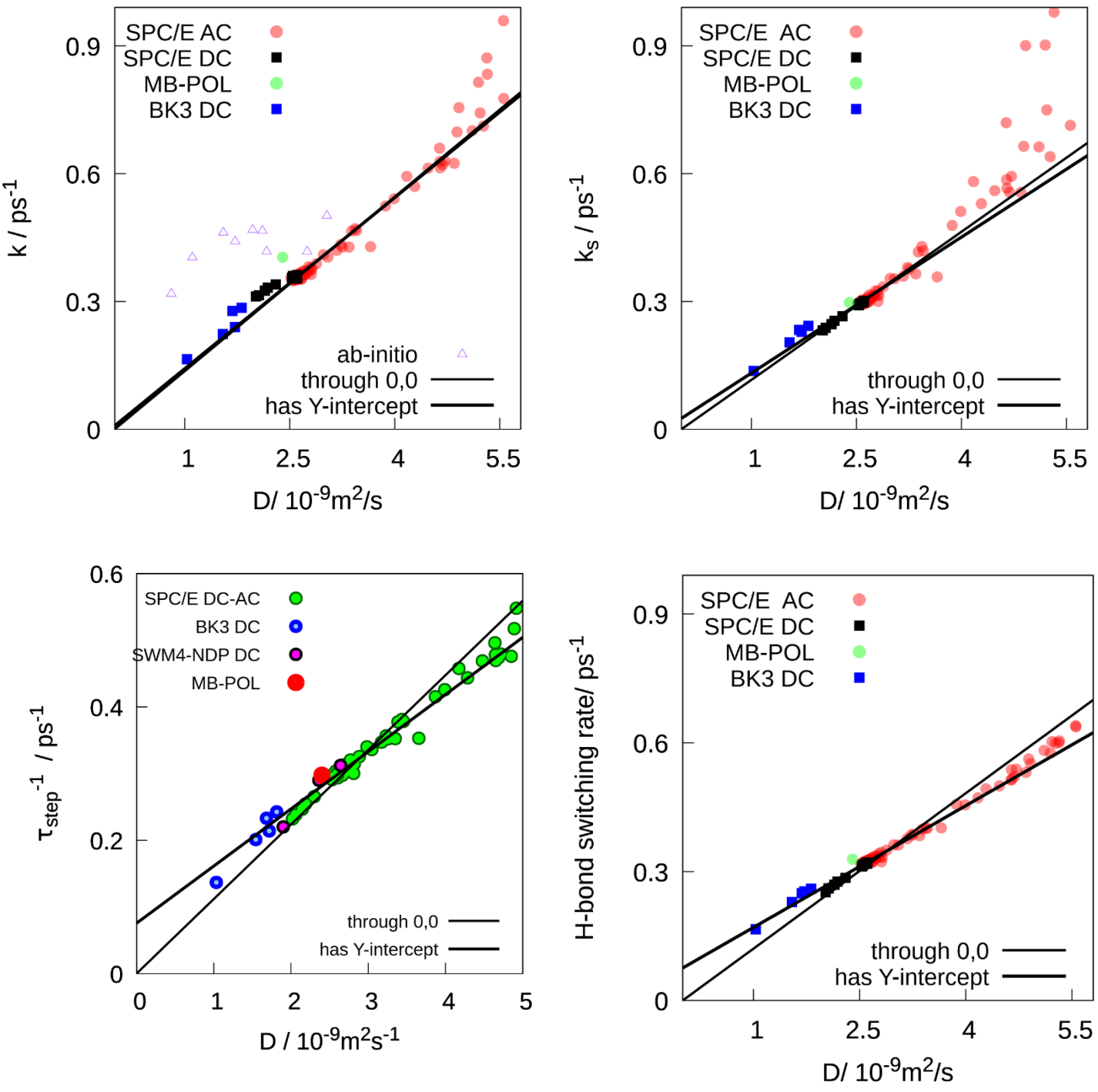

Figure 9. The correlation between the diffusion coefficient and the different H-bond breaking and reforming rate constants. The Paesani results are calculations using the MB-pol[185] water model using the trajectories that Paesani group shared with us. The fitted line can pass through (0,0) or can have a Y-intercept. Having a Y-intercept means that when the translational diffusion is zero, the molecules can still re-orient a little bit.

imposed by E-field, so $1/\ k_s$ is bigger than $\frac{1}{k} + \tau_D$, and under alternating E-fields, the H-bonds

switch fast but the molecules do not have time to separate, so $\frac{1}{k} + \tau_D > \frac{1}{k_s}$.

Another point to clear up is the difference between the two perspectives: Luzar and Chandler's model is about a pair of water molecules, while in this research, like the Laage and Hynes model, we worked with a tagged hydrogen, which is only one, out of four[130] ways of having an H-bond between a pair of water molecules. What is the probability that the pair reform an H-bond in any of the other three ways after switching the first bond? The probability of other-way-bonding can be calculated from:

$$n_O = c(t) - c_t(t) \qquad 28$$

In Figure S 7 we show that the probability of the "other-way re-bonding" increases with time and has a maximum around $6\ ps$. The other-way-re-bonding time is just a little longer than switching time, so these two processes: switching H^* to O_b and forming a new bond between O^* and O_a can happen simultaneously.

Finally, we comment about the coupling of translation and rotation[131] of water molecules: As Laage *et al.* explain, the rotation of water molecules is the result of the re-orientational jumps during switching of H-bond acceptors. We also showed here that the translational diffusion of water molecules happens during the jump like displacement of molecules during switching of H-bonds. So, hydrogen bonding governs and couples the rotation and translation of water molecules.[51]

This coupling breaks in two extreme cases: (1) When the number of hydrogen bonds per water molecule drops significantly, say less than three at high temperature, where water molecules are freer to rotate and translate without switching the H-bond allegiances. And (2) when the switching of a H-bond is not possible, for example for water under strong static electric field when water molecules still can rotate perpendicular to the field direction but cannot find any new acceptor to switch the bond. We will explain this in the next chapter. Another example is supercooled water when the roto-translational coupling is not broken,[132] but because of the structural constraints, the broken bond water molecules cannot diffuse away.[133] Galamba explains how it happens:[134] as the temperature goes down, the waiting time for reforming is longer than the waiting time for switching. This happens because the proton cannot find a nearby acceptor to switch and diffuse, instead, it reforms to the previous acceptor, i. e.; the probability of a *flop* increases and the probability of a jump decreases.

3.3. **Reconciliations with other descriptions**

The dynamics of hydrogen bonding have been studied from different viewpoints,[62,135] and it is widely accepted, and experimentally shown[136] that switching of a H-bond takes place during a very fast, less than $100\ fs,$ angular jump after a considerable waiting time, $2-3\ ps$.[117,119] The waiting time before breaking and switching of a hydrogen bond is also

shown to be more than $2\ ps$.[137] The effect of the fast switching events on the rotation of the water molecule is extensively investigated.[138] The difference between the method that we introduce in this research and the method that is used by Laage and Hynes, is that they see a switch back as a brand-new switch,[61] and they remove the re-crossings of the switching barrier by using a stable state picture, while we calculate the switching time after all re-crossings.

Laage and Hynes, in other research, show that the translational jump time is $\tau_T^{jump} = 0.55\ ps$.[139] They assume that every rotational jump happens with a translational jump, and since a water molecule has 4 hydrogen bonds, it takes $\frac{\tau_R^{jump}}{4} = \frac{3.1}{4}\ ps = 0.78\ ps$ for a water molecule to perform a translational jump. The point is that a water molecule does not need to re-orient with a jump when it changes a H-bond donor, so the re-orientational jump happen every $\frac{3.1}{2} = 1.5\ ps$. Instead, every flip can cause a translational jump, and hence a translational jump happens every $\frac{\tau_{flip}}{2} = 1.1\frac{ps}{2} = 0.55\ ps$ which is in good agreement with the simulation and experiment results.[139]

In Figure 10 we have compared the diffusion step time, τ_{step} and the jump time, τ_0. Please note that these two times are calculated from completely different perspectives: τ_{step} is the total time of one H-bond switch and a separation of a pair. On the other hand, τ_0 is the time for one stable switch. We can see from this figure that $\tau_0 \sim \tau_{step}$ and it means that a switch is stable only when the previous pair have been separated.

Kawasaki and Kim[67] have talked about the correlation between the diffusion coefficient and the hydrogen bond lifetime for water at different temperatures. Here we explained the mechanism of such correlation, and we calculate the H-bond lifetime from the dynamics of single water molecules, not from the relaxation of the total number of molecules. They mention that the reason of Stokes-Einstein violation[59,140] is a caging effect[66] at a low temperature. In our picture, the molecules may get trapped when they cannot find a new acceptor and do more flip-flops in the basin. We show a similar situation of water under static external E-field, see the next chapter. The correlation of the hydrogen bond dynamics and translational diffusion has been observed in several studies.[125,132,141–143] Here we show the mechanism of this correlation from the hydrogen bond dynamics point of view. In fact, switching the H-bond is what correlates the rotation and translation of water molecules.

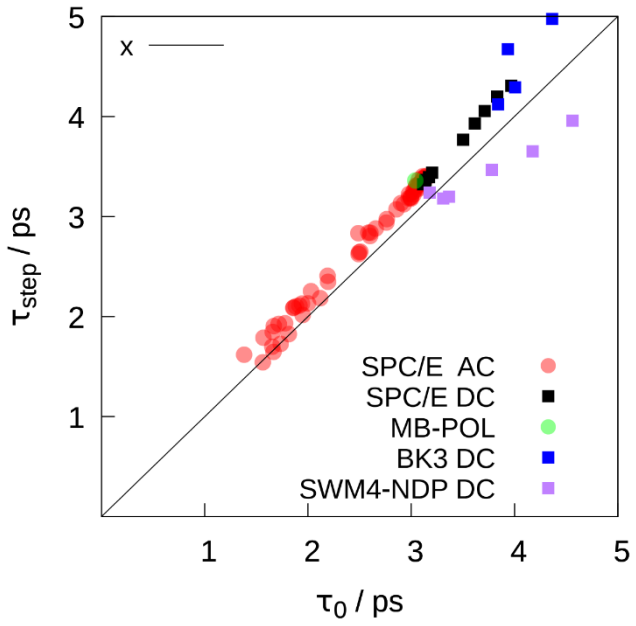

Figure 10. Reconciliation of the Laage and Hynes model and our suggested step time, eq. 27, for SPC/E, BK3, SWM4-NDP, and MB-pol water models.

3.4. **Conclusions**

We showed that the H-bond breaking in Luzar and Chandler model,[51] mostly coincides with a switching of the H-bond acceptor. The H-bond switching can be calculated using a reactive flux method which is in a good agreement with the SSP model results that applied at established H-bond definition but depends less on the H-bond criteria. The characteristic waiting time and distance of the random walk diffusion of water molecules are determined by the hydrogen bonding. The dynamics of hydrogen bonding determines both the translation and rotation of water molecules, resulting in the correlation between the translational and rotational diffusion coefficients.

.

Chapter 4. **Water under Static Electric Fields**

The behavior of water molecules under external electric fields has been the subject of many experimental and computational studies: Application of an external electric field can impose significant changes on properties like density[3,4,17,30] diffusion,[144] viscosity,[10,145] and permeability[13] of water in bulk[47] and confinement.[146] A direct current (DC) can generate a static electric field in a capacitor, so, traditionally we call a static E-field a DC field.

In pure water, the effect of an external electric field is an alignment of water dipole moments with the direction of the E-field. Water molecules can have up to 4 stable hydrogen bonds, and since the hydrogen bonds are strongly directional[70], the behavior of water under an electric field is non-trivial even for pure water in bulk.[20,21,25,28,37,38,41,147,148]

In this research, we measure the effects of the external E-fields on the dynamics of water molecules using the phenomenological model of hydrogen bonding introduced by Luzar and Chandler,[51] the extended jump model for the molecular rotation introduced by Laage and Hynes,[61] and our generalized framework described in chapter 3. We have explained the Luzar and Chandler model in section 1.2.1, and the Laage and Hynes model in section 1.2.2 and the details of the simulations are explained in section 2.1. We use a range of electric field strengths of $0 - 0.2\ V/\text{Å}$, not much smaller than $0.01\ V/\text{Å}$ since the effects will not be observable, and not much higher then $0.2\ V/\text{Å}$ since a water molecule dissociates at higher E-field.[32]

We have examined several structure functions, and as we have seen in the previous works,[27,149] the tetrahedral structure remains almost unchanged under static E-fields, while water becomes anisotropic and the change in the structure is observable in a plane perpendicular to the E-field direction. Then we look at thermodynamic properties of water under the static E-fields where we show that the energy landscape of hydrogen bonding cannot be interrupted under the range of E-fields that we apply. The dynamics of water molecules, however, slows down and we can see this slowing down in the translation and re-orientation of water molecules, and H-bond breaking and switching rates. Finally, we discuss the connections of the observed phenomena and we assess the theories that we developed in chapter 3 on water under static E-fields.

4.1. **Structure**

The dipole moment vector of a water molecule tries to align with the direction of the external E-field. In this section, we are interested in the average structure of water, not only one cluster of molecules.[38] Specifically, the question that we want to answer is: how will the tetrahedral structure of water resist the E-field induced alignment of water molecules? And how will the hydrogen bonds arrange when the molecules are forced to align with the E-field direction.

The average alignment of water molecules can be calculated from:[30]

$$\langle \cos(\theta_z) \rangle = \frac{p_z}{\vec{p}} \qquad 29$$

where θ is the angle of water dipole moment vector, $\vec{p}$, with the direction of the electric field, z. This average is plotted in Figure 11 showing that in the presence of a static E-field, the alignment increases almost linearly up to $0.03\ V/\text{Å}$ where $\langle \cos(\theta_z) \rangle$ reaches to 0.65.[28] Then, the alignment

increases at a lower rate and reaches to near 0.8 under $0.1\,V/\text{Å}$ where water alignment is saturated and the alignment never reaches 1.0.

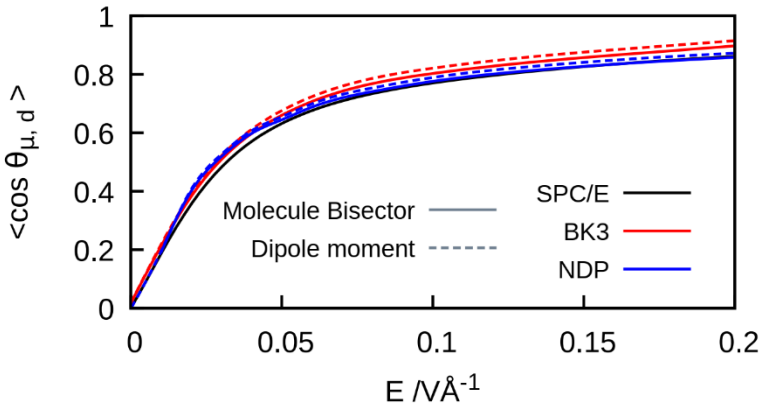

Figure 11. The average of the angle of the water dipoles and water molecule bisector vectors with the E-field direction. Below $E = 0.05\,V/\text{Å}$, the increase in the alignment is significant. The rate of the alignment of water with the field is almost negligible beyond $E = 0.1\,V/\text{Å}$.

The above results show that with fields weaker than $0.03\,V/\text{Å}$ there is little resistance of the water structure against alignment.[50,150] However, a strong state of saturation sets in at the alignment of more than 0.65 under stronger E-fields.[151] The system is at the room temperature, 300 K, and water molecules continue to re-orient and break their H-bonds,[35] and they continue to deviate from a full alignment to keep their dynamics, and that is why alignment never gets to 100%.

In Figure 12 we have plotted the distribution of the angle of the dipole moment of water molecules and the intra-molecular $O-H$ bonds with the field direction under different static E-fields.[145] There are differences between the two figures: For the dipole moment distribution plot, increasing the field strength continuously shifts the maximum to the smaller angles and reduces the standard deviation, which simply means a stronger alignment of water molecules with the field direction.

The distribution of the angle of the intermolecular O-H bonds behaves differently: Under the electric fields stronger than 0.05 V/A, the most probable angle does not change dramatically, but only the distribution narrows down. This is because a water molecule has two intramolecular $O-H$ polar bonds, if one of the $O-H$ bonds aligns more, the other one would be less aligned. Hence, the intermolecular bonds settle into a compromised angle with the E-field direction.

However, the distribution of $O-H$ angles is broader than that of the dipole's angles. This means that even under the highest electric fields, water molecules are still free enough to re-orient. We will show later in this thesis that this is because of the energy-entropy competition: a narrower distribution of the $O-H$ angle results in decreasing of the entropy of H-bond breaking, Figure 22, while the energy of the system also increases, Figure 22.

Despite these limitations on the molecular re-orientations, we will show that the main features of the structure of water are preserved under even very strong E-fields.[152] To assess this, we look at some structural properties of water: the radial distribution function, g(r), the triple angle distribution $\widehat{OOO}$,[153] tetrahedral order parameter called q, the second layer the tetrahedral order parameter, called Q_6, and at the end, we observe the spatial distribution function, SDF.

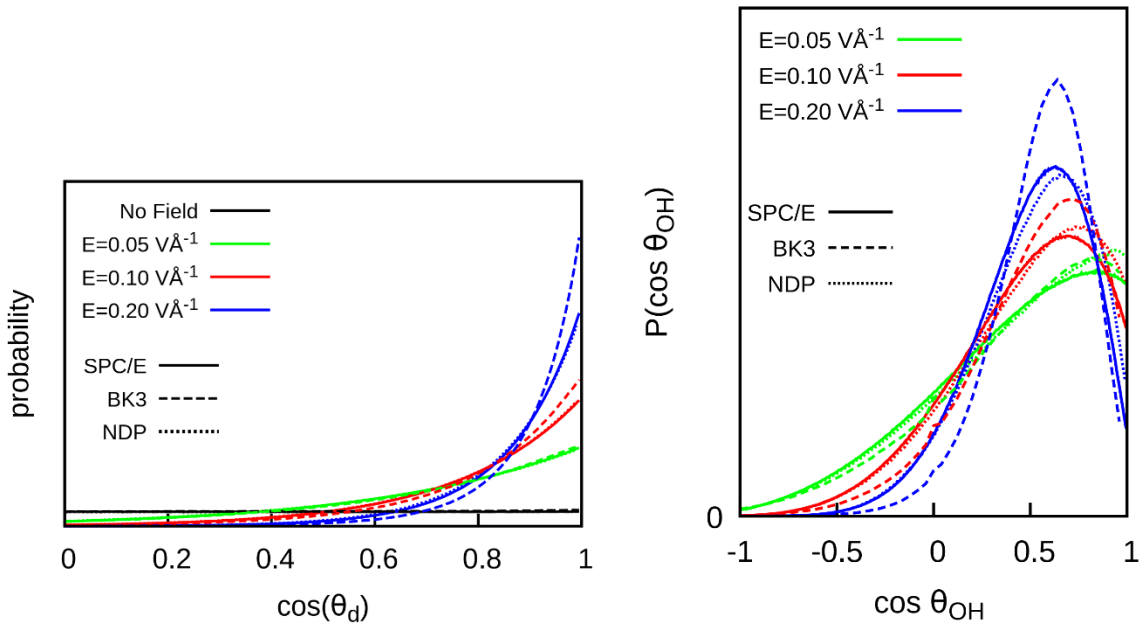

Figure 12. (Left) The distribution of the angle of water dipole moments with the E-field direction. Like the average alignment of dipole moment that increases dramatically bellow $0.05\ V/\text{Å}$*, the position of the distribution shifts to the higher angles. (Right) the intramolecular OH bond angle distribution with the E-field direction. After* $0.05\ V/\text{Å}$*, the maximum of the probability distribution does not shift, but the distribution gets narrower.*

4.1.1. The radial distribution function

The three radial distribution functions of water: oxygen-oxygen $g_{OO}(r)$, oxygen-hydrogen $g_{OH}(r)$, and hydrogen-hydrogen $g_{HH}(r)$ under external E-fields is plotted in Figure 14. This figure shows that the radial structure around a water molecule slightly changes under E-fields, and this is in agreement with the reported results.[19,145,150,154] This shows that the applied E-fields, only change the direction of water dipole moments, and the tetrahedral structure is compatible with a highly-aligned water system.

However, other distance distribution functions can help us to understand the structure of a bulk of aligned water molecules. We can look at the cylindrical distribution function: $g(l_{\parallel})$ where l is

the cylindrical distance to the central molecule in the $x-y$ plane, and $g(l_{\perp})$ is the same cylindrical distribution function, but in $x-z$ or $y-z$ plane.

The $g(l_{\perp})$ functions show a significant change of structure in each direction while the overall change is averaged out in $g(r)$. Under the strongest E-field where almost all the water molecules are aligned, the height and the distance of the first peak of $g(l_{\perp})$ has slightly changed, while its second peak is higher and in a longer distance. This shows that water in the z direction has been layered in the second shell under the E-field. For $g(l_{\perp})$, the height of the first peak has decreased dramatically, while its distance is not changed under the field. Moreover, the height of the second peak increases and it has been shifted to a closer distance. This implies that in the $x-y$ plain the water is structured by pushing the closest neighboring molecules away and having more order in the second coordination shell. We hypothesize that the second peak of $g(l_{\perp})$, is related to the molecules that share a common H-bond partner.

To assess the above hypothesis, we have plotted the distribution of the elements of the $O_a - O_a$ vectors in Figure 15, where O_a's are the H-bond acceptor oxygens of a central molecule. We explain our hydrogen bond criteria in section 4.1.6. Under zero field, we see absolutely no preference in the direction of the $\overrightarrow{O_a - O_a}$. Under the strongest field, however, we see that the two acceptors are mostly in the same z level, and the most probable distance of the acceptors in the $x-y$ plane is near $4\ \text{Å}$, which is the same distance of the second peak of $g(l)$. This layering can be seen as formation of water clusters under the different external static E-fields.[38,155]

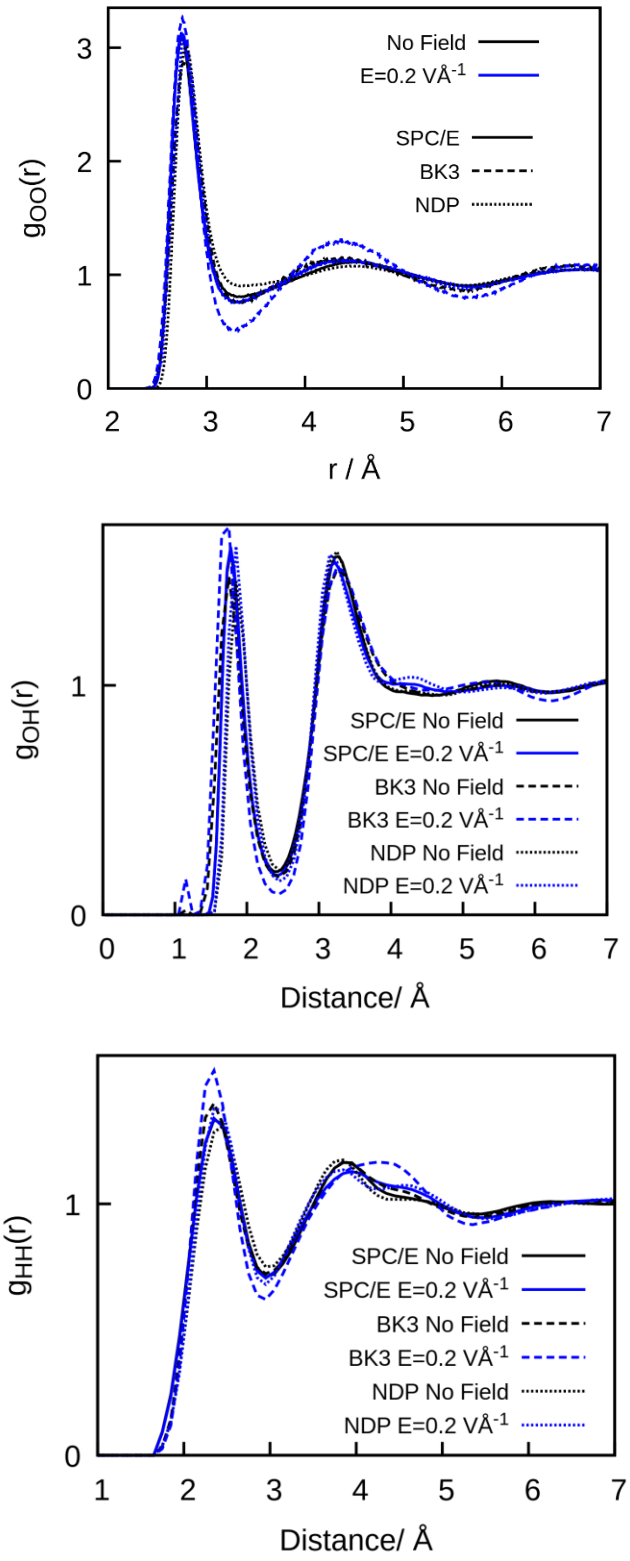

Figure 13. The radial distribution function of water: $g_{\mathrm{OO}}(r)$ (top), $g_{OH}(r)$(middle) and $g_{HH}(r)$ r (bottom).

The effect of an E-field is changing the direction of the water molecules, and RDF is not a

directional function, i. e., $g(r)$ averages all the neighboring molecules that have a distance of r to the central molecule. So, the conservation of $g(r)$ under E-fields, can mean that the tetrahedral structure of water molecules has not changed, but it has just been re-arranged. The aligned structure is therefore layers of water molecules perpendicular to the E-field direction. In the $x - y$ plane, the system becomes anisotropic: the first peak has decreases, and the second peak has come closer, and the first and the second peak seems to be in the same height.

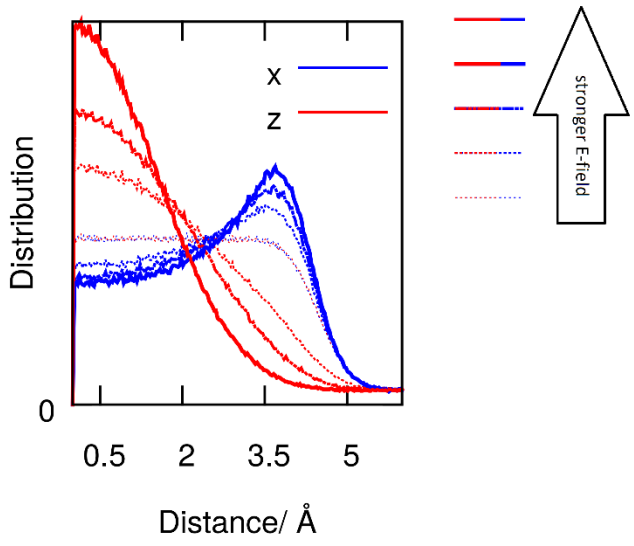

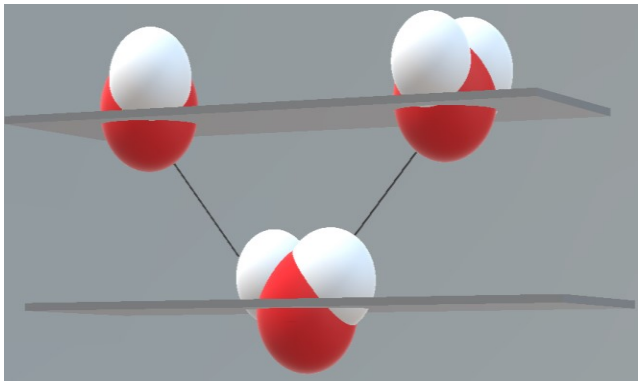

Figure 15. The distribution of the $O_a - O_a$ distance in the x and z directions. This plot shows that with increasing the static E-field, the z component of the $O_a - O_a$ distance goes toward shorter distances,

meaning that acceptors are almost in the same plane. In such a plane, the H-bond acceptors of the same molecule keep the distance of ~ 4 Å*.*

4.1.2. Tetrahedral order parameter

The first tool for calculating tetrahedrality is the tetrahedral order parameter calculated by[156]:

$$q = 1 - \frac{3}{8}\sum_{j=1}^{3}\sum_{k=j+1}^{4}\left(cos\psi_{jk} + \frac{1}{3}\right)^2 \qquad 30$$

where ψ_{jk} is the $\widehat{O_i O^* O_j}$ angle and i and j are the nearest neighbors of the central molecule O^*. An increase in q is required but not sufficient to prove the increase in tetrahedrality.[157] The results show that the tetrahedral structure has not changed under the static E-fields, see Appendix 1. We will show this conclusion again in the next section by plotting the triple oxygen angle distribution function.

We see that the tetrahedral structure of water is preserved when molecules are highly aligned. We proceed to evaluate the tetrahedrality in the second coordination layer, and we calculate the second layer structure order parameter[158]:

$$q_6 = \frac{1}{N}\sum_{i}^{N}\left[\frac{4\pi}{2\times 6+1}\sum_{m=-6}^{m=6}|\bar{Y}_{6m}|^2\right]^{\frac{1}{2}} \qquad 31$$

Where $\bar{Y}_{6m}$ is the average of $6th$ spherical harmonic over 12 nearest neighbors of the central molecule. This time, see Appendix 1, we observe absolutely no change in the q_6 parameter in the presence of the E-fields. This implies that a high alignment of water molecules does not make any crystal lattice structure like fcc or bcc at 300K.

4.1.3. Triplet angle distribution

Another well-known method for calculating the tetrahedrality of the system is plotting oxygen triplet angle distribution,[159] which is the distribution of the angles that nearest molecules make with the central oxygen[153]:

$$P(\cos\theta_{\mathrm{OOO}}) = \frac{1}{N(n_i-2)}\langle\sum_{i=1}^{N}\sum_{j=1}^{n_i-1}\sum_{k=j+1}^{n_i}\delta\left(\cos\theta_{\mathrm{OOO}} - \frac{r_{ij}.r_{ik}}{|r_{ij}|\,|r_{ik}|}\right)\rangle \qquad 32$$

where N is the number of molecules, n_i is the number of nearest neighbors of the central molecule inside the first coordination shell, and r_{ij} is the vector connecting oxygen i to oxygen j. The first peak in this function shows the "*tetrahedrality*" and the second peak is related to the *interstitial* molecules, see Figure 16. The angle of the tetrahedral peak reduces by almost 3%, and the height of that peak increases by less than 5% under the highest electric fields. Unlike q which only shows angular tetrahedral order and not translational order, the triplet angle distribution function is calculated by connecting the closest neighbors in the first coordination shell, so it shows angular as well as radial order.

As we show in section 4.1.6, the coordination number and the number of hydrogen bonds of water does not change dramatically under static fields, so the closest molecules stay at the H-bonding positions, and the triple oxygen tetrahedral parameter does not change. Since the H-bond donors and acceptors will not be in the $x-y$ plane, the planar structural changes that we mentioned in the previous section will not be projected in this function.

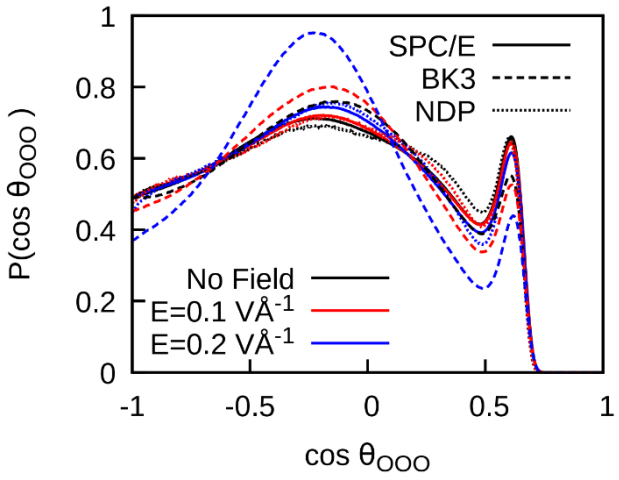

Figure 16. Triplet angle distribution function OOO in the presence of three water models under static electric fields.

We hence conclude that the tetrahedrality of water molecules is not changed under the applied external static electric fields, while the number of interstitial molecules is reduced by 7% under

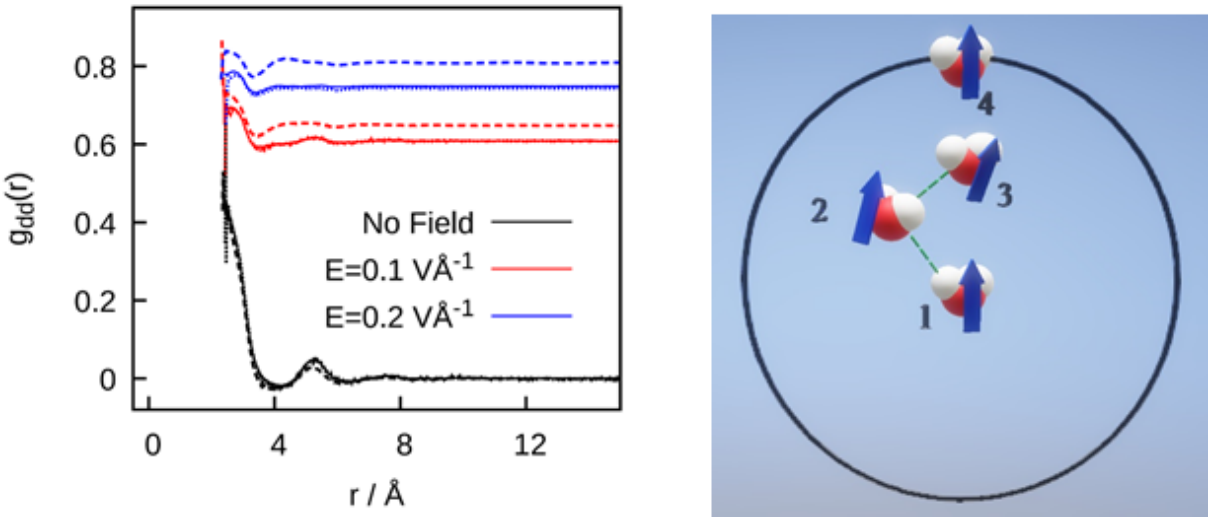

Figure 17. (Left) Distance-dependent orientational correlations in SPC/E water (solid lines), BK3 (dashed lines), and SWM4-NDP (dotted lines) under no field and under $E = 0.1\,V\text{Å}^{-1}$. All models behave qualitatively similar, although BK3 water molecules are stronger correlated than in other models. (Right): A schematic illustration of a possible configuration of H-bonded (2, 3) and non-H-bonded (4) water molecules. Molecule 4 is located at the boundary of the second coordination shell, lacking angular preferences due to H-bonding, which makes it relatively free to rotate.

the strongest E-field. This is an important result to understand the effect of the static E-fields on HB dynamics since the less interstitial molecules means that fewer molecules are available for hydrogen-bond switching process.

4.1.4. Average Orientational Correlations

It can be insightful to look at distance-dependent average orientational correlations measured using the water angle bisector vector $\vec{d}$:[160,161]

$$g_{dd}(r) = \frac{\langle \vec{d}(0)\vec{d}(r) \rangle}{\langle d \rangle^2}, \qquad 33$$

where $\hat{d}_i$ is the direction of the dipole moment of molecule i. The long-distance value of $g_{dd}(r)$ measures the average alignment of water molecules, which we calculated directly in in Figure 11.

The interesting point is the second peak of alignment in the ambient water, the blue line in Figure 17 (left) which vanishes under static E-fields. This peak is because the energetically ideal configuration of two dipoles is head-to-tail alignment like molecules 1 and 4 in Figure 17 (right). But this alignment can be faded because the molecules are connected by a chain of H-bonds, and the H-bonds forces the molecule to have other directions. Once the molecules go beyond the second coordination shell, there is a higher probability that the at least one bond in the chain of H-bonds between them is broken, so they are free to have the head-to-tail configuration. Under higher E-fields, the molecules are already aligned with the E-field, so the peak vanishes.

4.1.5. Spatial Distribution Function

From the results presented above, we learn that under the static E-fields: the tetrahedral structure of water inside the first coordination shell and the average number of molecules in each distance from a central molecule do not change, and water is more anisotropic. Now, we can observe these structures visually by looking at the spatial configuration of the neighboring molecules around a tagged water molecule.[126,162] The coordination system of the SDF plot is based on the central water molecule: x axis is in the direction of one intra-molecular $O-H$ bond, the z axis is parallel to the cross product

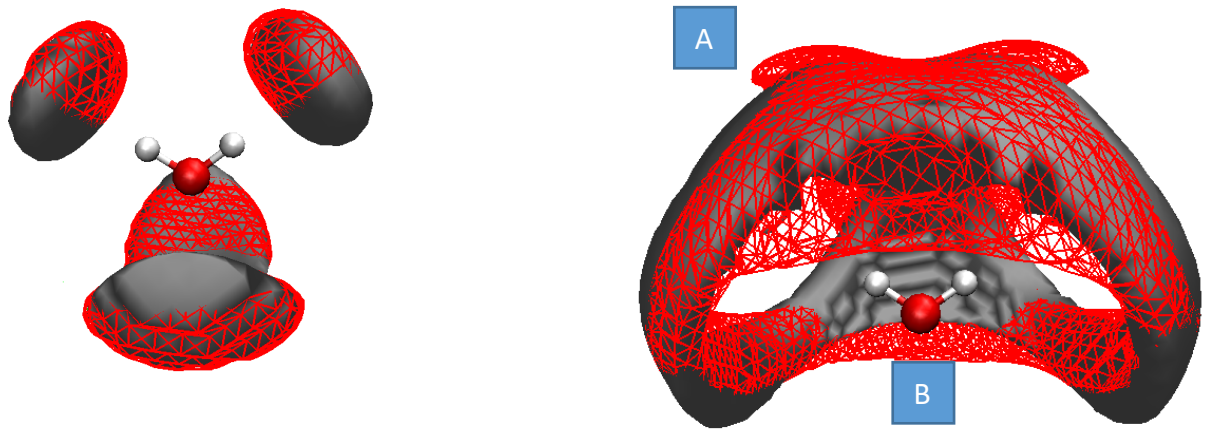

Figure 18. The spatial distribution function of SPC/E water in the first(left) and the second (right) shell for no field (blue) and $E = 0.2V/\text{Å}$ (red). Both plots for the first shell have an average iso-value density of 1.3 and for the second shell, the density iso-value is 1.8. The central molecules is added to show the relative positions of the lobes to a water molecule. In the first shell, the strong E-field does not change the probable position of the H-bond accepting molecules, but the positions of the H-bond donor molecules are more restricted. In the second shell, however, the shape of the density profile is more different under the strong static E-field.

of x axis and the other intra-molecular $O-H$ bond, means perpendicular to the $H-O-H$ plane, and $\vec{y}=\vec{x}\times\vec{z}$.

Inside the first shell, we see four lobes: two related to the positions of H-bond acceptors, and two lobes related to the positions of the H-bond donors. The former lobes are more distinguishable than the latter ones. Inside the first shell, the spatial distribution function hardly changes under static E-fields, neither the shape nor the position of the lobes. The only difference is that the two lobes that are related to the hydrogen bond donors are more distinct under our strongest E-field, but this has a small effect on the tetrahedral structure since the main lobes have not shifted.

In the second shell, the most probable positions of the neighboring molecules are off-above the lobes in the first coordination shell. According to Laage and Hynes,[163] the molecules in the second shell are the possible next H-bond acceptors that can enter the first shell to accept a proton and form a H-bond. These molecules also can be the molecules that have lost their H-bond and have left the first shell. The latter group, however, still have a chance to return to the first shell and take the previous H-bond back.

The electric field is more influential in the second shell. This is because the electric intermolecular interactions around the central molecule inside the first shell are stronger than the external field force, making the field less effective.

Under our strongest E-field: $0.2\ V/\text{Å}$, the water molecules highly align with the field, so the $x-y$ plane of the SDF plot is almost perpendicular to the $x-y$ plane in the laboratory frame. We can see a relatively higher density at a smaller distance to the central molecule in the $x-y$ plane

(laboratory frame) in area B in. This area is related to the neighbors in the second shell that are H-bonded to a common acceptor.[126] This agrees with the cylindrical distribution $x-y$ plane, Figure 14, where the second peak of $g(l_{\perp})$ is higher and at a relatively shorter distance. Since a water molecule re-orients to exchange the hydrogen bond mostly in the $x-y$ plane, the possible new acceptors are mostly positioned above the central molecule, area A.

4.1.6. Number of H-bonds

Here we assess our theory more in depth, but in the first step, we count the number of hydrogen bonds.

Before starting, we need a definition of a hydrogen bond. We use the geometric criteria for calling a pair of water molecules H-bonded.[120] According to Figure 19, in near 70% of the hydrogen bonds, the $H\text{-}\widehat{O^{*}\text{-}O_{a}}$ angle is less than 30 degrees, so we take it as a hydrogen bond cut off angle. The acceptor also needs to be in the first coordination shell of the central molecule, which is 3.5 Å according to the radial distribution function, Figure 14. In such a triangular, the maximum $H-O_{a}$ distance is 2.4 Å. In the EJM section we use a restricted H-bond criterion which is $H\text{-}\widehat{O^{*}\text{-}Oa}=30^{\circ}, d_{O^{*}-Oa}<3.1$Å and $d_{H-O_{a}}<2.0$ Å.

According to Figure 19, in the presence of the static electric fields, the number of hydrogen bonds as a function of the cutoff angle slightly increases, but in all the cases, near 70% of the bonds are within the 30 degrees cutoff angle. It means that the hydrogen bonds are not stretched to keep their bonds when the molecules are aligned.[150] In section 4.2 we see this conclusion again by showing that the water-water interactions do not change in the presence of a static electric

field, and since a huge percent of the interaction energy between a pair of water molecules is related to hydrogen bonding, we conclude that the hydrogen bonding does not change.

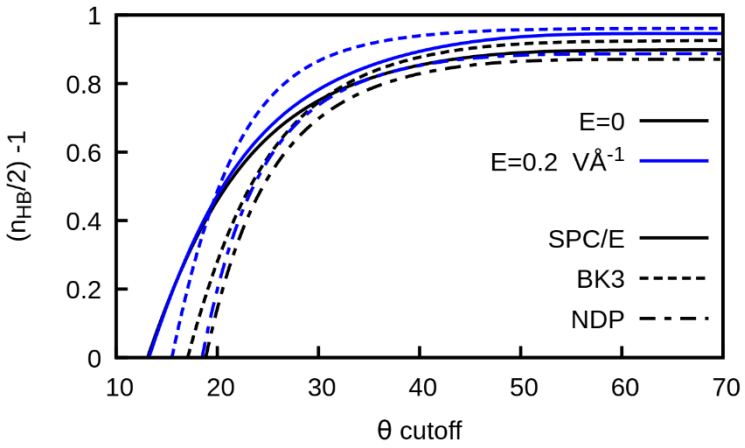

Figure 19. The Relation of the average number of H-bonds to the angular hydrogen bond criterion. The E-fields do not make any significant difference, so we stay with our traditional H-bond criteria when we study for SPC/E, BK3, and SWM4-NDP water models under static E-fields.

In Figure 20, we show that the number of H-bonds per water molecule under different electric fields changes around 1%[49,50,150,164] under the strongest E-field of $0.2\,\frac{V}{\text{Å}}$.

Similarly, the total number of neighbors in the first coordination shell of water molecules, simply called the coordination number decreases by only 1% after $0.05\,V/\text{Å}$. According to Luzar's model, the coordination number, n_c, plotted in Figure 20 is the number of accessible neighbors for forming an H-bond. A lower coordination number around a water molecule is the result of a higher number of hydrogen bonds. Under a strong electric field, however, we do not see any change in any of them. This result is in agreement with a very subtel change of the structure, implying that the alignment of water molecules with the E-field is compatible with the hydrogen bond tetrahedral structure. In section 4.3 we will show that unlike the structure of hydrogen bonds, the dynamics of hydrogen bonds is significantly influenced under E-fields.

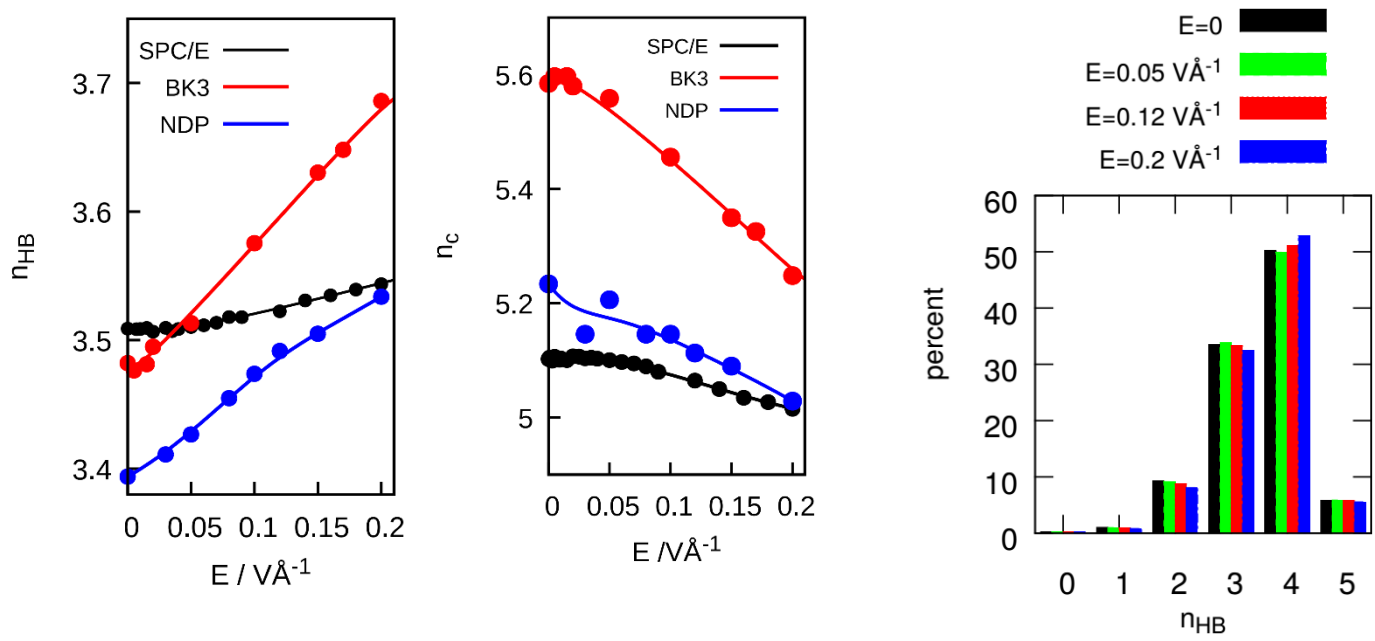

Figure 20. (left) number of H-bonds and (middle) coordination number which is the total number of neighboring molecules within the first coordination shell of a molecules, 3.5Å*. Despite the trend, the overall change of both values under DC fields is negligible: less than 1%. (right) The percentage of the water molecules that have a specific number of H-bonds. There is a very slight increase and decrease in the percent of the molecules with a higher and lower number of bonds respectively under the E-field of* $0.2\ V/\text{Å}$*, but the overall change in the number of H-bonds is negligible.*

4.1.1. Structure of polarizable models

The imposition of an electric field does not only align water molecules, but polarizes them as well. Here, we examine the field-induced change in the dipole moments of our polarized water models (Figure 21).

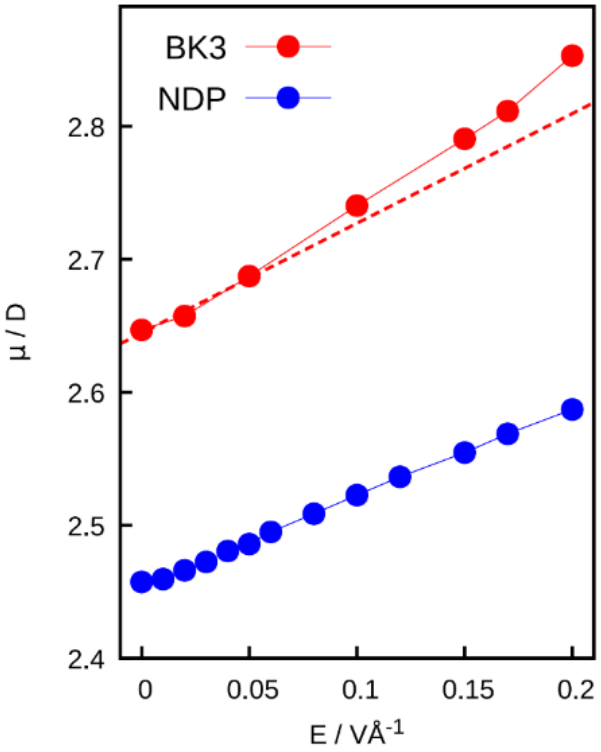

Figure 21. The change in the dipole moment of BK3, and SWM4-NDP water molecules under static electric fields. The dashed, red line shows how the dipole moment of BK3 water molecules deviates from a linear trend.

The reported static dipole moment and polarizability volume of BK3 water are $\mu_{BK3} = 2.64\ \mathrm{D}$ and $\alpha_{BK3} = 1.44\ \text{Å}^3$, respectively.[99] Within the linear response regime, the predicted change in the dipole moment upon application of an electric field of strength $0.2\ \mathrm{V\text{Å}^{-1}}$, $\Delta\mu_{BK3}$, should be $\sim 0.1\ \mathrm{D}$, which is $\sim 4\%$ while our results suggest that the dipole moment changes by $\sim 7\%$. While the low field polarizability resembles that of real water, the use of a suppressed, field-dependent polarizability has been suggested to alleviate the nonphysical

increase of the dipole moment at stronger E-fields[84], however, the proposed correction becomes significant only at fields well above the strongest field considered in our work.

With the SWM4-NDP model, on the other hand, $\alpha_{SWM4-NDP} = 1.5\ \text{Å}^3$ and $\mu_{SWM4-NDP} = 2.64\ \text{D}$ suggesting a change of $\Delta\mu_{SWM4-NDP} = 0.065\ \text{D}$, which is 2.65% and agrees well with our observed change of 2.59%.

4.2. Thermodynamics

We conclude that from the static point of view, H-bonds are very resilient to the change under a static E-fields. Here we study the change of the energy of the system.

A useful approach would be calculating the water-water part of the potential energy. This water-water part, or *cohesive energy*, is the total interaction energy between the molecules and is equal to the total potential energy of the system minus the water-E-field interaction energy[151] $\Delta U = \hat{P}.\hat{E}$:

$$\langle \Delta \mathrm{E}_{\mathrm{coh}} \rangle = \langle \Delta \mathrm{E}_{\mathrm{pot}} - \mathrm{E}_{\mathrm{field}} \rangle. \qquad 34$$

By calculating ΔE_{coh} in this way, we can see if the H-bond network is energetically weaker in the presence of the field or not. Our result in Figure 22 confirms that the intermolecular energy of the system does not change substantially in the presence of an E-field. This means that the hydrogen bonds are not under stress while they keep their H bonds when the molecules are aligned with the E-field. This agrees with the static picture in Figure 20 that an H-bond angle is not affected by the presence of the DC fields.

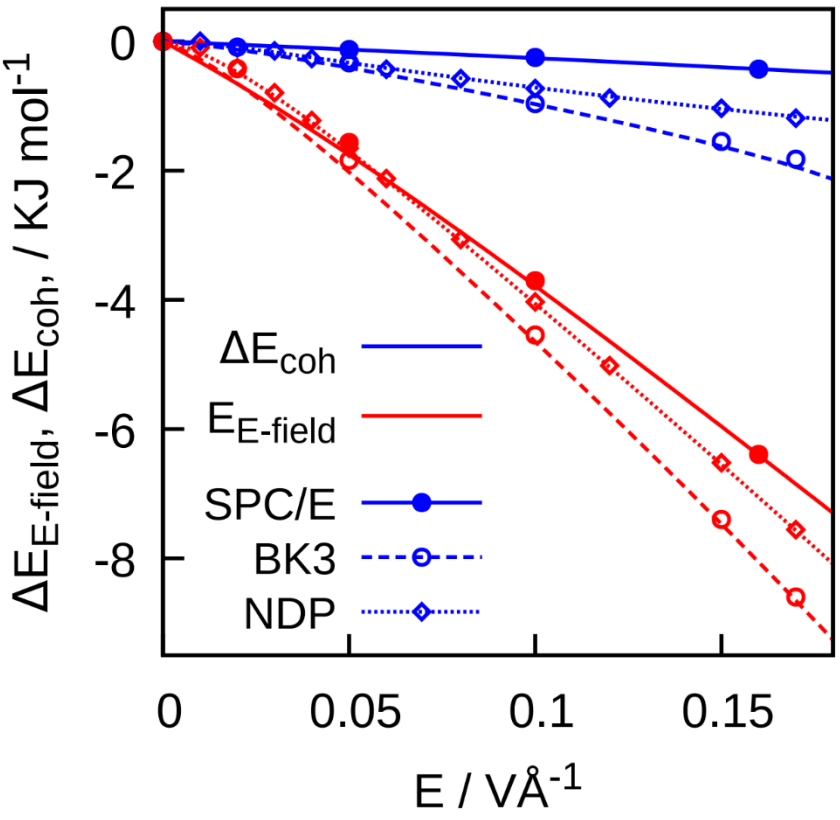

Figure 22. The change in the energy of the system under static E-fields. We see that the main change in the energy of the system is due to the change of the interaction of the field with water molecules. The change in water-water energy (cohesive energy, black line) is less than 2%.

Water thermal intermolecular energy is of the order of $k_B T = 2.5 \frac{kJ}{mol}$. When the imposed energy of the electric fields is higher than the rotational energy of water molecules,[165] the water dynamics is suppressed, means the molecules hardly can rotate and break the hydrogen bonds, and the dynamics of water molecules would be slower. We will explain this process in section 4.3.1. The significant changes in dynamics, for example in the hydrogen bond rate constants: k and k', are observable at the electric fields stronger than $\approx 0.05 \frac{\mathrm{V}}{\mathrm{\AA}}$, and this is almost the electric field that the water-E-field interaction energy exceeds $k_B T$.

We can also interpret the change in the number of hydrogen bonds by calculating the standard free energy, ΔG° of formation of an H-bond from the probability of bond formation. This probability is the total number of H bonds divided by the total *possible stable* number of H-bonds:

$$r = \frac{e^{-\beta \Delta G^{\circ}}}{e^{-\beta \Delta \mathrm{G}^{\circ}} + 1} \qquad 35$$

The maximum number of stable H-bonds is equal to 4. In Figure 20, we have shown the distribution of the number of hydrogen bonds; we see that the probability of having the 5th H-bond is very small. This is because the 5th bond is an unstable bifurcated bond that happens during a H-bond switching.[61] So, we set the maximum number of H-bonds to four and $r = \frac{n_{HB}}{4}$. The number of H-bonds for different E-fields are plotted in Figure 20, and the entropy of bond breaking can be calculated using the above-mentioned free energy: $S^{\circ} = -dG^{\circ}/dT$. Figure 22 shows the change of the entropy of the hydrogen bonding with the strength of the static electric field. The alignment of water molecules is not entropically favorable, since the entropy is decreasing under the static fields. We also observe that above the alignment is not energetically favorable either, so the alignment remains only under strong E-fields and relaxes rapidly after removing the E-field.

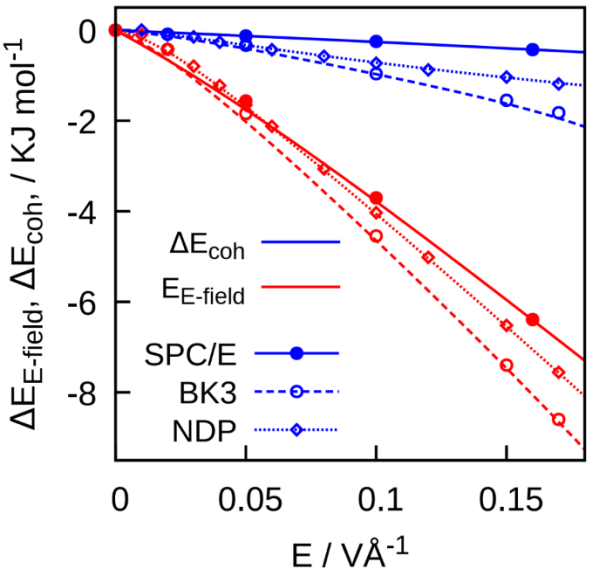

Figure 23. Changes in average cohesive and electric field energy of the system, $\langle \Delta E_{coh} \rangle$ and $\langle E_{field} \rangle$, with and electric field for various water models. For $E = 0$, $E_{coh}^{SPC/E} = -46.6\ kJ\ mol^{-1}$, $E_{coh}^{BK3} = -43.4\ kJ\ mol^{-1}$, and $E_{coh}^{SWM4-NDP} = -43.3\ kJ\ mol^{-1}$

4.3. Dynamics

4.3.1. H-bonds dynamics

In the Luzar and Chandler model,[51] see section 1.2.1, the hydrogen bonding and un-bonding states of a pair of molecules interconvert with each other with rate constants k and k' respectively. To measure the dynamics of H-bonding using the Luzar and Chandler model, and switching of H-bond dynamics using the phenomenological relation suggested in section 1.2.1 under the static E-fields, at first, we need to see how these models works in the presence of an electric field. In Figure 24 we have plotted the correlation functions for both models under the static field of $0.2\ V\text{Å}^{-1}$ and as we see, the correlation plots are good enough and we can calculate the rate constants from them.

Besides, under the strongest E-fields, the rotation of water molecules can only happen in the $x-y$ plane.[115]

In the next step, we look at the hydrogen bond rate constants. In the presence of the static E-fields weaker than $0.05\,V\text{Å}^{-1}$, the change in the rate constants of H-bond breaking, k, and reforming, k', is insignificant. This means that in this E-field range, and while water molecules show no resistance against alignment, the electric field imposes no limitation on the breaking and reforming of the hydrogen bonds.

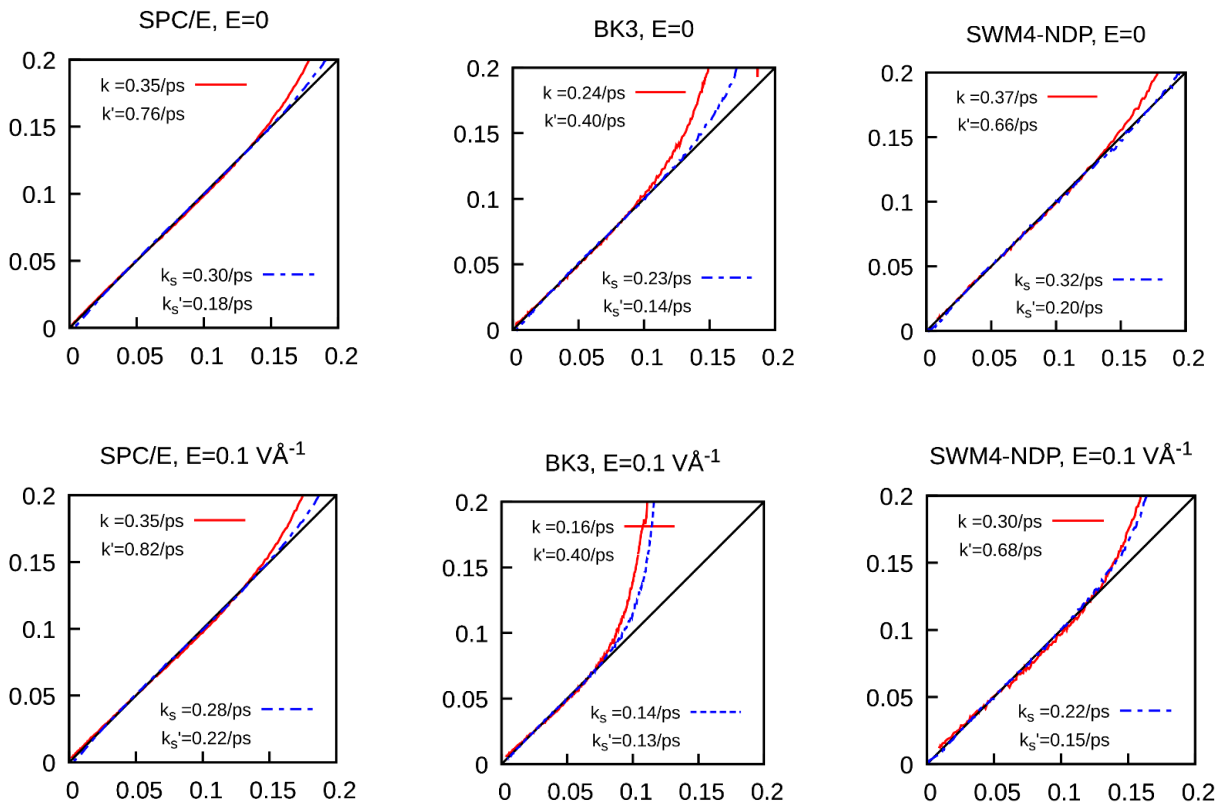

Figure 24. Hydrogen bond kinetics correlation plots. For classic model, red lines, showing the best fit between $k(t)$ (y-axis) and $k\,c(t)-k'n(t)$ (x-axis) to find the rate constantst k and k'. For the new model, the blue lines shows the best fit between $k_s(t)$ (y-axis) and $k_s\,c(t)-k_s'n_s(t)$ (x-axis) to find the a pair of rate constants k_s and k_s'.in SPC/E (left), BK3 (middle) and SWM4-NDP (right) for zero field (top) and $E=0.1\,V/\text{Å}$ (bottom).

The hydrogen bond lifetime highly depends on the temperature. Temperature determines how fast molecules librate and break the hydrogen bonds. But in this research, the temperature is kept constant, so the short time librations of molecules are mostly unchanged. The breaking of H-bonds due to the fast librations can be seen in the very short time, $< 300fs,$ behavior of $k(t)$ function in Figure 27. The continuous lifetime of a hydrogen bond depends highly on the librations of water molecules and can be calculated from $\tau_{cont}^{HB} = \frac{1}{k_{TST}}$. In Figure 27 we have also calculated τ_{cont}^{HB} and we show that the overall short time behavior of water molecules change less than 1% under the E-field of $0.2\ V/\text{Å}$ compared to zero field. This clearly shows that the ability of a strong E-field to limit the librations of the molecules cannot be the sole reason of the change in the dynamics of water under E-fields. This is because the internal E-field of the partial charges of water molecules is huge in a close distance, and the external E-fields that we apply are way weaker than these E-fields.[166]

The reason for the increasing the H-bond lifetime under static E-fields is the increase in the number of re-crossings per H-bond breakings, $1/\kappa$. In other words, under the E-fields, when a hydrogen bond breaks, there is a higher probability that the bond reforms, and a lower probability that the H-bond switches, as compared to no field, see Figure 27. The reason is that under the strong E-fields, finding a new nearby H-bond acceptor is more difficult for a hydrogen than under zero field. Hence, the broken bond reforms instead of switching. We will show this more specifically in section 4.3.3.

In Luzar's model, two dynamics with close specific times are distinguished: inside the first coordination shell, the rotation of water molecules determines the hydrogen bond kinetic rate constants k and k', and the diffusion of water molecules, with the characteristic time of τ_D, determines how fast water molecules exit the first shell after breaking the H-bond. The $k_{in}(t)$ function, eq. 11 measures the relaxation of H-bonds inside the first coordination shell and $k(t)$ measures the hydrogen bond dynamics in and out of the first coordination shell. To find the

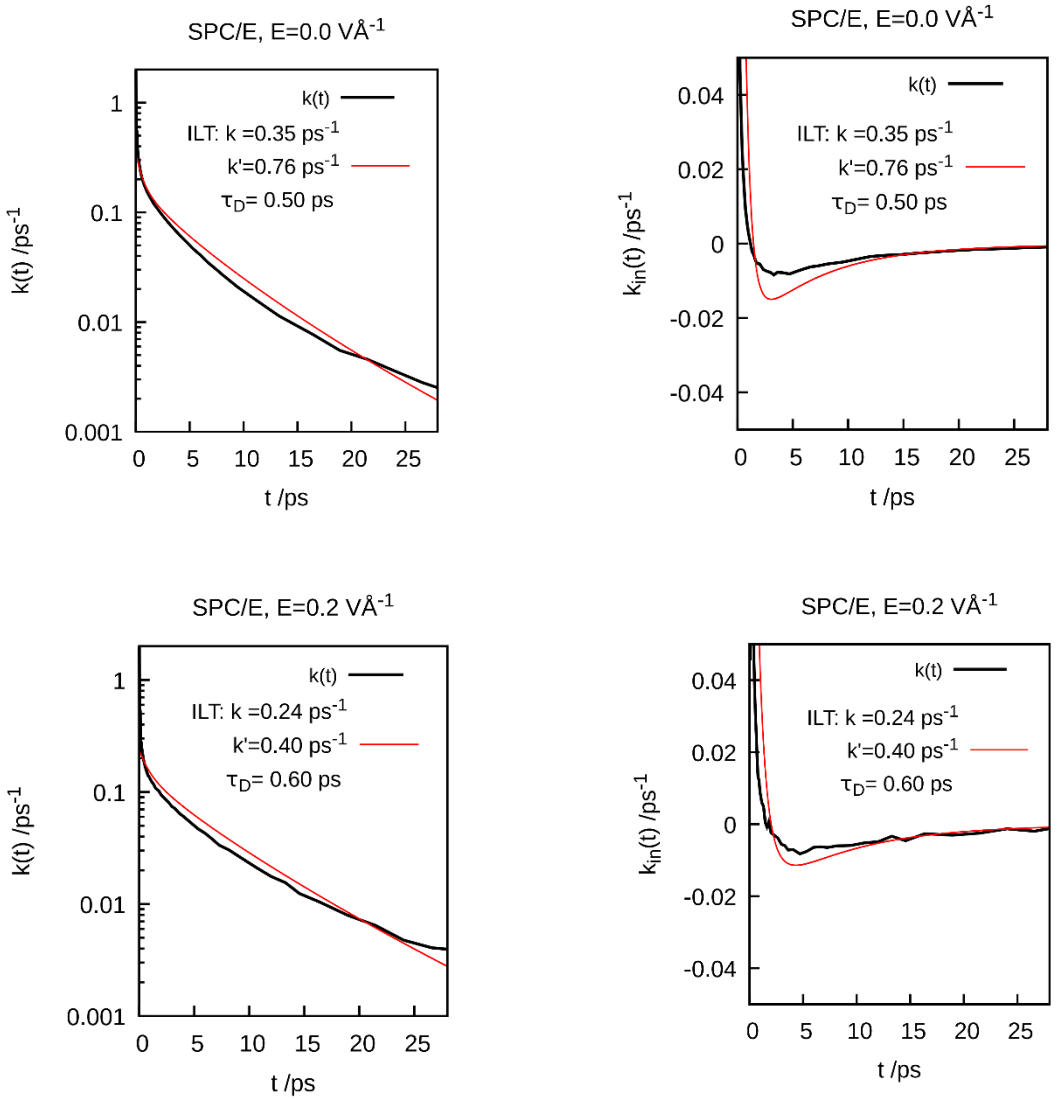

Figure 25. k(t) (left) and $k_{in}(t)$ (right) functions (black line) along with the analytic line (red line) calculated from eq. 10 and eq. 11 using the rate constants k and k' calculated from the correlation plots, Figure 24, and fitted the best value of τ_D. The qualitative agreement does exist between the model and the. The results for BK3 and SWM4-NDP water are in Appendix 6.

diffusion time, we need to try different τ_D in eq. 10 until we find the best value that fits $k(t)$ and $k_{in}(t)$ at the same time. These functions have been plotted in Figure 25 for a specific τ_D.

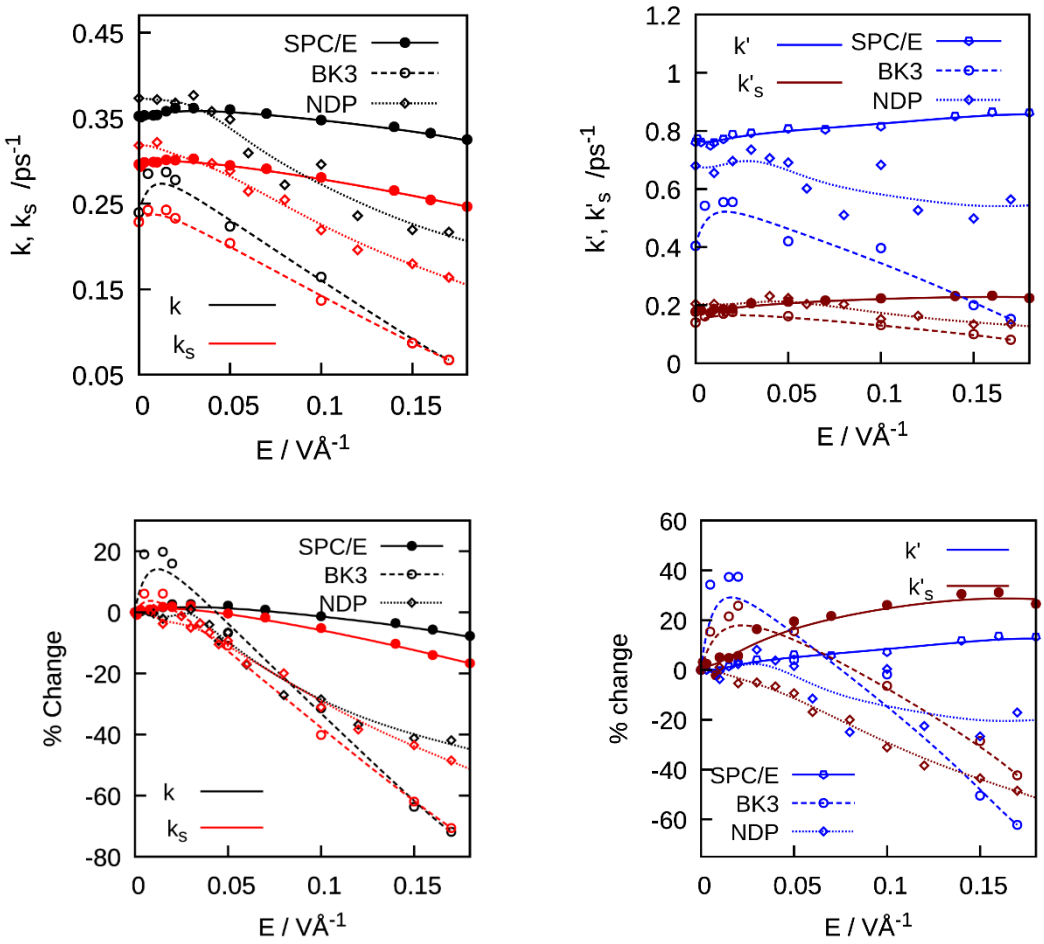

Figure 26. The rate constants of hydrogen bond breaking k and switching k_s (top, left), as well as the rates of H-bond reforming, k' and switching back k_s' (top, right) for three water models under electric fields ranging from 0 to $0.2\ V\text{Å}^{-1}$. Bottom panels: The percentual change of the same quantities. Lines are meant to guide the eye.

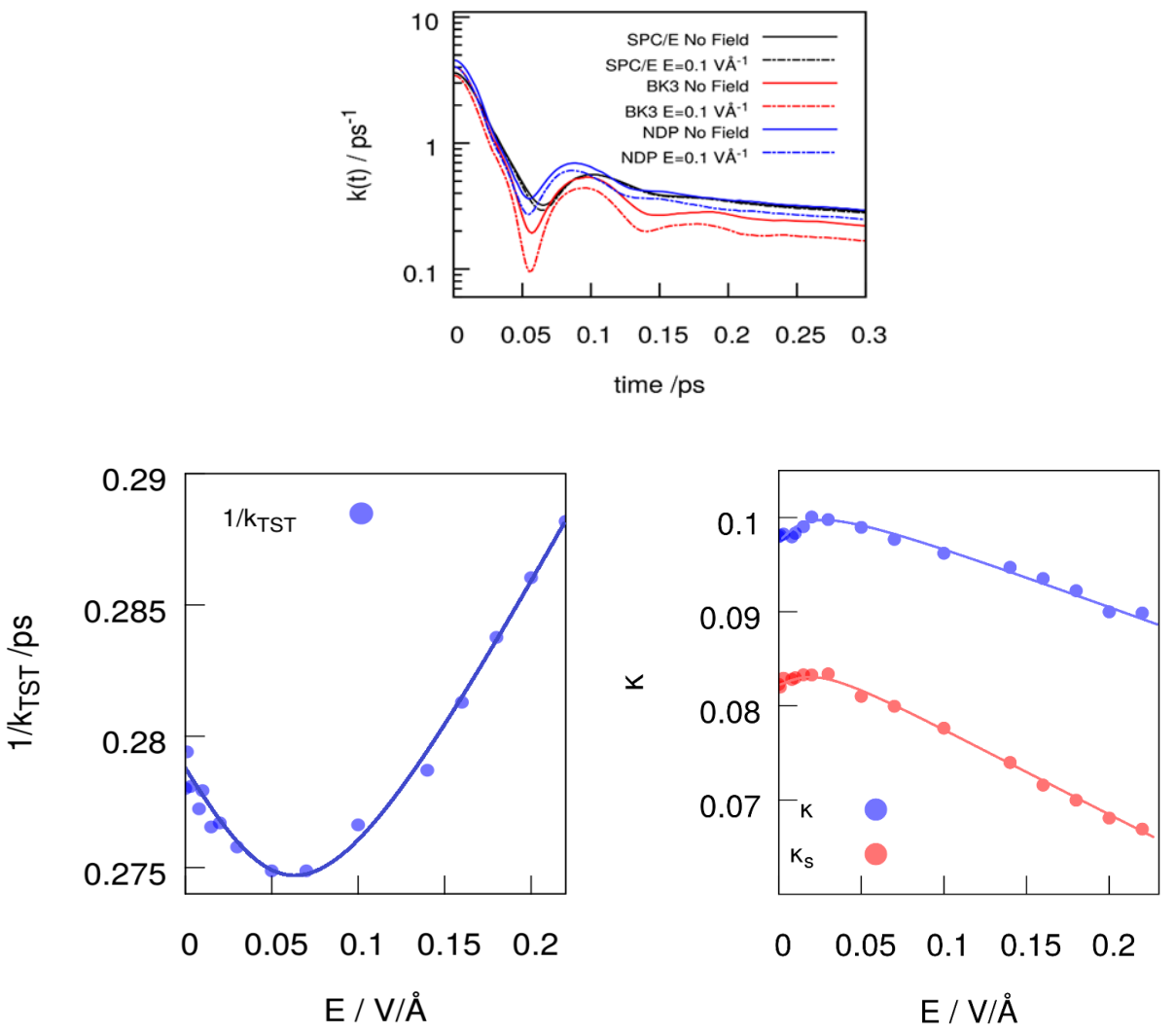

Figure 27. (Top) The transient time behavior of $k(t)$ under the different static E-fields. This plot shows that the librations of water molecules do not change under static E-fields. (Bottom left) the numeric value of $\tau_{cont}^{HB} = 1/k_{TST}$ versus E-fields. We still see minimum at around $0.05\ V/\text{Å}$, but the overall change is less than 4% between 0 to $0.2\ V/\text{Å}$. On the other hand, the transmission coefficient of breaking and switching a H-bond (Bottom right) decreases over 8% and 17%, respectively, in the same range of E-fields.

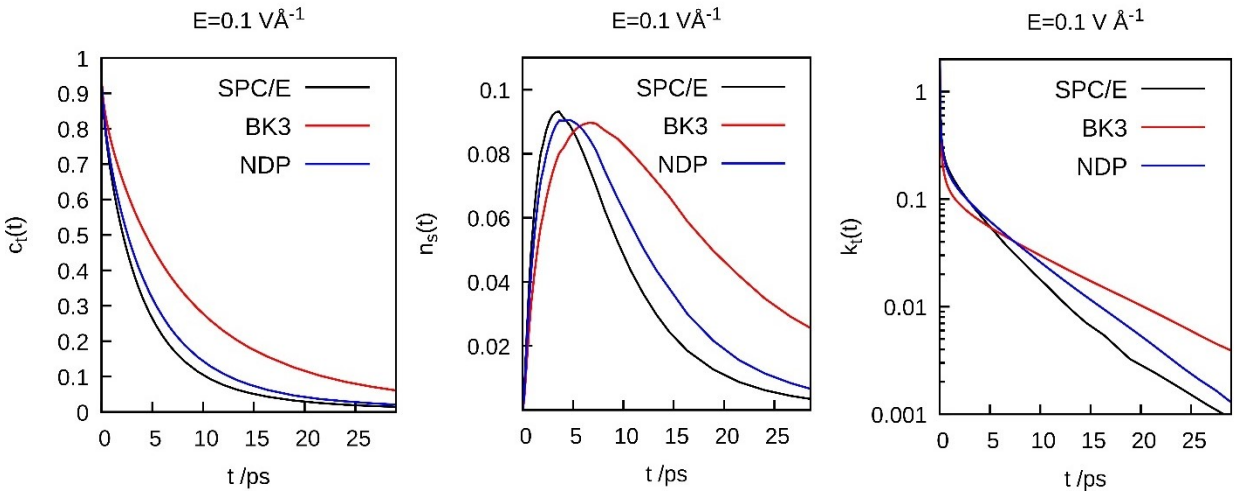

Figure 28. The hydrogen bond time correlation functions (from left to right) $c(t)$, $n(t)$, and $k(t) = -dc/dt$ for various water models $E = 0.1\ V/\text{Å}$.

In the diffusion part of Luzar's model, the diffusion constant is equal to $D_i = \tau_D^{-1} q_c^{-2}$, where $q_c = \frac{(6\pi^2)^{\frac{1}{3}}}{a}$ and $a \approx 1.5\ \text{Å}$ is the range of distances where a neighboring molecule may move without breaking a bond, and the index i denotes the inter-diffusion of a pair. For zero field, $\tau_D = 0.5\ ps$, and $D_i \approx 2.9 \times \frac{10^{-9} m^2}{s}$ which is close to the diffusion coefficient calculated from the mean square displacement,[85] $D = 2.59 \times \frac{10^{-9} m^2}{s}$.

From our structure analysis, we know that a should not change significantly under a DC E-field. Besides, there is no significant change in τ_D, so the change of D_i is insignificant under DC E-fields. The reason that τ_D does not change under the static E-fields, is the same as that of k_{TST}: the electric field due to the charges of nearby water molecules is much stronger than the applied external E-field, and the interactions that push a pair of molecules away after breaking of the H-bond is much stronger than the impact of the external E-field.

However, we will see in section 4.3.4 that the translational diffusion changes by almost 20% under the E-field range of $0 - 0.2\ V/\text{Å}$. We will show later in section 4.3.5 that the diffusion of the water molecules is correlated with the "residence time" that we explained in the Chapter 3.

4.3.2. Extended jump model

In this section, we consider the extended jump model (EJM) of Laage and Hynes[45] (see SI) under a range of static electric fields. According to this model, water molecules reorient through large amplitude jumps from one acceptor to another. This process is concerted with the diffusion of the new and the previous acceptor in and out of the first coordination shell of the donor. We do not observe fundamental changes in the jump mechanism (see SI) and can thus assume the model to remain valid even under strong electric fields.

In accord with the model, we calculated jump times τ_0, jump angles θ, and the frame re-orientation times τ^{frame}. Field effects influence the various elements of water re-orientation differently, see Figure 29. Under the strong E-field of $0.2\ V/\text{Å}$, the jump time, τ_0 increases by 27% for SPC/E, by about 90% for SWM4-NDP, and by a factor of almost 4 in BK3, compared to zero E-field.

The jump angle does not change significantly under E-fields, since it depends primarily on the local hydrogen bond network structure, which is hardly changed under electric fields (see Appendix 3).

Putting the jump time and the re-orientation angle during a H-bond switching jump in the Ivanov model:

$$\tau_n^{JM} = \tau_0 \left\{ 1 - \frac{1}{2n+1} \frac{\sin[\left(n+\frac{1}{2}\right)\Delta\theta]}{\sin(\frac{\Delta\theta}{2})} \right\} \quad 36$$

Here we only compare second order re-orientation time, τ_2^{JM}. Under a field of $0.2\, V\text{Å}^{-1}$, τ_2^{JM} changes by 40%, 380%, and 110% in SPC/E, BK3 and SWM4-NDP water models respectively. The significant reduction of the re-orientation is because the strong electric field almost completely blocks re-orientation against the electric field, and the re-orientation perpendicular to the E-field is slowed down due to the considerably longer waiting time, τ_0, for performing a switch.

The re-orientation of the frame of the jump is always slower than the re-orientation of the molecules, and it is not dependent on the H-bond switching, so it is less influenced under E-field. Considering the re-orientation of the frame, we can calculate the re-orientation time of a molecule from the extended jump model:[45,61]

$$\frac{1}{\tau_2^{EJM}} = \frac{1}{\tau_2^{JM}} + \frac{1}{\tau_2^{frame}} \quad 37$$

the results for τ_2^{EJM} are presented in Figure 29, showing a moderate change under E-field in all three water models. The difference between τ_2^{JM} and τ_2^{EJM} increases because despite the extensive slowing down of the H-bond switching, the molecules can still re-orient due to the re-orientation of the frame.

We can compare the model results by the direct calculation of the re-orientation time of the water dipole moment from the relaxation time of the following function:

$$C_2(t) = \langle P_2[\vec{u}(0).\vec{u}(t)]\rangle \qquad 38$$

where $\vec{u}$ is a vector attached to the molecule. The relaxation time of water dipole moment, means $\vec{u} = \vec{p}$, is τ_2^p and it is in qualitatively good agreement with τ_2^{EJM}, see Figure 29. On the other hand, the E-field imposes an anisotropy on the re-orientation of the molecules. When the molecules are aligned with the field, the molecules are relatively freer to re-orient around their dipole moment in a plane perpendicular to the E-filed direction. We can show this re-orientation with $\vec{u} = \vec{q}$ where $\vec{q}$ is a unit vector perpendicular to water's plane of symmetry. In Figure 29 we show that the re-orientation time τ_2^q agrees even better with the EJM model, and that is because the effect of the E-field on τ_2^q is mostly via reducing the H-bond switching rate, but τ_2^p is directly affected by the restrictions of the molecular re-orientation. The difference between τ_2^q

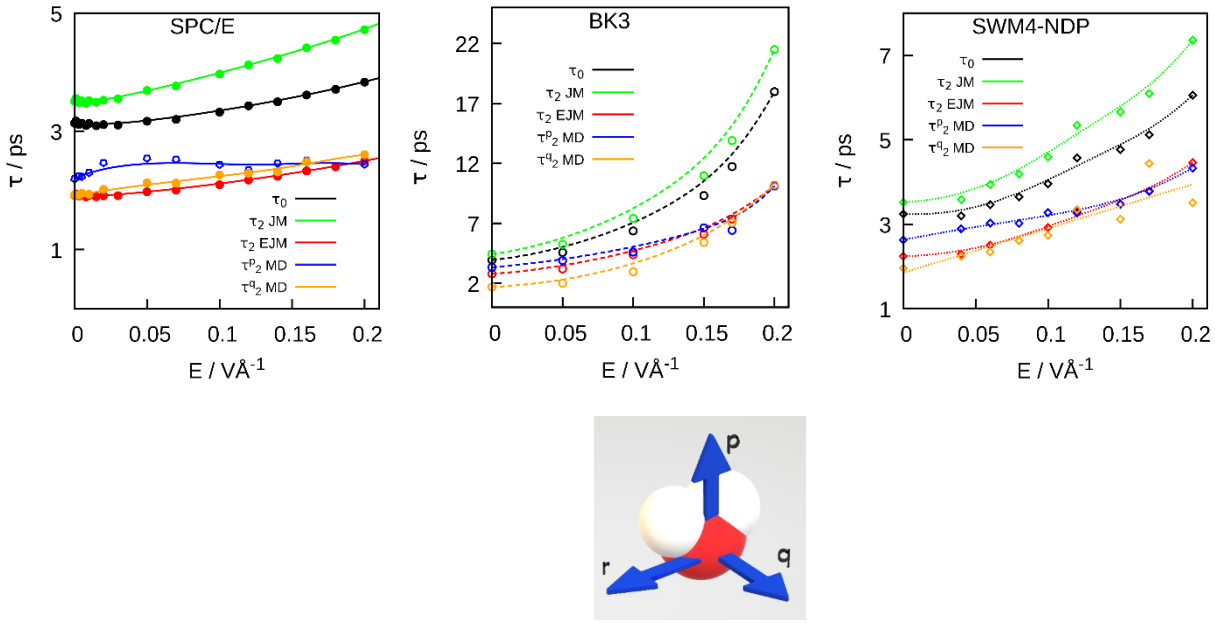

Figure 29. (Top)Field-dependence of jump time, τ_0, the second order re-orientation time from jump model, τ_2^{JM}, the second order re-orientational jump model from the extendend jump model, τ_2^{EJM} along with the re-orientation time calculated directly form molecular dynamic of $\vec{p}$ and $\vec{q}$ vector under E-fields for three water models . (Bottom) and a scheme defining the molecular vectors $\vec{p}$ and $\vec{q}$ for a water molecule.

and τ_2^p , however, diminishes under stronger E-fields since the partial freedom of the re-orientation in the plane perpendicular to the E-field is removed.

As we explained in the previous sections, the dynamics of water molecules are strongly related to the hydrogen bond switching. In this section, we study the extended jump model introduced by Laage and Hynes,[45] see section 1.2.2, under a range of static electric fields.

In section Appendix 3 we have plotted the trajectories and the H-bond angles in the frame of the central molecule, the previous, and the next H-bond acceptor for zero fields and 0.2 VÅ^{-1}. We can see from the plots that the jump mechanism does not change under even the strongest E-field. Again, the reason is that the electrical interactions of the molecules during an exchange of a hydrogen bond is way stronger than the external electric fields,[166] and the external electric field cannot affect the jump mechanism.

4.3.3. Switching correlation function

Under the static E-fields, the rate constants k and k_s decrease by near 13% and 20% respectively, so the difference between k and k_s increases, which means that the probability of finding a dangling hydrogen (a non-bonded hydrogen) should increase. So, the average number of H-bonds, on one hand should increase since the lifetime of a H-bond increases, and on the other hand, it should decrease since the dangling time increases. This is the reason that the number of H-bonds, Figure 20, does not change under the static E-fields.

The rate constant of other-way-bonding decreases by 20% under the strongest E-field. This is because switching the way of H-bonding, especially swapping the donor-acceptor role is more difficult under static E-fields.

As we mentioned before, $\frac{1}{k_s}$ and τ_0 are similar quantities that have been calculated using different methods. The value, $\frac{1}{k_s}$ depends less on the H-bond criteria. Please see Table 4 for details.

Table 4. The H-bond switching time calculated using jump time, τ_0, and from the reactive flux method, $\frac{1}{k_s}$ The H-bond criteria are explained in section 4.1.6. Regular: $H-\widehat{O^*}-O_a = 30^\circ, d_{O^*-Oa} < 3.5$ Å and $d_{H-O_a} < 2.4$ Å and restricted: $H-\widehat{O^*}-Oa = 30^\circ, d_{O^*-Oa} < 3.1$ Å and $d_{H-O_a} < 2.0$ Å.

Time (ps)	τ_0		$\frac{1}{k_s}$	
	Reg.	Restrct.	Reg.	Restrct.
No field	2.37	3.13	3.38	3.45
$0.2\ V\text{Å}^{-1}$	2.91	3.83	4.33	4.55

The differences in the final switching time values is that for calculating k_s we do not force the bond to be stable, and for calculating the jump time, τ_0, we do not force the previous pair to leave the first shell. Although, usually a stable state bond forms when the previous pair has left the first shell, but in some cases, like water under strong static E-fields, the average switching time is longer than the jump time. This is because when the bond between a pair of molecules breaks, leaving the first shell takes a long time. In short, a complete switch happens when the bond is switched, the previous pair leave, and the bond is stabilized.

$$\tau_{step} = \frac{1}{k_d} + \tau_{trans} + \tau_r \qquad 39$$

where τ_{trans} is the time that it takes until a non-stable bond becomes a stable bond, and τ_r is the time between switching the bond and the separation of the previous pair of water molecules.

$\frac{1}{k_d}$ is the switching time before the previous pair separate. So: $\frac{1}{k_s} = \frac{1}{k_d} + \tau_r$ and $\tau_0 = \frac{1}{k_d} + \tau_{trans}$. Please note that τ_{trans} and τ_r are independent times and each of them can be shorter or longer than the other one. Under the static E-fields, τ_r is longer than τ_{trans} and that is why $\frac{1}{k_s}$ is longer than τ_0.

4.3.4. Diffusion

Figure 30 shows the change of translational diffusion, D, calculated from mean square displacement, see section 24, under the applied static electric fields.[150] Within the E-field range of $0 - 0.2 V/\text{Å}$, the translational diffusion decreases by nearly 20%.

The trend is not the same for all three coordinates: the translational diffusion in the $x - y$ plane increases under the E-field range of $0 - 0.05\ V/\text{Å}$. This is because the alignment of water molecules linearly increases with the field, see Figure 11, so water molecules keep rotating and translating, but mostly in the x-y plane. As we explained in section 4.2, under fields stronger than $0.05\ V/\text{Å}$, the electric field limits even small re-orientations of water molecules, these re-orientations are necessary for breaking and exchanging H-bonds and diffusion of water molecules. So, fewer hydrogen bonds break, and the translational and rotational diffusion decrease under E-field stronger than $0.05\ V/\text{Å}$.

In the z direction, however, the translational diffusion decreases monotonically from zero field. Diffusion in the z direction and $x - y$ plane reduce by $\sim 36\%$ and $\sim 13\%$, respectively under the strongest E-fields compared to zero E-field. Jung *et al* [152] report that under static E-fields the

diffusion enhances in the z direction, but that probably happens at very low temperature,

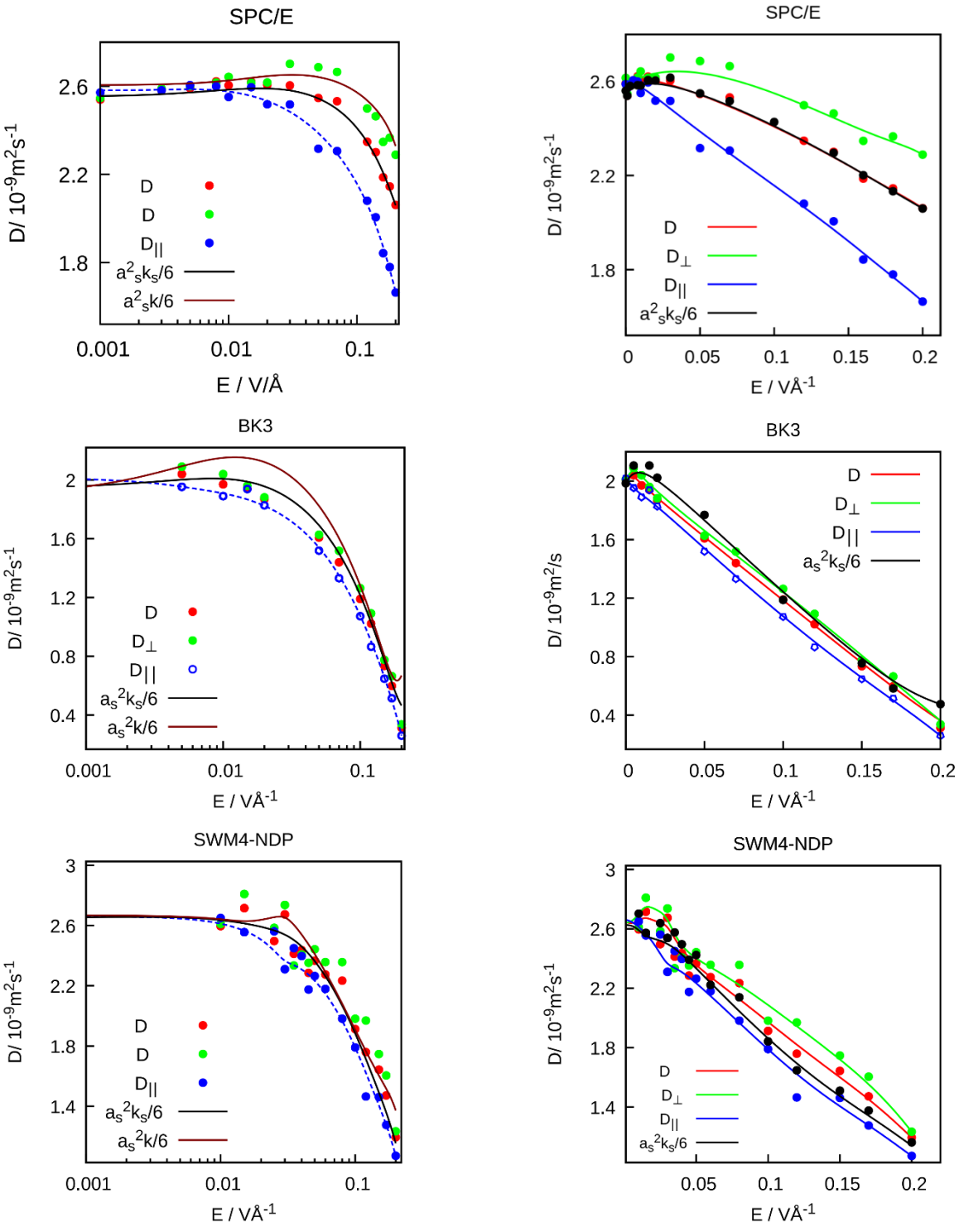

Figure 30. Isotropic diffusion coefficients D as well as the parallel $D_{\|}$ and perpendicular components $D_{\perp}$ of the diffusion tensor in SPC/E water (top) BK3 water (middle) and SWM4-NDP water(bottom). The left panels are semi-log plots to show the increase in $D_{\perp}$ in weak E-fields and right panels show the overall trend. The black line is the best fit of the overall diffusion using the H-bond switching as the random walk waiting time, eq. 26. Brown line is the same, but using the breaking rate constant, k to fit eq. 26.

-30 ℃ , and under very strong E-fields, near $0.5\ V/\text{Å}$.

The trends that we see for the diffusion coefficients and hydrogen bond rates are similar and we can assess our theory about the random walk of water molecules by hydrogen bond waiting time, see eq. 26. In section 4.3.1 we see that under static E-fields, the rate of H-bond breaking, k, is always bigger than the rate of H-bond switching, k_s. So, the rate limiting step in the diffusion of water molecules, se eq. 27 is the switching of H-bonds, so under static E-fields, $\tau_{step} = 1/k_s$.

We can find the best s_D value for the relation: $D = \frac{s_D^2 k_s}{6}$. The optimal value is $s_D = 2.27$ Å, which is close to the value that we found in the previous chapter, 2.4 Å and the two plots are in an excellent agreement over a wide range of applied DC E-fields. This is an interesting result indicating that the waiting time of the random walk diffusion of water molecules is the H-bond switching time.[67]

To conclude, the application of the static E-fields slows down the diffusion of molecules[40] but this slowing down is mostly because the molecules cannot switch their H-bonds.[167]

4.3.5. Roto-translational coupling

We can measure the rotation of water molecules by calculating the mean square rotation:[60]

$$MSR_i(t) = < \left(\phi_i(t) - \phi_i(0)\right)^2 > \qquad 40$$

where ϕ_i is the direction of the vector i which can be $\hat{p}$ or $\hat{q}$ or $\hat{r}$, see Figure 11. The rotational diffusion is the slope of $MSR(t)$:

$$R_i = \lim_{t\to\infty} \frac{\mathrm{MSR_i(t)}}{4\mathrm{t}} \qquad 41$$

and the overall R is $\sqrt{R_p^2 + R_q^2 + R_r^2}$. The rotational diffusion coefficients R_p, R_q, and R_r are not affected equally under the static E-fields. In Figure 31 we show that the application of the E-fields limits the rotation of water molecules up to nearly 60%. We observed in Figure 30 that the translation of water does not change up to this percent, so what happens to the roto-translation coupling of water molecules,[42,131] and what is the role of hydrogen bonding in that?

We show in the structure section that water molecules are more structured in the $x - y$ plane under E-fields stronger than $0.05\ V/\text{Å}$. Water molecules in this situation only can rotate around their $\hat{p}$ axis, and the translational diffusion of water is reduced less in the $x - y$ plane compared to the E-field direction, z. The rotation in this plane can be measured by R_{q_z}. In Figure 31 we see that the rotational diffusion of R_{q_z} is reduced by near 30%, much less than the overall R reduction. Since the molecules are mostly aligned to the E-field, the dipole vector, $\vec{p}$, cannot rotate against the E-field direction, so R_{p_x}, reduces dramatically under the E-fields.

Finally, we have shown the correlation between translational and rotational diffusion in Figure 31. We see that R_q and R_r are indeed correlated with the translational diffusion. The source of this diffusion is hydrogen bonding, since each translational step of a water molecules is accompanied with a rotation of the molecule and that happens every time that a hydrogen bond is switched.

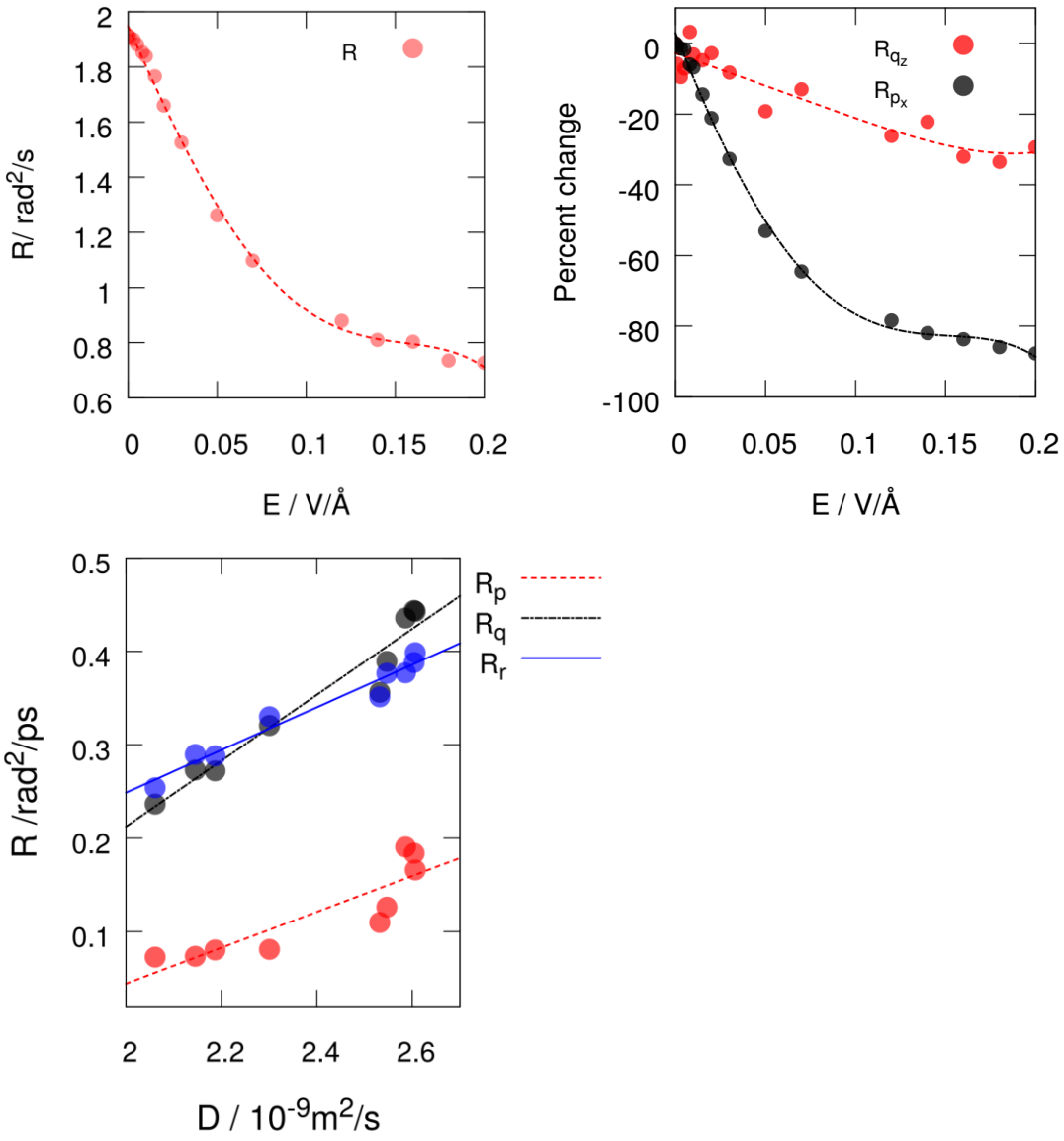

Figure 31. (top-left) The rotational diffusion is calculated using eq. 41. The difference in the trend of the rotational diffusion of the p, q, and r axes is due to the different effects of hydrogen bonding under the E-fields on those axes. (top-right) The percentage change of two different rotations of a water molecule. (bottom) The roto-translational coupling of water molecules under static E-fields. The correlation of R_q and R_r remains mostly unchanged with the alignment of water, since when the molecules are aligned with the field, the $\vec{q}$ and $\vec{r}$ vectors are parallel to the x-y plane, so their rotation and translation is less affected under the static E-fields.

Finally in Table 5 we compare the effect of polarizability on the change of the dynamic variables of water under E-fields. As we explained before, the interaction of BK3 water with the external E-field is much stronger than SWM4-NDP since a BK3 water molecule has three charge-on-

springs. So, under static E-fields, the H-bond rate constants and diffusion coefficient of BK3 water drop significantly under static E-fields, while the dynamic variables of swm4-NDP water change moderately.

Table 5. The effect of the polarizability on the water dynamics properties: rate constant of H-bond breaking, k, the rate constant of H-bond switching, k_s, the jump time, τ_0, and the translational diffusion coefficient, D.

	SPC/E no field	SPC/E $0.2\ V/\text{Å}$	BK3 No field	BK3 $0.1\ V/\text{Å}$
$k\ /ps^{-1}$	0.35	0.31	0.23	0.20
$k_s\ /ps^{-1}$	0.30	0.24	0.23	0.16
$\tau_0\ /ps$	3.14	3.83	3.93	6.03
$\frac{D}{10^{-9}m^2s^{-1}}$	2.59	2.06	2.01	1.0

4.4. Conclusion and Remarks

We applied a range of static electric fields on bulk water. First, we examined the change of structure of water by looking at different structure factors. We observe no significant change in the radial distribution function, oxygen triple angle distribution, q order parameter, and Q_6 second layer order parameter. We have also plotted the spatial distribution function of water molecules in the first and second coordination shell. These plots emphasize that the change of structure in the first shell is minor. In the second shell, however, we see a more directional distribution that is related to the hydrogen bond acceptors that have left the first shell but still have a chance to return to the first shell and re-form the hydrogen bond.

From the dynamics point of view, application of the static E-fields reduces the rate of hydrogen bond breaking and increases the rate of H-bond re-forming. This is because under strong static E-fields, it is harder for protons to go out of the H-bond cone and find a new acceptor. Instead, when a bond is broken due to the thermal fluctuations, the H-bond will reform faster. Because of the same reason, the hydrogen bond switching time $1/k_s$ and jump time, τ_0 increases. The H-bond switching time, $1/k_s$ increases more than the jump time, τ_0, since after breaking the H-bond diffusion of water molecules out of the first shell is slower under static E-fields.

At the same time, the translational and rotational diffusion coefficients decrease with different rates with the applied external electric field. Even under weak E-fields, the change of the rotational diffusion is significant, since water molecules' dipole moments cannot rotate against the field direction. Under the E-field range of 0 to $0.05\ V/\text{Å}$, the diffusion in the $x-y$ plane increases, but under the stronger E-fields, diffusion starts to slow down because the E-field limits the molecular re-orientations and switching the H-bonds even in the $x-y$ plane.

Chapter 5. **Water under Alternating Electric Field**

We have investigated the effect of an external alternating electric field on bulk water. The main question that we want to answer is that how the hydrogen bonds resist against the E-field imposed dipole re-orientation. We have assessed the hydrogen bond dynamics and water re-orientation models under a wide range of alternating electric field strengths and frequencies. We confirm that the change in the tetrahedral structure of water is limited, while the dynamics of hydrogen bond switching, and diffusion change significantly. We have also studied the effects of E-field-generated rotation on the translation and rotation of water molecules, and we show that these kinetics are all controlled by the hydrogen bonding.

The change of the properties of water under alternating electric fields has been the subject of many experimental and modeling studies due to its considerable applications in science and technology.[48,168–171] English and Waldon have reviewed a wide range of these applications in a nice review.[15]

Water molecules establish a high number of hydrogen bonds in liquid, that is 3.6 on average[172] at room temperature, and hence form a loose tetrahedral structure.[1] The hydrogen bonding of water molecules is highly dynamic, and the bonds change every few picoseconds.[118,173] A water molecule has a net dipole moment (experiment: $2.95\ D$,[95] SPC/E: 2.35 D[76]), and application of an external electric field imposes a torque on the water dipole moment to align it with the field direction.

$$\vec{\boldsymbol{\tau}} = \vec{\boldsymbol{p}} \times \vec{\boldsymbol{E}} \qquad 42$$

where $\vec{\boldsymbol{\tau}}$ is the torque imposed by the electric field, $\vec{\boldsymbol{E}}$, on water dipole moment, $\vec{\boldsymbol{p}}$. The water molecules feel external electric field in different situations, either when an electromagnetic wave is passed through water,[20] or the strong electric fields around hydrated ions,[174] inside nano-tubes[36] or nano-surface.[175] In a simple example, an alternating electric current, (AC), can generate an external alternating electric field inside a capacitor, so in this paper, we call an alternating electric field an AC field. The goal of this research is studying the effect of the alternation of the external E-field on the hydrogen bond dynamics of bulk water. We simulate bulk water under a sinusoidal one dimensional electric field:

$$E = E_0 \sin(2\pi\upsilon t) \qquad 43$$

where E_0 is the amplitude of the E-field of the order of $10^{-9}\ V/\text{Å}$, and υ is the frequency of the field of the order of GHz, t is a time of the order of picoseconds. We use the range of E_0 strengths of $0 - 0.2\ V/\text{Å}$, since a water molecule dissociates at higher E-fields,[32] and the range of frequencies below $1\ THz$ since for the faster frequencies, we would need to take the intra-molecular vibrations into account, which is not possible using classical molecular dynamics simulation, while the hydrogen bond dynamics of water molecules happen in order of picosecond time range.

The behavior of water under static and alternating electric fields has enjoyed enormous attention in the past 20 years, see Chapter 1, but our focus in this research is on hydrogen bonding. First, we study the structure of water under AC E-fields and show like many other researchers,[150,176] that the structural changes are not significant. Then we show that AC E-fields can indeed

influence the hydrogen bond dynamics. Finally, we apply our suggested analysis in Chapter 3 to understand the translation and rotation of water molecules under AC E-fields.

5.1. Results and Discussion

5.1.1. Structure

An alternating external electric field continuously re-orients the water molecules. However, since hydrogen bonds are directional, the rotation a water molecule involves breaking existing H-bonds and forming new ones. We will study how much the breaking and re-forming of H-bonds speeds up under the AC E-fields in the next sections, but first, we want to know to what extent water molecules follow the oscillation of the E-field, and how much the H-bond network is affected by following the E-field reversion.

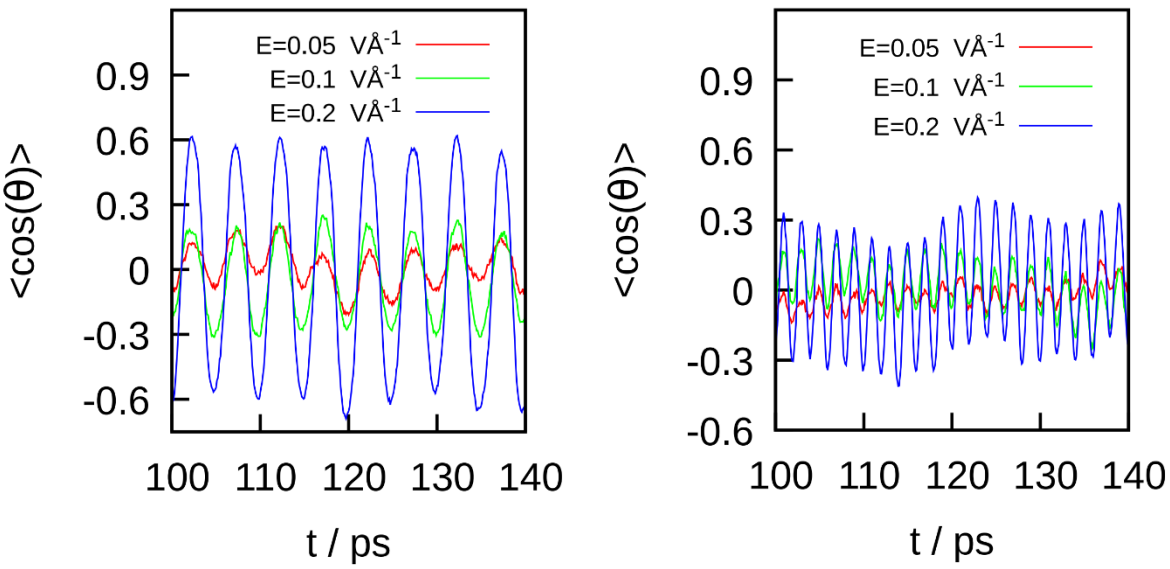

Figure 32. The average alignment of water molecules $< cos(\alpha) >$ where α is the angle of the water dipole moment with the field direction in a range of E_0 strengths and two frequencies: 100GHz (left) and 200GHz (right). When the E-field is strong enough, on average, water molecules follow the field, even at the increased frequencies.

Figure 32 shows the average alignment of water molecules to the E-field direction, z :

$$\overrightarrow{P_z} = \sum_{all\ molecules} \vec{p}_z \qquad 44$$

where p_z is the dipole moment of one water molecule and $\vec{P}$ is the overall dipole moment of the system. We see that for all the fields stronger than $0.12\ V/\text{Å}$, the system generally follows the field oscillations. We should note that when the average direction of the water molecules, $< \cos(\alpha) >$ follows the E-field reversion, it does not mean than all the water molecules are actually aligned with the field.[10] The re-orientation with the field reversal is a collective behavior, and in the section 5.1.7 we show that the rotation of water molecules can be much slower than the field reversal. Despite the average alignment at any moment, the distribution of the molecular alignments broadens as we increase the frequency, see Figure 33. This means that the direction of water molecules is less correlated to each other, and we show this again in Figure 38. The average alignment of the system decreases with the frequency, for instance, when $E_0 = 0.2\ V/\text{Å}$, the maximum of the average alignment is near 60% under $200GHz$ and less than 40% under 500GHz AC E-field. This makes sense since the water molecules are H-bonded to the neighboring molecules, and the faster the field is reversed, the harder it is for water dipoles to re-orient with the field.[10,41]

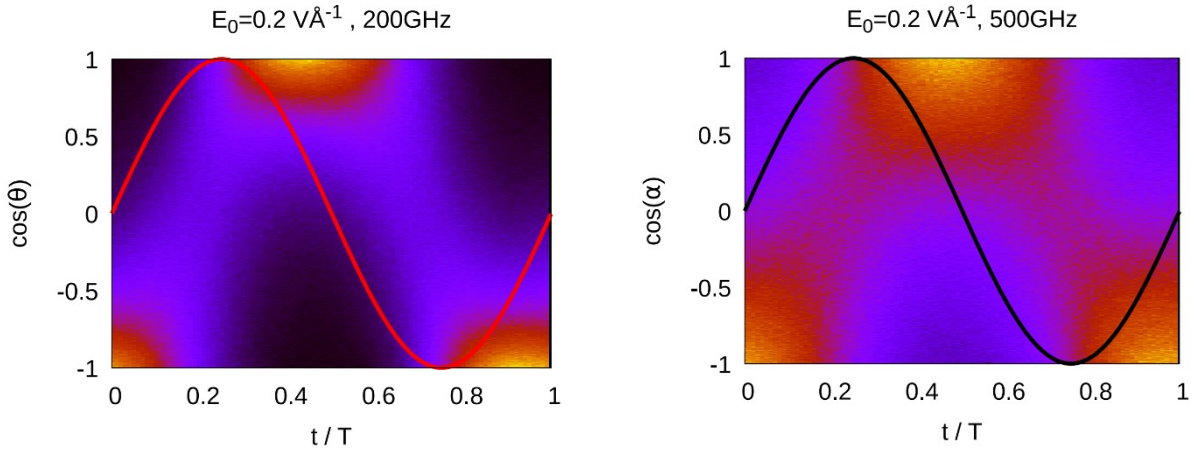

Figure 33. The distribution of the angle of water molecule with the E-field direction, z, per each moment of the period time. The time is normalized by T, the period time, and $x = time/T$. The solid lines are just $sin(t/T)$ indicating the phase of the E-field. The distribution is apparently narrower under $200\ GHz$. We use the different colors for the solid lines to show it better. The retardation of the maximum alignment, shown as the brightest point, relative to the E-field maximum at $x = 0.25$ is observable in both figures.

The reversal of the net dipole moment, however, is with a delay. In Figure 33 we have plotted the distribution of the water dipole moment angles with the field direction. In this picture, we see that the maximum alignment, corresponding to the brightest points, happens at a time later than when the E-field is maximum, i. e. $t = T/4$, where T is the oscillation period time. The average of the alignment at each time t/T is also plotted in Figure 34 showing that the maximum alignment is at around $T/2$ for all the systems, but the maximum of the average alignment decreases with the E-field frequency.

The retardation is because the molecules need time to break their hydrogen bonds and align with the E-field. For instance, when $E = E_0 \sin\left(\frac{\pi}{2}\right)$, it has been the $T/2$ of time that the upward E-field has been applied to the system, although with a variable strength, and the molecules still try to re-arrange their network and align with the E-field in this time. After $T/2$, the E-field is reversed, and the molecules begin adapting to the new E-field direction.

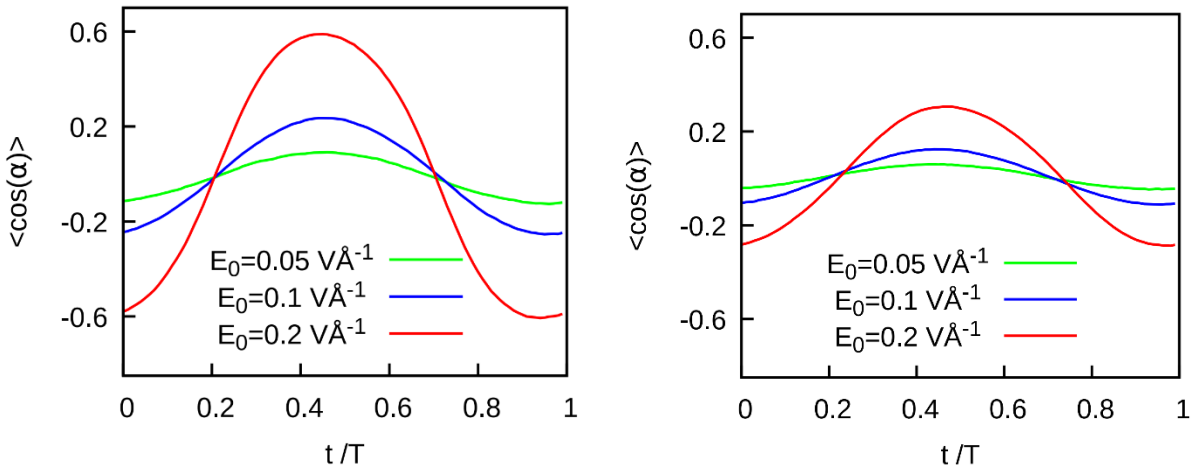

Figure 34. The average of the distribution of the molecular alignment (left) $200GHz$ and (right) 500GHz, in every moment of the phase, $time/T$ where T is the period of the AC field. Increasing the E-field strength and the frequency increases and decreases the maximum alignment respectively.

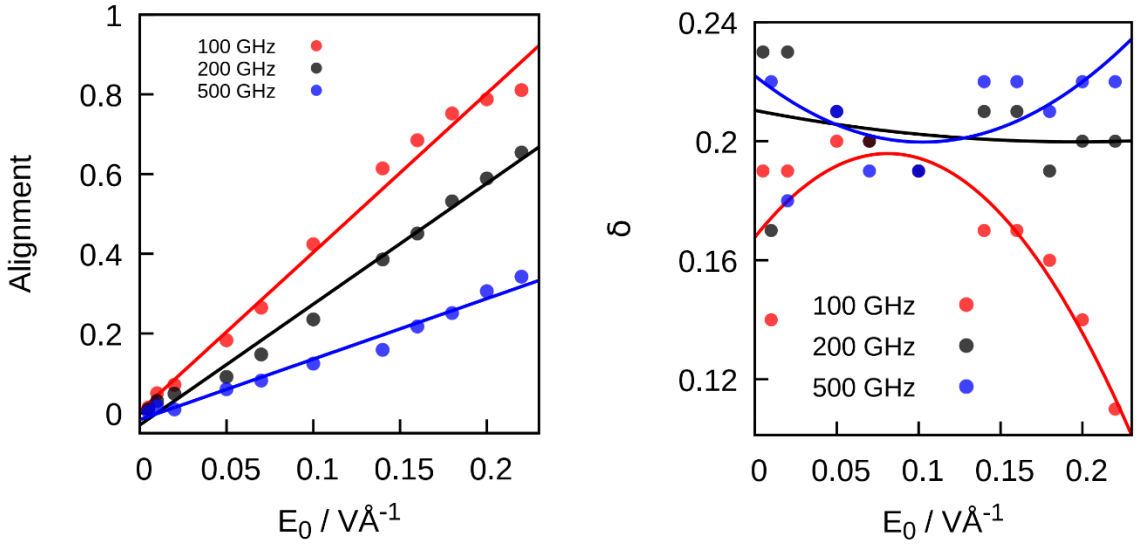

Figure 35. (left) the maximum of the average alignment of water molecules in Figure 33 The maximum alignment increases with E_0 and decreases with frequency. (right) The maximum alignment happens with a delay time after the maximum E-field at (T/4). In this figure we have plotted the $\delta = \frac{t_{max}}{T} - 0.25$ where

t_max is the time of maximum alignment in Figure 34. There is almost no trend in the retardation phase under AC E-fields. The lines are eye guides.

We have plotted the retardation versus frequency in Figure 35. The trend of the delay time of $100\ GHz$ is clear, indicating that the delay time increases with E-field until $0.05\ V\text{Å}^{-1}$ and then decreases.

5.1.2. Number of hydrogen bonds

For studying the hydrogen bonding behavior of water molecules under AC fields, the first property to observe is the average number of hydrogen bonds. We use the geometric H-bond criteria[120] explained in section 4.1.6.

As the re-orientation of water molecules forces the molecules to break their H-bond and form new ones, the average number of hydrogen bonds explains how much the AC field disconnects a water molecule from its neighbors, and how freely the molecule can rotate. Figure 36 shows that the change in the average number of hydrogen bonds is insignificant.[150] The percentage of the changes depends on the E_0 and the frequency, but the maximum change is below 4%. Please note that this small change is when the field is extremely strong and the E-field direction is reversed as fast as every $\frac{T_{500GHz}}{2} = 1\ ps$, and around 60% of water molecules follow the E-field reversion. This is a very interesting phenomenon since the water molecules cannot re-orient without breaking their H-bonds,[120] and the conservation of the number of H-bonds with such fast re-orientations means that the H-bonds break and form almost with the same rate. In section 5.1.6 we measure these rates and, we show they are indeed close to each other.

The conservation of the number of hydrogen bonds and coordination number suggests that the tetrahedral structure of water is not influenced under the AC fields. In other words, the very fast

and strong applied E-field, fails to disrupt the hydrogen bond structure. As Laage and Hynes showed,[45] the switching of a H-bond happens in a short time about $\approx 70fs$, which is much shorter than the waiting time between sequential switches, $\approx 3ps$, so increasing the number of switches under AC E-fields does not influence the structure of water dramatically. We will assess this hypothesis in detail in the next sections, but before, we need to confirm the preservation of the structure of water.

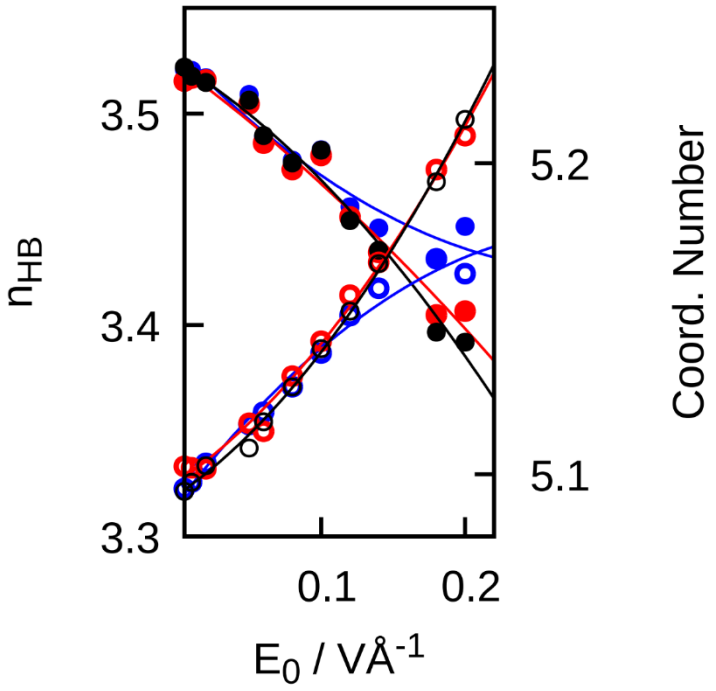

Figure 36. The number of H-bonds per water molecules (filled circles-left axis) and the coordination number, means the number of neighboring molecules within 3.5 Å of the central molecule (hollow circles-right axis) under the different AC E-fields for SPC/E water. For both sets, blue is 100GHz, red is 200GHz, and black is 500GHz. Application of the AC E-fields decreases the number of H-bonds, but the percentage of the change under such high intensity and fast reversing alternating E-fields is less than 6%.

In Figure 36 we have also plotted the coordination number, n_c, under the different AC E-fields. Decreasing the number of H-bonds allows the molecules to come closer to each other, and we see that the coordination number has slightly increased. n_c is the summation of the H-bonded and non-H-bonded molecules inside the first coordination shell, so the number of interstitial water molecules $n_c - n_{HB}$ increases with increasing E_0 and ν, but only by 6% and this increase is not observable in the interstitial peak of oxygen triplet angle distribution.

5.1.3. Radial distribution functions and tetrahedral order parameters

We have assessed the most important structural functions to see how they change with the different E-field strengths and frequencies. The first function to observe is the radial distribution function, RDF or $g(r)$. Figure 37 shows that the change in RDF is insignificant.[150] The position of the peaks is remained constant,[176] but the height of the peaks has slightly reduced under the strong E-fields. If the system had really disturbed under the such E-fields, we would see a bigger reduction of the peaks, and/or we would see a shift in them, while none of them really happens.

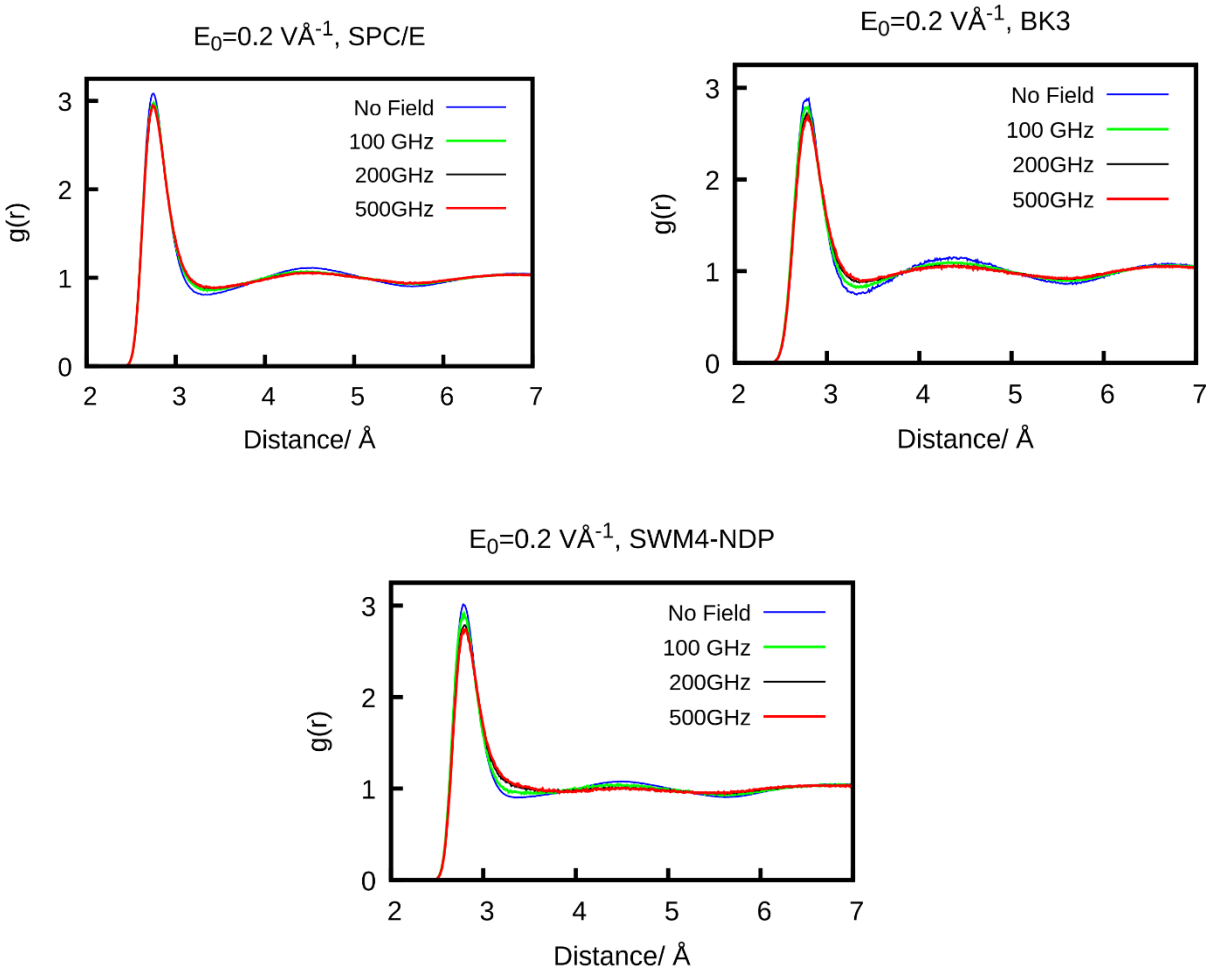

Figure 37. The radial distribution function of water under different AC field frequencies with a very strong E-field strength of $0.2\ V/\text{Å}$ *for SPC/E (top left), BK3 (top right), and SWM4-NDP water models (bottom). The difference between the height and the position of the peaks for the different frequencies is small.*

The radial distribution function only specifies how radially layered is the structure of water around a central molecule, and the spatial position of the adjacent molecules is averaged out. The oxygen triplet angle, $O-O-O$ function measures the tetrahderality of the system by calculating the angle that two nearest molecules make with the central molecule.[27] The first big hump of $O-O-O$ is related to the tetrahedrality, and the second peak is related to the interstitial non-H-bonded water molecules. The change in the main peak is less than 10% which is indeed small under such strong and fast changing E-fields. Apparently, there is a less than a

10% change[177] in the tetrahedrality of water under an extreme E-field: $E_0 = \frac{0.2V}{\text{Å}}, \nu = 500\ GHz$, compared to zero E-field.

Table 6. The tetrahedral order parameter, q and the second coordination shell order parameter, Q_6 under different AC-fields.

Frequency/ GHz	E-field/ $V/\text{Å}$	q	q_6
	0	0.63	0.21
100	0.1	0.62	0.21
	0.2	0.61	0.21
200	0.1	0.62	0.21
	0.2	0.60	0.21
500	0.1	0.61	0.21
	0.2	0.60	0.21

We also calculate the tetrahedrality as a number from the tetrahedral order parameter from the eq. 30.[156] Besides, we have studied the second coordination orientational order, Q_6, see ref. [158], to see the relation of the tetrahedral structures to each other in the second shell. The results of q and Q_6 are presented in Table 6 showing that the change in the tetrahedrality is insignificant under the AC E-fields.

5.1.4. Average Orientational Correlations

When water molecules are forced to re-orient by the E-field, the amount of the re-orientation of each water molecule depends on how the molecule is H-bonded to the neighboring molecule. The g_{dd} function, see section 4.1.4 measures how entangled is a water molecule with the neighboring molecules.[161] Figure 38 shows that the relative alignment of the neighboring

molecules decreases with the frequency. The maximum angular correlation is under $100GHz$, where the dynamics is slowest, and E-field aligns the molecules.

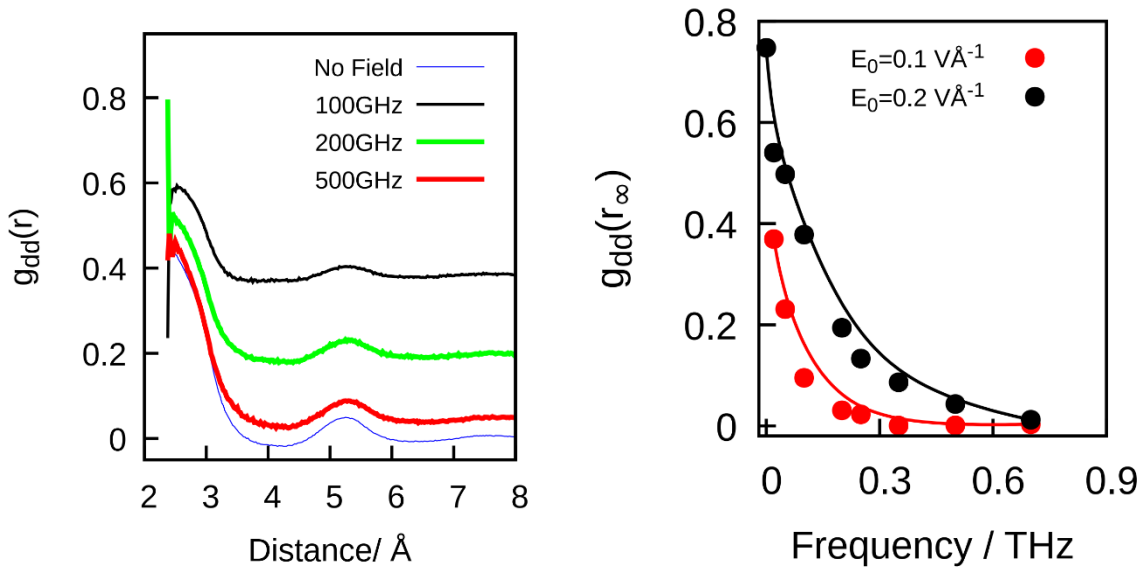

Figure 38. (left) The relative alignment of water molecules, $g_{dd}(r)$ under $E_0 = 0.2\ \frac{V}{Å}$ for different frequencies. Application of the E-field aligns the adjacent molecules, but increasing the frequency, decreases this alignment since the nearby molecules cannot rotate with the same rate, because they have different H-bonding states. (right) The ultimate value of the $g_{dd}(r)$ at a long enough distance (10 Å). Like many other plots, we see a sharp decrease in the relative alignment of water molecules, indicating that despite maintaining the structure, at a long distance, there is more chaos in bulk water under the fast reversing AC E-fields.

Under low frequencies like $100GHz$, increasing the E-field strength enhances the average alignment, and the second peak of $g_{dd}(r)$, which we explained in section 4.1.4, vanishes. Under high frequency E-fields, since the H-bonds break in a much higher rate, the average mutual alignment decreases, and the second peak is more observable. In Figure 38- right, we have also plotted the long-distance angular correlation of water molecules. This figure shows that the collective behavior of water molecules in the long distance sharply decreases until the frequency of near $200\ GHz$.

So, the above results prove that the directional structure changes moderately while the radial structure remains mostly unchanged.[41,178]

5.1.5. Re-orientation of water molecules and Extended Jump model under AC E-fields

When it comes to the rotation of water molecules, the very first method for measuring the rotation time is the Extended Jump Model (EJM) introduced by Laage and Hynes,[45,61] that we explained in the section 1.2.2. The main elements of the EJM model are the waiting time in between of the H-bond switches, τ_0, the average angle of the water re-orientation during a H-bond switch, and the rotation of the switching frame.

We have calculated the changes of each EJM element under the different AC E-fields.[179] The waiting time, τ_0, is calculated from a Stable State Picture, SSP, measuring the time between when the donated hydrogen is stably bonded to the first acceptor, and when it is stably H-bonded the second one. The stable H-bonds are identified using geometrically stricter criteria: $d_{O^*-O_a} < 3.1\text{Å}$, and $d_{H^*-O_b} < 2.0$ and $H\widehat{-O^*-O_a} = 20^\circ$, and the waiting time is calculated from eq. 13. The waiting times have been plotted for the different E_0 strengths in Figure 39. This figure clearly shows that τ_0 changes significantly with E_0.[42,52,180] The reduction of the waiting time in between of H-bond switching shows that the rotation of the water molecules is significantly faster under AC fields. In Figure 39 we see that the difference between the jump time, τ_0, and the reorientation time, τ_2, reduces with increasing the E-field strength, that is because the re-

orientation angle increases with E-field strength under the alternating E-field, see Figure 40, and that decreases the angular factor in Ivanov model in eq. 15.

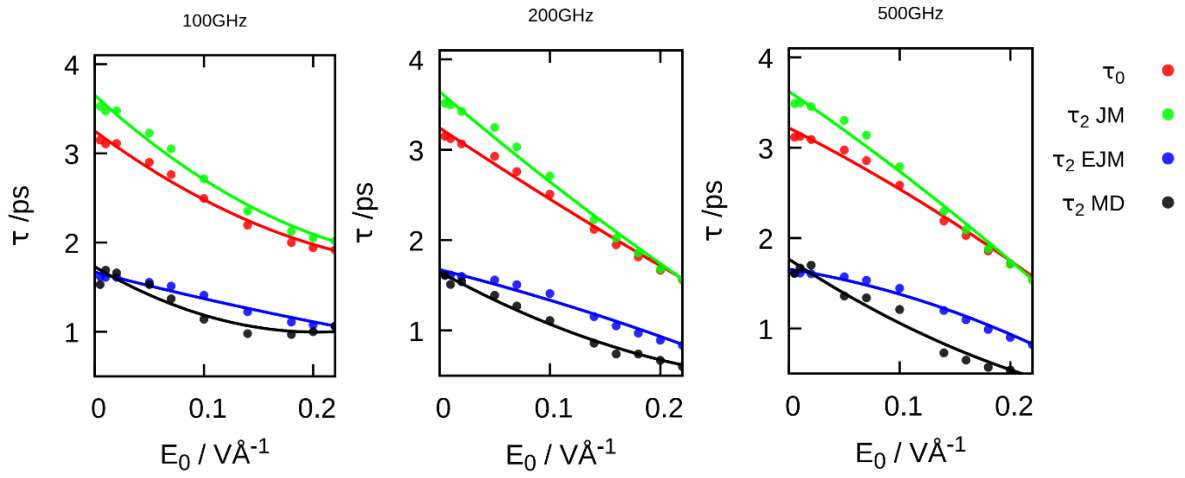

Figure 39. The jump and extended jump model for the reorientation time of water molecules under the different E_0 strengths and frequencies.[61]

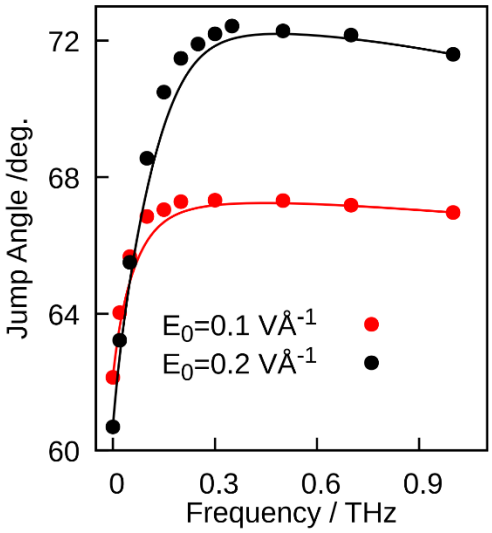

Figure 40. The jump angle, which is the average re-orientation angle of water molecules during a H-bond stable to stable switching. Increasing the E-field strength and frequency increases the jump angle.

In Figure 41 we show the effect of the frequency on τ_0. There is a sharp decrease of τ_0 with the frequency before $200\ GHz$ and after that τ_0 increases a little bit. This is very puzzling behavior, indicating that before $200GHz$, the water molecules speed up switching their H-bond acceptor as the E-field reversion forces them to re-orient. Under the faster frequencies, the waiting time for a switch increases, which means that it takes more time for the molecule to find a new acceptor and to form a stable H-bond. Besides, the average jump angle, shown in Figure 40, increase up to 20% when $E_0 = \ 0.2\ V/\text{Å}$ and at around $\nu = 300\ GHz$, while the trend is similar to the trend of H-bond dynamics.

Finally, we compare the rotation time calculated from the EJM under the AC fields with the direct calculation of the relaxation time of the orientational correlation function,[61] see eq. 16. The results in Figure 41 show that there is a good agreement between the EJM model (blue points) prediction of rotation time and the rotation time calculated directly from MD simulations (black points).

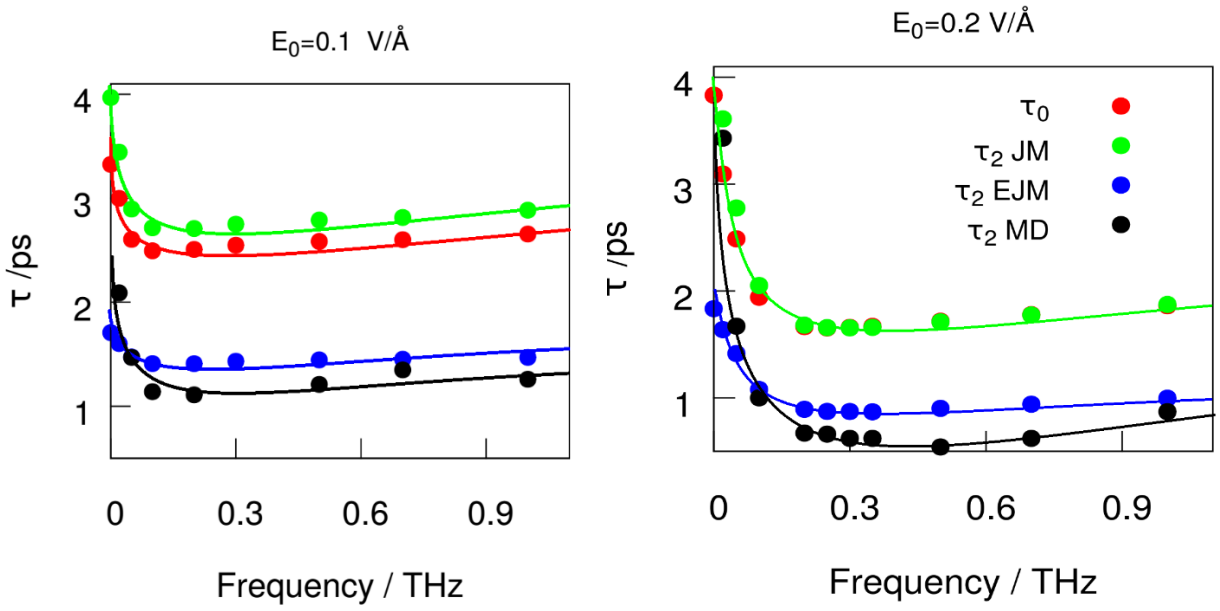

Figure 41. The change in the JM and EJM re-orientation time, τ_2, under AC E-fields, and comparing them with the MD results. There is a minimum in all of them at around $200GHz$. We will show in the next sections that these minimums are related to the response of the H-bond dynamics of the molecules to the E-field induced re-orientation.

5.1.6. Hydrogen Bonding kinetics

In this section, we calculate the hydrogen bond dynamics and the influence of a wide range of AC E-fields on the H-bonding rate constants. The classic model of hydrogen bonding, introduced by Luzar and Chandler[181] is the first tool that we use for measuring the hydrogen bond lifetime.[179,182] We explained this model in section 1.2.1.

In the first step, we assess if this phenomenological model works under AC E-fields. We have plotted the correlation functions along the calculated rates for some E_0 and frequencies in Figure 42, and we see that under all the E-fields, this relation works very well, so the resulting rate constants are reliable measures of the dynamics of H-bonding in AC field.

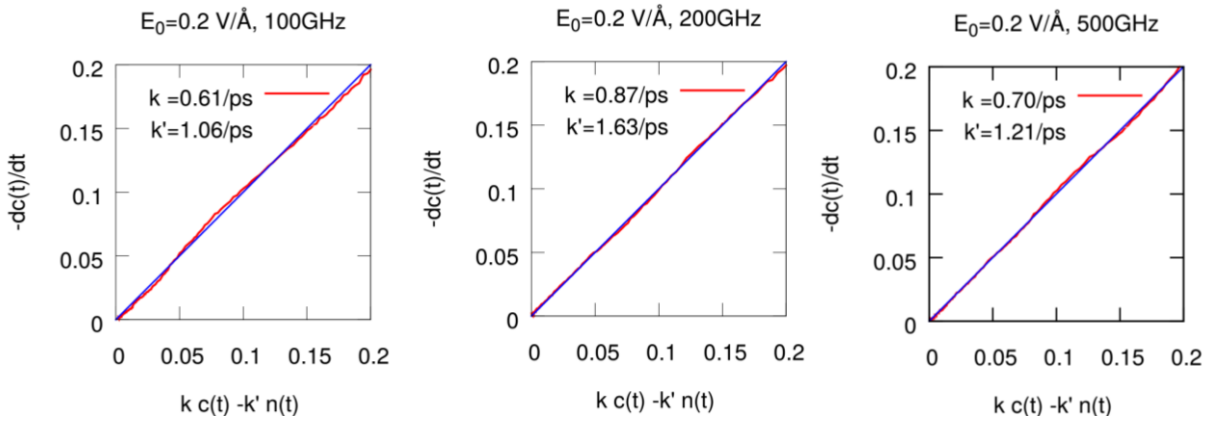

Figure 42. The correlation between the left and the right side of eq. 8, and the best pair of k and k'. We chose our highest E_0 to show that the phenomenological relation does not break even under such a strong E-field and when the field direction is changing so fast.

In the next step we study the trend of the hydrogen bond rate constants, k, for the different frequencies for under $E_0 = 0.1\, V\text{Å}^{-1}$ in Figure 43. The H-bond breaking rate constant, k, increases significantly with frequency before $200GHz$. There is maximum at around $200GHz$ for the H-bond breaking rate, k, in Figure 43, and we will talk about this maximum shortly.

In Figure 43, we also show the results of the H-bond switching rate constants, k_s. All these rates are calculated from the good correlation plots. The trend of all the rate constants with frequency is the same: a sharp increase until around $200GHz$ and then a moderate decrease until $1\ THz$.

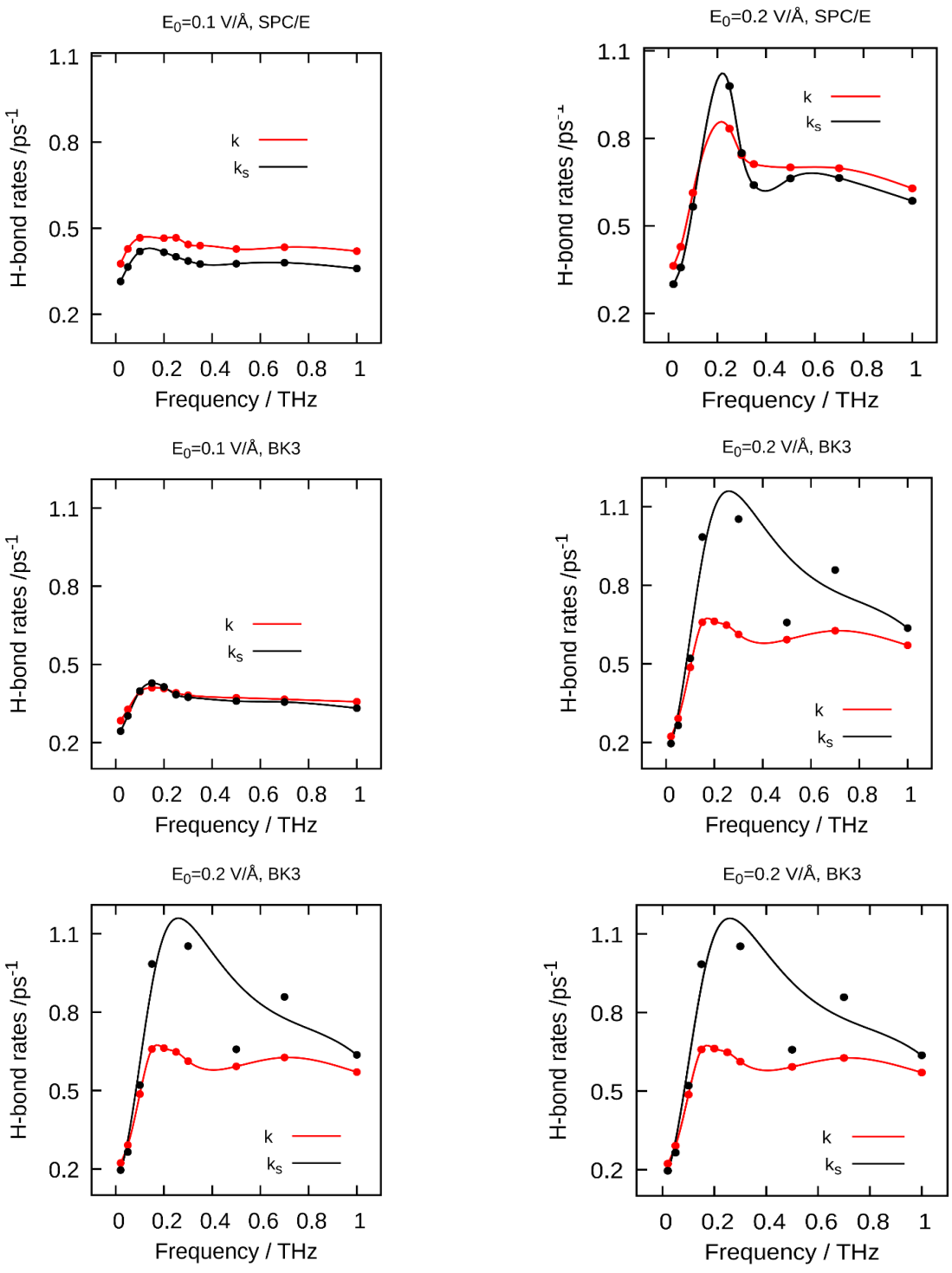

Figure 43. The different rates constants of hydrogen bonding from the methods that we presented in this report for two different E_0 strengths versus frequencies. All the rates constants are calculated from the correlation plots, the application of the AC field may interrupt the first order kinetics and make the correlation plots non-linear only in a few cases of k_s which we explain later. We have eliminated those numbers from data set before plotting them in this figure. Still almost all the rates constants show a maximum in the $200\ GHz$.

When increasing the frequency increases the H-bond rate, it means that the dynamics of water molecules can adapt itself with the faster E-field inversion. In other words, water molecules are ready to re-orient after $T/2$ with no resistance.

The resistance happens when the molecules cannot respond to the E-field reversal. As we explained in Chapter 3, the process of H-bond breaking and switching, consists of several re-forming and switching back, in other words, when a H-bond breaks, it can have two destinations: switching the acceptor (Large Jump Model) or re-forming (Luzar and Chandler model). The longer the H-bond lives, the higher the probability for a switch to happen and the lower the probability for a re-form to happen. Increasing the E-field frequency, forces the molecules to switch their H-bond faster. When $T/2$ is so short, the duration of E-field is not long enough to force the molecules to do a switch, so the E-field is left behind and the lifetime of the H-bond increases. Under stronger E-fields, increasing the H-bond breaking rates can happen until faster frequencies, and the peak in Figure 43 shifts to the right.

Figure 44 shows the relation of $\frac{1}{k_s}$ and $\frac{T}{2}$: as long as $\frac{T}{2}$ is smaller than $\frac{1}{k_s}$, the faster E-field results in faster H-bond dynamics. But when $\frac{T}{2}$ becomes smaller than $\frac{1}{k_s}$, the higher the frequency is, the longer is the switching time. The frequency in which $\frac{1}{k_s} \sim \frac{T}{2}$ happens is around 150 GHz, and it means that the H-bond survives during a half-period.

Imagine that a bond is formed when the E-field direction is $-z$. When the E-field direction changes, during a period of $T/2$ the E-field remains in $+z$ direction and tries to re-orient the

molecules and break the H-bond, but if $\frac{1}{k_s} > \frac{T}{2}$ the E-field, on average, fails to break the bond in this time. The water molecule simply needs more time to break and form a new H-bond. After $t > T/2$, the E-field is reversed, so there is less pressure on the bond to break. In this situation, the higher frequency means the shorter frustrated time, means the longer switching time.[42,179] Therefore, the H-bond characteristic times: $\frac{1}{k}$, $\frac{1}{k_s}$ and the waiting time, τ_0, increase after around

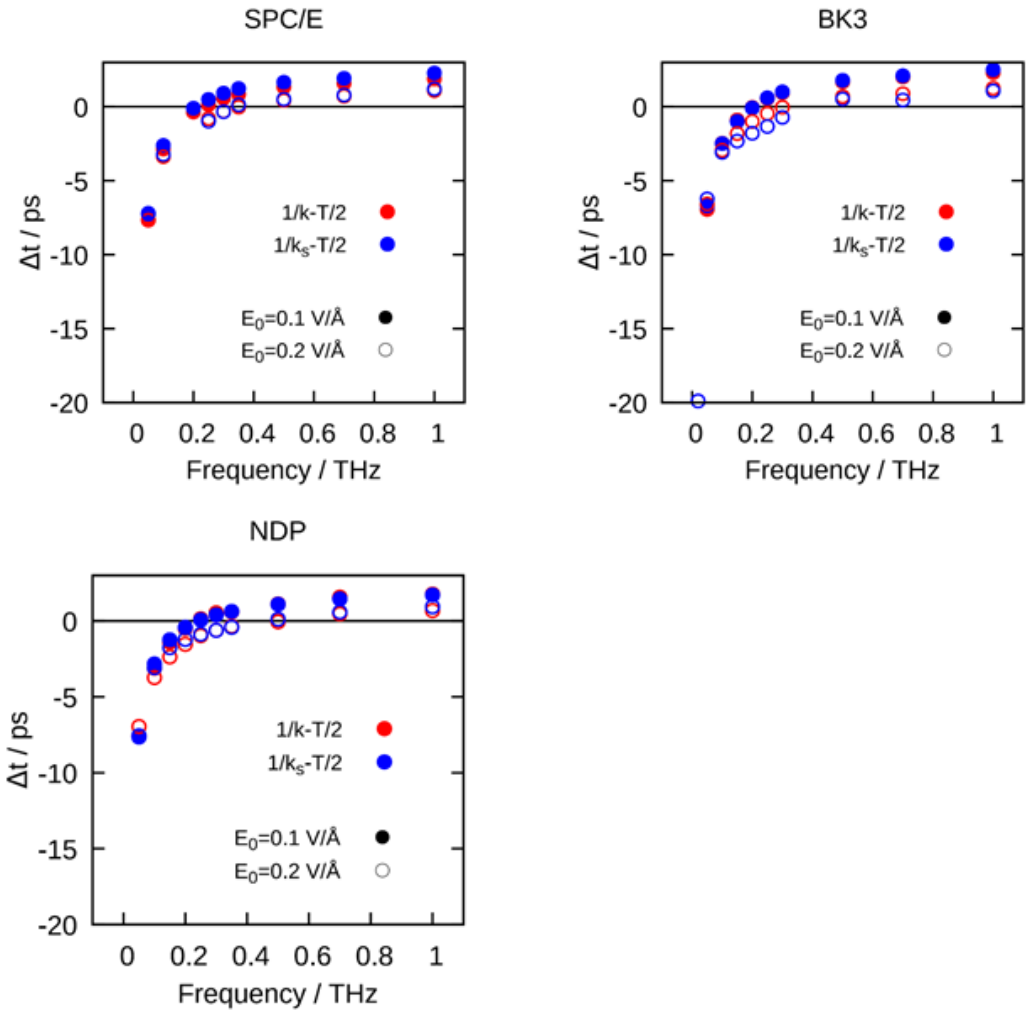

Figure 44. The relation of Δt, which is the time difference between AC field half period time, $\frac{T}{2}$, and H-bond switching time, $1/k_s$, or H-bond breaking time $1/k$, and the E-field frequency. When the hydrogen bond breaking time is smaller than the half period, means $\Delta t < 0$, the higher E-field frequency results in a higher H-bond breaking rate, and we have faster dynamics. But when the half period is shorter than $1/k$, the water dynamics cannot follow the E-field reversal, and the breaking of hydrogen bond slows down with frequency, see Figure 43.

$200GHz$. This critical frequency increases slightly to around $300\,GHz$ for polarizable water models, but the overall trend is the same for BK3 and SWM4-NDP water models.

To sum up, the H-bonds have an inherent *"response time"* that is a characteristic of water molecules to switch their H-bond and the water molecules cannot respond to the external E-field faster.

Table 7. The different H-bond breaking rate constants, k, H-bond switching rate constant, k_s, and the diffusion step time, τ_{step} switching time (eq. 27), for three frequencies for SPC/E water.

Frequency	$\frac{T}{2}\,(ps)$	E_0	$\tau_{step}(ps)$	$\frac{1}{k(ps)}$	$\frac{1}{k_s(ps)}$
Zero E-field			1.13	2.83	3.38
100	5	$0.1\,V/\text{Å}$	1.01	2.14	2.38
		$0.2\,V/\text{Å}$	0.93	1.63	1.77
200	2.5	$0.1\,V/\text{Å}$	1.01	2.14	2.40
		$0.2\,V/\text{Å}$	0.83	1.14	0.97
500	1	$0.1\,V/\text{Å}$	1.02	2.33	2.65
		$0.2\,V/\text{Å}$	0.81	1.43	1.51

5.1.7. Diffusion

Translational Diffusion:

The straightforward effect of the change of the dynamics of water under AC fields is the change in the translational and rotational diffusion.[20,21] We showed in the previous section that the application of the AC E-field does not change the number of hydrogen bonds. However, the dynamics of water molecules are much faster under AC fields. In this section, we show that while each water molecule is still connected with the neighboring molecules, the faster H-bond dynamics results in a faster diffusion of water molecules.

We calculate the translational diffusion from the slope of the mean square displacement (MSD), see section 2.2. The 3-dimensional diffusion coefficient and the diffusion coefficient in the z direction have been plotted in Figure 45 for different E-fields and frequencies. As we expected, the diffusion coefficient increases with the E-field strengths at all measured frequencies. On the other hand, for the same E_0, the diffusion coefficient increases with frequency until around 200 GHz, and then slightly decreases.

We explain in Chapter 3 that the diffusion of water has a complex behavior which depends on several parameters. In short, a water molecule first needs to switch its H-bond acceptor, then leave the previous partner and transfer to the H-bonding area of the new acceptor. Application of the E-field influences these steps differently, but the main change is related to the H-bond lifetime. We showed in the previous section that there is a sharp increase in k before around $200\ GHz$, and a moderate decrease until $1000\ GHz$. We see almost the same trend in the diffusion rate in Figure 45. When the H-bond switches, the next step is the separation of the water molecules away from each other, which is τ_D or τ_r time. Since the calculation of τ_r is more

accurate we have plotted that in Figure 44-right, showing that the diffusion time is a little

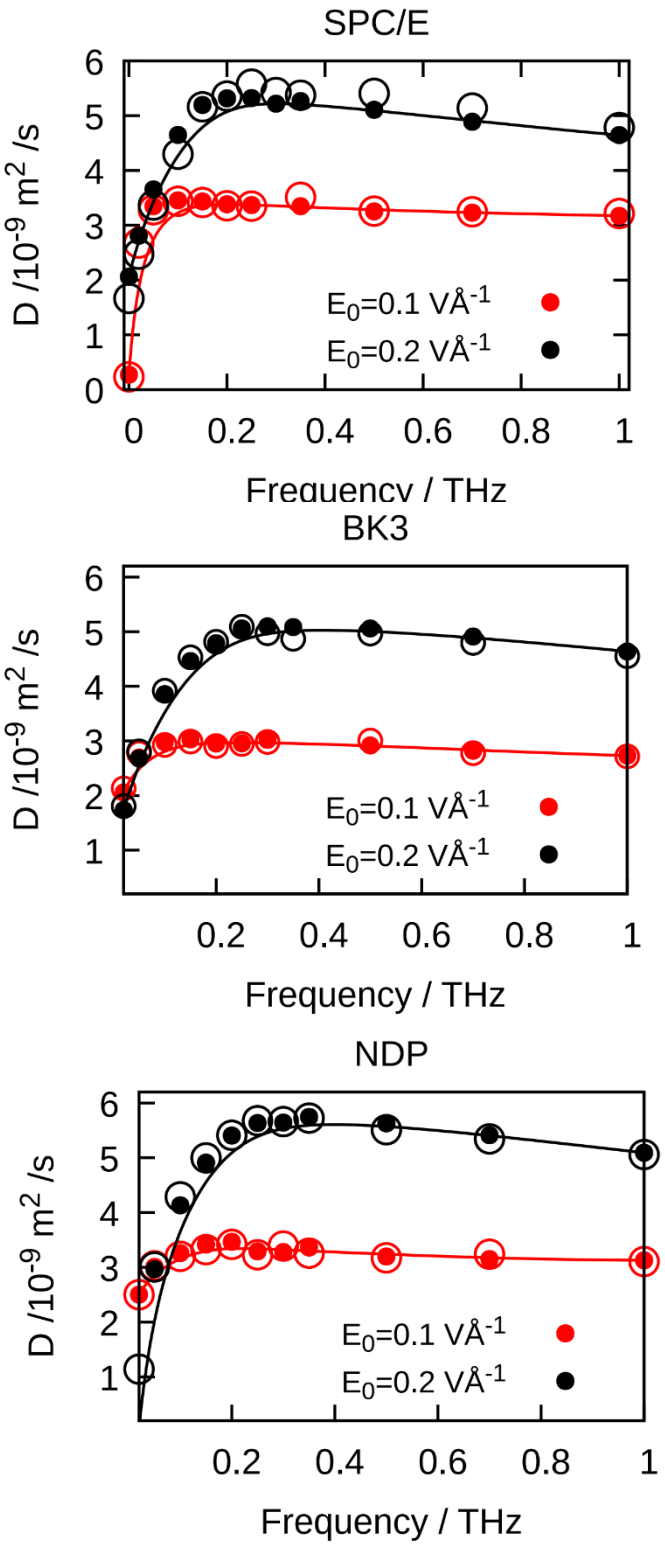

Figure 45. Translational diffusion for two E_0 strengths for a range of frequencies for SPC/E (top left) BK3 (top right) and SWM4-NDP water model (bottom). The filled circles and lines are for overall 3D diffusion coefficient, and the thin lines and hollow circle are for D_z. Diffusion has the same trend as the H-bond rates constants has, and we showed in section 4.3.4 the diffusion is highly correlated to the H-bonding. The diffusion in z direction follows the same trend.

decreasing with frequency, that makes the rise and fall of the diffusion coefficient less sharp than that of k_s. For instance, at $E_0 = \frac{0.1V}{A}$, the diffusion coefficient decreases by near 8% from its maximum at near $150\,GHz$ to $1\,THz$, while the k_s decreases 14% in the same range of frequencies.[150]

In Chapter 3, we suggested a step time τ_{step}, which is the average waiting time before one diffusional random walk step. In Figure 43 we reported the H-bond rate constants, k and k_s. Unlike under static E-fields, the breaking of the H-bond, with resident time $\frac{1}{k} + \tau_D$ is the rate limiting step under AC E-fields, so the step time is equal to the residence time, $\tau_{step} = \frac{1}{k} + \tau_D$. The diffusion coefficient and the residence time are included in the diffusion versus τ_{step} time in Figure 45 .

Our diffusion results for SPC/E water is in excellent agreement with *ab-initio* simulation done by Futera and English[40] both in trend and values, indicating the current results are independent of the choice of water model.

Rotational Diffusion

We calculate the rotational diffusion using the method explained by Mazza *et al*[60,183]:

$$D_{R_p} = \lim_{t\to\infty} \frac{1}{4t} < \left|\overrightarrow{\phi_p}(t) - \overrightarrow{\phi_p}(0)\right| >$$

where $\overrightarrow{\phi_p}(t)$ is the rotation vector of the dipole moment vector, p, using the right hand rule for rotation. The rotational diffusion, as well as translational diffusion, depends highly on the H-bond dynamics.[71] Here we see again that the trend of the change of rotational diffusion is very similar

to the trend in the H-bonding dynamics. The reason is simple: when the H-bonds switch faster, the water molecules can travel and rotate freer.[177]

In Figure 46 we also show the rotation of the dipole moment, $\vec{p}$ of a molecule in x, y, z directions. Please note that R_{p_x} measures how fast the dipole moment rotates in the $y-z$ plane, and so on. In both plots in Figure 46 the R_{p_x} and R_{p_y} have the same value, and are greater than R_{p_z} which show that AC E-field mostly increases the up-down rotation. The rotation of molecules inside $x-y$ plane increases monotonically until around $200\,GHz$ and after that it mostly remains constant.

We showed that the structure and the number of hydrogen bonds of a water molecule do not change much under AC E-fields. We also showed in Figure 38 that the angular correlation of the neighboring molecules reduces drastically under AC E-fields.

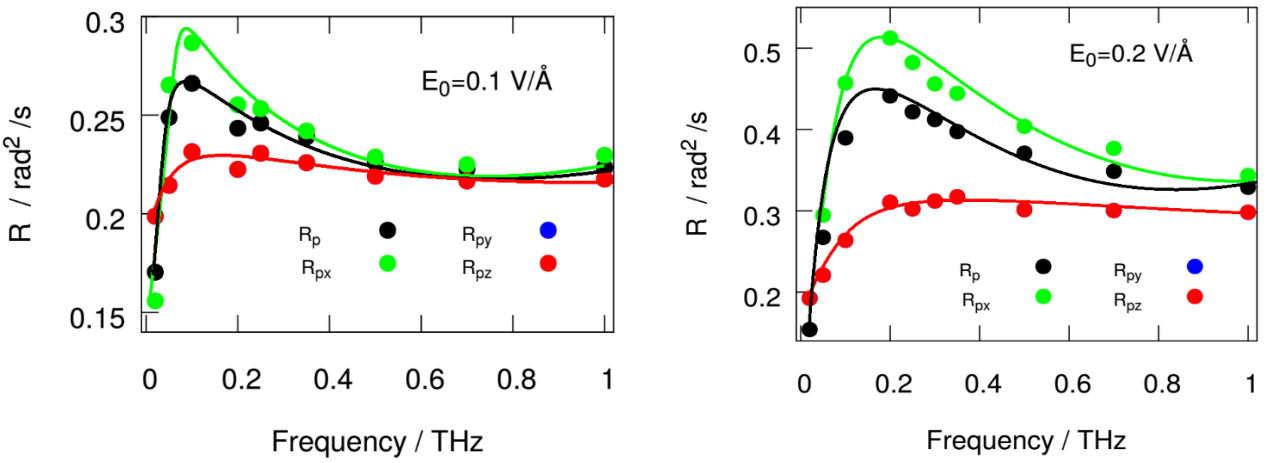

Figure 46. Rotational diffusion of the water dipole moment for two E_0 strengths in a range of frequencies. The maximum difference between the p_z component and p_x component happens when the H-bond rate, and translational and rotational diffusion is maximum.

5.2. Conclusion

We have studied the effect of external alternating electric on the structure and dynamics of bulk water. We show that when the field is strong enough, the average alignment of water molecules reverses after the direction of the field is flipped, although the magnitude of the net dipole moment decreases as the frequency of the field increases.

The structure of water becomes less tetrahedral under the alternating electric fields. We show that by plotting the radial distribution function, oxygen triple angle distribution, and tetrahedral order parameter, q.

The dynamics of the system is also significantly influenced by the external AC field. The external field tries to re-orient the dipole moment of water molecules, but before a re-orientation, at least a few H-bonds of the molecule should break. We have studied the dynamics of hydrogen bonds using the Luzar and Chandler model[51] and dynamic of H-bond switching using the method that we explained in chapter 3. As we expected, the dynamics of the H-bonds increases with frequency of the E-field, but there is a maximum at around 200 GHz; under higher frequencies, the H-bond dynamics moderately slows down. This is because when the field frequency is more than 200 GHz, the half-period time, which is the maximum time before a field reversal, is shorter than $2.5\ ps$ but the H-bond needs more time to break and switch, so the bond remains intact. When the field cannot break the H-bond, increasing the frequency reduces the duration time that the field tries to rotate the molecule (frustration time), and hence the dynamic slows down.

We see the same trend in the translational and rotational diffusion, and the diffusion coefficient, D, remains correlated with H-bond dynamics under alternating E-fields.

The further steps can be studying other effects on the dynamics of the water, for example a confinement or the presence of solvated ions.

Chapter 6. **Summary and Outlook**

This thesis is about the effects of the external electric fields on water. We use molecular dynamic simulations to study what happens when the external force of an electric field controls the orientation of water dipole moments. We have carefully chosen three water models: one non-polarizable, SPC/E, and two polarizable models, BK3 and SWM4-NDP, and we study the effect of polarizability on the effect of the external E-field on water.

In the case of static (or DC) electric fields, the field limits the re-orientation of water molecules and aligns the molecules. We show that the structure and dynamics of water molecules become anisotropic with layers that are perpendicular to the applied field and the H-bond acceptors of a molecule are mostly in one layer above the donor molecule. Still, averaging over all directions, the tetrahedral structure is less influence by the field. The breaking and switching of H-bonds happen relatively fast in the layers perpendicular to the E-field, and the diffusion parallel to the E-field is much slower compared to the diffusion parallel to the layers.

Under alternating electric field, or AC field, the change in the structure is more significant because the electric field forces the molecules to break their H-bonds and rotate, and this reduces the tetrahedrality of the structure. Increasing the frequency of the E-field increases the dynamics of the molecules, but after a certain frequency, around 200 GHz, the dynamics slows down. We show that the time that the E-field remains in one direction, a half-period time, becomes shorter

than the time a H-bond needs to break. So, the molecules cannot follow the E-field reversal and the dynamics slows down after around 200GHz.

During studying the effects of the electric field on water, we realized that the models for describing the H-bond dynamics, Luzar and Chandler model, and describing the re-orientation of molecules by Laage and Hynes, are related but their connection is not described thoroughly. We introduce a method for calculating the rate of switching a tagged hydrogen bond using a reactive flux method. We also provide a generalized framework for studying the H-bond breaking and switching, and we show that this generalized picture is consistent with the previous models. Finally, we show that the random walk translational diffusion of water molecules is correlated with a hydrogen bond characteristic time, $1/\tau_{step}$. This characteristic time is the time that two conditions are met: the previous bond breaks and a new bond can reform, so: $\tau_{step} = \max(\tau_{res}, \frac{1}{k_s})$. We show that this correlation exists for water under static and alternating electric fields.

It would be interesting to assess in depth the relaxation of confined water reorientation in an electric field. In confinement, there are two elements that change the water molecules dynamics: (1) there will be water-surface interaction forces, and (2) change of hydrogen bonding structure because the tetrahedral structure of water cannot be formed completely at the surface elements. The second just increases the water mobility by reducing hydrogen bonding. We can also study a superposition of static and alternating electric field, and study how the response time of water H-bond dynamics changes at confinement.

Bibliography

1 D. Eisenberg and W. Kauzmann, *The Structure and Properties of Water*, Oxford University Press, 2005.

2 P. G. Kusalik, "Determination of the transient polarization response of a dipolar fluid," Mol. Phys. **76**, 337 (1992).

3 M. Von Domaros, D. Bratko, B. Kirchner and A. Luzar, "Dynamics at a Janus interface," J. Phys. Chem. C **117**, 4561 (2013).

4 D. Bratko, C. D. Daub, K. Leung and A. Luzar, "Effect of field direction on electrowetting in a nanopore," J. Am. Chem. Soc. **129**, 2504 (2007).

5 N. Ojaghlou, H. V. Tafreshi, D. Bratko and A. Luzar, "Dynamical insights into the mechanism of a droplet detachment from a fiber," Soft Matter (2018).

6 B. Shapiro, H. Moon, R. L. Garrell and C. J. Kim, "Equilibrium behavior of sessile drops under surface tension, applied external fields, and material variations," J. Appl. Phys. **93**, 5794 (2003).

7 D. Bratko, R. A. Curtis, H. W. Blanch and J. M. Prausnitz, "Interaction between hydrophobic surfaces with metastable intervening liquid," J. Chem. Phys. **115**, 3873 (2001).

8 S. Joseph and N. R. Aluru, "Pumping of confined water in carbon nanotubes by rotation-translation coupling," Phys. Rev. Lett. **101**, 1 (2008).

9 S. De Luca, B. D. Todd, J. S. Hansen and P. J. Daivis, "Electropumping of water with rotating electric fields," J. Chem. Phys. **138**, 154712 (2013).

10 S. De Luca, B. D. Todd, J. S. Hansen and P. J. Daivis, "Molecular Dynamics Study of Nanoconfined Water Flow Driven by Rotating Electric Fields under Realistic Experimental Conditions," Langmuir **30**, 3095 (2014).

11 J. Badur, P. J. Ziółkowski and P. Ziółkowski, "On the angular velocity slip in nano-flows," Microfluid. Nanofluidics **19**, 191 (2015).

12 W. F. D. Bennett, N. Sapay and D. P. Tieleman, "Atomistic simulations of pore formation and closure in lipid bilayers," Biophys. J. **106**, 210 (2014).

13 M. Tokman, J. H. Lee, Z. A. Levine, M.-C. C. Ho, M. E. Colvin, P. T. Vernier and J. M. Sanchez-Ruiz, "Electric Field-Driven Water Dipoles: Nanoscale Architecture of Electroporation," PLoS One **8**, e61111 (2013).

14 E. Neumann, M. Schaefer-Ridder, Y. Wang and P. H. Hofschneider, "Gene transfer into mouse lyoma cells by electroporation in high electric fields.," EMBO J. **1**, 841 (1982).

15 N. J. English and C. J. Waldron, "Perspectives on external electric fields in molecular simulation: Progress, prospects and challenges," Phys. Chem. Chem. Phys. **17**, 12407 (2015).

16 G. Ciccotti, R. Kapral and A. Sergi, in *Handbook of Materials Modeling*, ed. S. Yip, Springer, Dordrecht, 2005, vol. I, pp. 1–17.

17 J. L. England, S. Park and V. S. Pande, "Theory for an order-driven disruption of the liquid state in water," J. Chem. Phys. **128**, 1 (2008).

18 A. Singh, N. J. English and K. M. Ryan, "Highly ordered nanorod assemblies extending over device scale areas and in controlled multilayers by electrophoretic deposition," J. Phys. Chem. B **117**, 1608 (2013).

19 I. M. Svishchev and P. G. Kusalik, "Electrofreezing of Liquid Water: A Microscopic Perspective," J. Am. Chem. Soc. **118**, 649 (1996).

20 N. J. English and J. M. D. Macelroy, "Molecular dynamics simulations of microwave heating of water," J. Chem. Phys. **118**, 1589 (2003).

21 N. J. English and J. M. D. MacElroy, "Hydrogen bonding and molecular mobility in liquid water in external electromagnetic fields," J. Chem. Phys. **119**, 11806 (2003).

22 N. J. English, D. C. Sorescu and J. Karl Johnson, "Effects of an external electromagnetic field on rutile Tio2: A molecular dynamics study," J. Phys. Chem. Solids **67**, 1399 (2006).

23 D. J. Evans and B. L. Holian, "The Nose–Hoover thermostat," J. Chem. Phys. **83**, 4069 (1985).

24 D. Frenkel and B. Smit, in *Understanding Molecular Simulation*, Academic Press, 2002, pp. 63–107.

25 M. Avena, P. Marracino, M. Liberti, F. Apollonio and N. J. English, "Communication: Influence of nanosecond-pulsed electric fields on water and its subsequent relaxation: Dipolar effects and debunking memory," J. Chem. Phys. **142**, 141101 (2015).

26 G. Bussi, D. Donadio and M. Parrinello, "Canonical sampling through velocity rescaling," J. Chem. Phys. **126**, 14101 (2007).

27 D. Bratko, C. D. Daub and A. Luzar, "Field-exposed water in a nanopore: liquid or vapour?," Phys. Chem. Chem. Phys. **10**, 6807 (2008).

28 G. Sutmann, "Structure formation and dynamics of water in strong external electric fields," J. Electroanal. Chem. **450**, 289 (1998).

29 A. Vegiri, "Reorientational relaxation and rotational-translational coupling in water clusters in a d.c. external electric field," J. Mol. Liq. **110**, 155 (2004).

30 D. Vanzo, D. Bratko and A. Luzar, "Nanoconfined water under electric field at constant chemical potential undergoes electrostriction," J. Chem. Phys. **140**, 074710 (2014).

31 D. Vanzo, D. Bratko and A. Luzar, "Dynamic Control of Nanopore Wetting in Water and Saline Solutions under an Electric Field," J. Phys. Chem. B **119**, 8890 (2015).

32 A. M. Saitta, F. Saija and P. V. Giaquinta, "Ab initio molecular dynamics study of dissociation of water under an electric field," Phys. Rev. Lett. **108**, 1 (2012).

33 A. Vegiri, "Translational dynamics of a cold water cluster in the presence of an external uniform electric field," J. Chem. Phys. **116**, 8786 (2002).

34 A. Amadei, M. E. F. Apol, G. Brancato and A. Di Nola, "Theoretical equations of state for temperature and electromagnetic field dependence of fluid systems, based

on the quasi-Gaussian entropy theory," J. Chem. Phys. **116**, 4437 (2002).

35 J. L. Aragones, L. G. MacDowell, J. I. Siepmann and C. Vega, "Phase diagram of water under an applied electric field," Phys. Rev. Lett. **107**, 1 (2011).

36 S. Vaitheeswaran, J. C. Rasaiah and G. Hummer, "Electric field and temperature effects on water in the narrow nonpolar pores of carbon nanotubes.," J. Chem. Phys. **121**, 7955 (2004).

37 J. Hernández-Rojas, B. S. González, T. James and D. J. Wales, "Thermodynamics of water octamer in a uniform electric field," J. Chem. Phys. **125**, 1 (2006).

38 Y. C. Choi, C. Pak and K. S. Kim, "Electric field effects on water clusters (n=3–5): Systematic ab initio study of structures, energetics, and transition states," J. Chem. Phys. **124**, 094308 (2006).

39 X. Zhang, "Hydrophobicity at a Janus Interface," Science (80-.). **295**, 663 (2002).

40 Z. Futera and N. J. English, "Communication: Influence of external static and alternating electric fields on water from long-time non-equilibrium ab initio molecular dynamics," J. Chem. Phys. **147**, 031102 (2017).

41 M. Tanaka and M. Sato, "Microwave heating of water, ice, and saline solution: molecular dynamics study," J. Chem. Phys. **126**, 034509 (2007).

42 N. J. English, P. G. Kusalik and S. A. Woods, "Coupling of translational and rotational motion in chiral liquids in electromagnetic and circularly polarised electric fields," J. Chem. Phys. **136**, 094508 (2012).

43 N. J. English, "Molecular dynamics simulations of liquid water using various long-range electrostatics techniques," Mol. Phys. **103**, 1945 (2005).

44 R. Reale, N. J. English, P. Marracino, M. Liberti and F. Apollonio, "Dipolar response and hydrogen-bond kinetics in liquid water in square-wave time-varying electric fields," Mol. Phys. **112**, 1870 (2014).

45 D. Laage and J. T. Hynes, "A molecular jump mechanism of water reorientation.," Science **311**, 832 (2006).

46 R. Reale, N. J. English, P. Marracino, M. Liberti and F. Apollonio, "Translational and rotational diffusive motion in liquid water in square-wave time-varying electric fields," Chem. Phys. Lett. **582**, 60 (2013).

47 N. J. English, "Molecular dynamics simulations of microwave effects on water using different long-range electrostatics methodologies," Mol. Phys. **104**, 243 (2006).

48 P. K. Nandi, N. J. English, Z. Futera, A. Benedetto, A. DeVries, M. Gruebele, D. M. Leitner, M. Havenith, A. Schulte, P. J. Steinbach, A. H. Xie, R. D. Young, D. Tobias and M. Weik, "Hydrogen-bond dynamics at the bio–water interface in hydrated proteins: a molecular-dynamics study," Phys. Chem. Chem. Phys. **19**, 318 (2017).

49 S. J. Suresh, A. V. Satish and A. Choudhary, "Influence of electric field on the hydrogen bond network of water," J. Chem. Phys. **124**, 074506 (2006).

50 S. J. Suresh, "Disruption of hydrogen bond structure of water near charged electrode surfaces," J. Chem. Phys. **126**, 204705 (2007).

51 A. Luzar and D. Chandler, "Hydrogen-bond kinetics in liquid water," Nature **379**, 55 (1996).

52 K. Takae and A. Onuki, "Fluctuations of local electric field and dipole moments in water between metal walls," J. Chem. Phys. **143**, 154503 (2015).

53 J. Teixeira, A. Luzar and S. Longeville, "Dynamics of hydrogen bonds: how to probe their role in the unusual properties of liquid water," J. Phys. Condens. Matter **18**, 2353 (2006).

54 S. I. Miller and J. I. Dickstein, "Nucleophilic substitution at acetylenic carbon. The last holdout," Acc. Chem. Res. **9**, 358 (1976).

55 A. Luzar, "Water hydrogen-bond dynamics close to hydrophobic and hydrophilic groups," Faraday Discuss. **103**, 29 (1996).

56 F. H. Stillinger, "Water Revisited," Science **209**, 451 (1980).

57 F. S. Csajka and D. Chandler, "Transition pathways in a many-body system: Application to hydrogen-bond breaking in water," J. Chem. Phys. **109**, 1125 (1998).

58 C. Dellago, P. G. Bolhuis, F. S. Csajka and D. Chandler, "Transition Path Sampling and the Calculation of Rate Constants," J. Chem. Phys. **108**, 1964 (1998).

59 D. A. Turton and K. Wynne, "Stokes−Einstein−Debye Failure in Molecular Orientational Diffusion: Exception or Rule?," J. Phys. Chem. B **118**, 4600−4604 (2014).

60 M. G. Mazza, N. Giovambattista, F. W. Starr and H. E. Stanley, "Relation between rotational and translational dynamic heterogeneities in water," Phys. Rev. Lett. **96**, 2 (2006).

61 D. Laage and J. T. Hynes, "On the molecular mechanism of water reorientation," J. Phys. Chem. B **112**, 14230 (2008).

62 R. H. Henchman and S. J. Irudayam, "Topological Hydrogen-Bond Definition to Characterize the Structure and Dynamics of Liquid Water," J. Phys. Chem. B **114**, 16792 (2010).

63 R. H. Henchman, "Water's dual nature and its continuously changing hydrogen bonds," J. Phys. Condens. Matter **28**, 384001 (2016).

64 F. Paesani, S. Yoo, H. J. Bakker and S. S. Xantheas, "Nuclear Quantum Effects in the Reorientation of Water," J. Phys. Chem. Lett. **1**, 2316 (2010).

65 J. Chowdhary and B. M. Ladanyi, "Hydrogen Bond Dynamics at the Water / Hydrocarbon Interface," J. Phys. Chem. B **113**, 4045 (2008).

66 E. Rabani, J. D. Gezelter and B. J. Berne, "Calculating the hopping rate for self-diffusion on rough potential energy surfaces: Cage correlations," J. Chem. Phys. **107**, 6867 (1997).

67 T. Kawasaki and K. Kim, "Identifying time scales for violation/preservation of Stokes-Einstein relation in supercooled water," Sci. Adv. **3**, 1700399 (2017).

68 J. E. Jones, "On the Determination of Molecular Fields. II. From the Equation of State of a Gas," Proc. R. Soc. A Math. Phys. Eng. Sci. **106**, 463 (1924).

69 R. Car and M. Parrinello, "Unified Approach for Molecular Dynamics and Density-

Functional Theory," Phys. Rev. Lett. **55**, 2471 (1985).

70 The Secret Nature Of Hydrogen Bonds -- ScienceDaily, https://www.sciencedaily.com/releases/1999/01/990121074852.htm, (accessed 15 March 2018).

71 H. J. Bakker, Y. L. A. Rezus and R. L. A. Timmer, "Molecular reorientation of liquid water studies with femtosecond midinfrared spectroscopy," J. Phys. Chem. A **112**, 11523 (2008).

72 D. Laage, G. Stirnemann, F. Sterpone and J. T. Hynes, "Water jump reorientation: From theoretical prediction to experimental observation," Acc. Chem. Res. **45**, 53 (2012).

73 J. Ono and K. Ando, "Semiquantal molecular dynamics simulations of hydrogen-bond dynamics in liquid water using multi-dimensional Gaussian wave packets," J. Chem. Phys. **137**, 174503 (2012).

74 M. Rami Reddy and M. Berkowitz, "The dielectric constant of SPC/E water," Chem. Phys. Lett. **155**, 173 (1989).

75 S. Tazi, A. Boţan, M. Salanne, V. Marry, P. Turq and B. Rotenberg, "Diffusion coefficient and shear viscosity of rigid water models," J. Phys. Condens. Matter **24**, 284117 (2012).

76 H. J. C. Berendsen, J. R. Grigera and T. P. Straatsma, "The Missing Term in Effective Pair Potentials," J. Phys. Chem. **91**, 6269 (1987).

77 M. A. Gonzalez and J. L. F. Abascal, "The shear viscosity of rigid water models," J. Chem. Phys. **132**, 2008 (2010).

78 C. Vega and E. De Miguel, "Surface tension of the most popular models of water by using the test-area simulation method," J. Chem. Phys. **126**, 154707 (2007).

79 M. W. Mahoney and W. L. Jorgensen, "A five-site model for liquid water and the reproduction of the density anomaly by rigid, nonpolarizable potential functions," J. Chem. Phys. **112**, 8910 (2000).

80 M. W. Mahoney and W. L. Jorgensen, "Diffusion constant of the TIP5P model of liquid water," J. Chem. Phys. **114**, 363 (2001).

81 R. Fuentes-Azcatl and J. Alejandre, "Non-polarizable force field of water based on the dielectric constant: TIP4P/ε," J. Phys. Chem. B **118**, 1263 (2014).

82 J. Alejandre, G. A. Chapela, H. Saint-Martin and N. Mendoza, "A non-polarizable model of water that yields the dielectric constant and the density anomalies of the liquid: TIP4Q," Phys. Chem. Chem. Phys. **13**, 19728 (2011).

83 P. Kiss, M. Darvas, A. Baranyai and P. Jedlovszky, "Surface properties of the polarizable Baranyai-Kiss water model," J. Chem. Phys. **136**, 114706 (2012).

84 A. Baranyai and P. T. Kiss, "Polarizable model of water with field-dependent polarization," J. Chem. Phys. **135**, 234110 (2011).

85 P. Mark and L. Nilsson, "Structure and Dynamics of the TIP3P , SPC , and SPC / E Water Models at 298 K," J. Phys. Chem. A **105**, 9954 (2001).

86 D. Van Der Spoel, P. J. Van Maaren, H. J. C. Berendsen, D. van der Spoel, P. J. van Maaren and H. J. C. Berendsen, "A systematic study of water models for molecular simulation: Derivation of water models optimized for use with a reaction field," J. Chem. Phys. **108**, 10220 (1998).

87 M. R. Stukan, A. Asmadi and W. Abdallah, "Bulk properties of SWM4-NDP water model at elevated temperature and pressure," J. Mol. Liq. **180**, 65 (2013).

88 Z. Steinczinger and L. Pusztai, "Comparison of the TIP4P-2005, SWM4-DP and BK3 interaction potentials of liquid water with respect to their consistency with neutron and X-ray diffraction data of pure water," Condens. Matter Phys. **16**, 1 (2013).

89 W. Yu, P. E. M. Lopes, B. Roux and A. D. Mackerell, "Six-site polarizable model of water based on the classical Drude oscillator A simple polarizable model of water based on classical Drude oscillators Modeling induced polarization with classical Drude oscillators: Theory and molecular dynamics simulation algorithm Mapping the Drude polarizable force field onto a multipole and induced dipole model Six-site

polarizable model of water based on the classical Drude oscillator," J. Chem. Phys. J. Chem. Phys. J. Chem. Phys. J. Chem. Phys. , DOI:10.1063/1.4774577.

90 S. Rick, S. Stuart and B. Berne, "Dynamical fluctuating charge force fields: Application to liquid water," J. Chem. Phys. **101**, 6141 (1994).

91 M. L. Laury, L.-P. P. Wang, V. S. Pande, T. Head-Gordon and J. W. Ponder, "Revised Parameters for the AMOEBA Polarizable Atomic Multipole Water Model," J. Phys. Chem. B **119**, 9423 (2015).

92 L.-P. Wang, T. Head-Gordon, J. W. Ponder, P. Ren, J. D. Chodera, P. K. Eastman, T. J. Martinez and V. S. Pande, "Systematic improvement of a classical molecular model of water.," J. Phys. Chem. B **117**, 9956 (2013).

93 R. Qi, L. P. Wang, Q. Wang, V. S. Pande and P. Ren, "United polarizable multipole water model for molecular mechanics simulation," J. Chem. Phys. **143**, 014504 (2015).

94 P. T. Kiss and A. Baranyai, "Anomalous properties of water predicted by the BK3 model," J. Chem. Phys. **140**, 154505 (2014).

95 Martin Chaplin, Water models, http://www1.lsbu.ac.uk/water/water_models.html, (accessed 12 January 2018).

96 A. V. Gubskaya and P. G. Kusalik, "The total molecular dipole moment for liquid water," J. Chem. Phys. **117**, 5290 (2002).

97 K. R. Harris and L. A. Woolf, "Temperature and volume dependence of the viscosity of water and heavy water at low temperatures," J. Chem. Eng. Data **49**, 1064 (2004).

98 N. R. Pallas and Y. Harrison, "An automated drop shape apparatus and the surface tension of pure water," Colloids and Surfaces **43**, 169 (1990).

99 P. T. Kiss and A. Baranyai, "A systematic development of a polarizable potential of water," J. Chem. Phys. **138**, 204507 (2013).

100 G. Lamoureux, E. Harder, I. V. Vorobyov, B. Roux and A. D. MacKerell, "A

polarizable model of water for molecular dynamics simulations of biomolecules," Chem. Phys. Lett. **418**, 245 (2006).

101 S. Plimpton, "Fast Parallel Algorithms for Short-Range Molecular Dynamics," J. Comput. Phys. **117**, 1 (1995).

102 Weblet Importer, http://lammps.sandia.gov, (accessed 13 January 2018).

103 B. Hess, C. Kutzner, D. van der Spoel and E. Lindahl, "GROMACS 4: Algorithms for Highly Efficient, Load-Balanced, and Scalable Molecular Simulation," J. Chem. Theory Comput. **4**, 435 (2008).

104 M. Sega, BK3-water-model, https://github.com/Marcello-Sega/gromacs.

105 M. E. Foulaadvand and N. Ojaghlou, "Structural and elastic properties of a confined two-dimensional colloidal solid: A molecular dynamics study," Phys. Rev. E **86**, 021405 (2012).

106 M. Ebrahim Foulaadvand and M. Mehdi Shafiee, "One-dimensional Brownian motion in hard rods: The adiabatic piston problem," EPL (Europhysics Lett. **104**, 30002 (2013).

107 L. Levrel and A. C. Maggs, "Boundary conditions in local electrostatics algorithms," J. Chem. Phys. **128**, 214103 (2008).

108 H. J. C. Berendsen, J. P. M. Postma, W. F. van Gunsteren, A. DiNola and J. R. Haak, "Molecular dynamics with coupling to an external bath," J. Chem. Phys. **81**, 3684 (1984).

109 M. Brehm and B. Kirchner, "TRAVIS - A Free Analyzer and Visualizer for Monte Carlo and Molecular Dynamics Trajectories," J. Chem. Inf. Model. **51**, 2007 (2011).

110 W. Humphrey, A. Dalke and K. Schulten, "VMD: visual molecular dynamics," J. Mol. Graph. **14**, 33 (1996).

111 I.-C. Yeh, I.-C. Y. and, G. Hummer*, I.-C. Yeh and G. Hummer, "System-Size Dependence of Diffusion Coefficients and Viscosities from Molecular Dynamics Simulations with Periodic Boundary Conditions," J. Phys. Chem. B **108**, 15873

(2004).

112 H. Kubinyi, in *Pharmacokinetic Optimization in Drug Research*, eds. B. Testa, H. van de Waterbeemd, G. Folkers and R. Guy, Verlag Helvetica Chimica Acta, Zürich, 2007, pp. 513–524.

113 E. Gianti, V. Carnevale, W. F. Degrado, M. L. Klein and G. Fiorin, "Hydrogen-bonded water molecules in the m2 channel of the influenza a virus guide the binding preferences of ammonium-based inhibitors," J. Phys. Chem. B **119**, 1173 (2015).

114 S. Fischer and C. S. Verma, "Binding of buried structural water increases the flexibility of proteins.," Proc. Natl. Acad. Sci. U. S. A. **96**, 9613 (1999).

115 H. Eslami and N. Heydari, "Hydrogen bonding in water nanoconfined between graphene surfaces: A molecular dynamics simulation study," J. Nanoparticle Res. **16**, 2154 (2014).

116 A. Chandra, "Effects of ion atmosphere on hydrogen-bond dynamics in aqueous electrolyte solutions," Phys. Rev. Lett. **85**, 768 (2000).

117 Q. Zhang, T. Wu, C. Chen, S. Mukamel and W. Zhuang, "Molecular mechanism of water reorientational slowing down in concentrated ionic solutions.," Proc. Natl. Acad. Sci. U. S. A. **114**, 10023 (2017).

118 J. Teixeira, "Recent experimental aspects of the structure and dynamics of liquid and supercooled water," Mol. Phys. **110**, 249 (2012).

119 D. Laage, T. Elsaesser and J. T. Hynes, "Water Dynamics in the Hydration Shells of Biomolecules," Chem. Rev. **117**, 10694 (2017).

120 A. Luzar, "Resolving the hydrogen bond dynamics conundrum," J. Chem. Phys. **113**, 10663 (2000).

121 J. Teixeira, "The contribution of small angle and quasi-elastic scattering to the physics of liquid water," J. Phys. Conf. Ser. **848**, 012003 (2017).

122 S. N. Wanasundara, R. J. Spiteri and R. K. Bowles, "A transition state theory for calculating hopping times and diffusion in highly confined fluids," J. Chem. Phys.

140, 24505 (2014).

123 B. Mukherjee, "Microscopic origin of temporal heterogeneities in translational dynamics of liquid water," J. Chem. Phys. **143**, 054503 (2015).

124 N. Agmon, "Liquid Water: From Symmetry Distortions to Diffusive Motion," Acc. Chem. Res. **45**, 63 (2012).

125 J. Qvist, H. Schober and B. Halle, "Structural dynamics of supercooled water from quasielastic neutron scattering and molecular simulations," J. Chem. Phys. **134**, 144508 (2011).

126 F. Rao, S. Garrett-Roe and P. Hamm, "Structural inhomogeneity of water by complex network analysis," J. Phys. Chem. B **114**, 15598 (2010).

127 J. Russo and H. Tanaka, "Understanding water's anomalies with locally favoured structures.," Nat. Commun. **5**, 3556 (2014).

128 Y. Wu, H. L. Tepper and G. A. Voth, "Flexible simple point-charge water model with improved liquid-state properties Comparison of simple potential functions for simulating liquid water Flexible simple point-charge water model with improved liquid-state properties," J. Chem. Phys. **1241**, 24503 (2006).

129 W. A. M. Madhavi, S. Weerasinghe and K. I. Momot, "Rotational-Diffusion Propagator of the Intramolecular Proton–Proton Vector in Liquid Water: A Molecular Dynamics Study," J. Phys. Chem. B **121**, 10893 (2017).

130 A. K. Soper, J. Teixeira and T. Head-Gordon, "Is ambient water inhomogeneous on the nanometer-length scale?," Proc. Natl. Acad. Sci. U. S. A. **107**, E44; author reply E45 (2010).

131 I. M. Svishchev and P. G. Kusalik, "Roto-translational motion in liquid water and its structural implication," Chem. Phys. Lett. **215**, 596 (1993).

132 J. Qvist, C. Mattea, E. P. Sunde and B. Halle, "Rotational dynamics in supercooled water from nuclear spin relaxation and molecular simulations.," J. Chem. Phys. **136**, 204505 (2012).

133 G. Stirnemann and D. Laage, "Communication: On the origin of the non-Arrhenius behavior in water reorientation dynamics," J. Chem. Phys. **137**, 031101 (2012).

134 N. Galamba, "On the hydrogen-bond network and the non-Arrhenius transport properties of water," J. Phys. Condens. Matter **29**, 015101 (2017).

135 D. M. Wilkins, D. E. Manolopoulos, S. Pipolo, D. Laage and J. T. Hynes, "Nuclear Quantum Effects in Water Reorientation and Hydrogen-Bond Dynamics," J. Phys. Chem. Lett. **8**, 2602 (2017).

136 S. T. Roberts, K. Ramasesha and A. Tokmakoff, "Structural rearrangements in water viewed through two-dimensional infrared spectroscopy," Acc. Chem. Res. **42**, 1239 (2009).

137 Y. Ni, S. M. Gruenbaum and J. L. Skinner, "Slow hydrogen-bond switching dynamics at the water surface revealed by theoretical two-dimensional sum-frequency spectroscopy," Proc. Natl. Acad. Sci. U. S. A. **110**, 1992 (2013).

138 A. C. Fogarty, E. Duboué-Dijon, D. Laage and W. H. Thompson, "Origins of the non-exponential reorientation dynamics of nanoconfined water," J. Chem. Phys. **141**, 18C523 (2014).

139 D. Laage, "Reinterpretation of the Liquid Water Quasi-Elastic Neutron Scattering Spectra Based on a Nondiffusive Jump Reorientation Mechanism," J. Phys. Chem. B **113**, 2684 (2009).

140 S.-H. Chen, F. Mallamace, C.-Y. Mou, M. Broccio, C. Corsaro, A. Faraone and L. Liu, "The violation of the Stokes-Einstein relation in supercooled water," Proc. Natl. Acad. Sci. **103**, 12974 (2006).

141 R. A. Nicodemus, K. Ramasesha, S. T. Roberts and A. Tokmakoff, "Hydrogen bond rearrangements in water probed with temperature-dependent 2D IR," J. Phys. Chem. Lett. **1**, 1068 (2010).

142 F. N. Keutsch, R. S. Fellers, M. G. Brown, M. R. Viant, P. B. Petersen and R. J. Saykally, "Hydrogen bond breaking dynamics of the water trimer in the translational and librational band region of liquid water," J. Am. Chem. Soc. **123**, 5938 (2001).

143 K. Shinokita, A. V Cunha, T. L. C. Jansen and M. S. Pshenichnikov, "Hydrogen bond dynamics in bulk alcohols Anharmonic exciton dynamics and energy dissipation in liquid water from two-dimensional infrared spectroscopy Hydrogen bond dynamics in bulk alcohols," J. Chem. Phys. **1421**, 212450 (2015).

144 P. Kumar and S. Han, "Dynamics of two-dimensional monolayer water confined in hydrophobic and charged environments," J. Chem. Phys. **137**, 114510 (2012).

145 D. Zong, H. Hu, Y. Duan and Y. Sun, "Viscosity of Water under Electric Field: Anisotropy Induced by Redistribution of Hydrogen Bonds," J. Phys. Chem. B **120**, 4818 (2016).

146 C. D. Daub, D. Bratko and A. Luzar, "Nanoscale wetting under electric field from molecular simulations," Top. Curr. Chem. **307**, 155 (2012).

147 A. Vegiri, "Dynamic response of liquid water to an external static electric field at T = 250 K," J. Mol. Liq. **112**, 107 (2004).

148 S. Acosta-Gutiérrez, J. Hernández-Rojas, J. Bretón, J. M. G. Llorente and D. J. Wales, "Physical properties of small water clusters in low and moderate electric fields," J. Chem. Phys. **135**, 124303 (2011).

149 K. a Maerzke and J. I. Siepmann, "Effects of an Applied Electric Field on the Vapor-Liquid Equilibria of Water , Methanol ," J. Phys. Chem. B 4261 (2010).

150 D. Li and G.-Z. Jia, "Dielectric properties of SPC/E and TIP4P under the static electric field and microwave field," Physica A **449**, 348 (2016).

151 J. Y. Yan, S. D. Overduin and G. N. Patey, "Understanding electrofreezing in water simulations," J. Chem. Phys. **141**, 074501 (2014).

152 D. H. Jung, J. H. Yang and M. S. Jhon, "The effect of an external electric field on the structure of liquid water using molecular dynamics simulations," Chem. Phys. **244**, 331 (1999).

153 R. D. Mountain and D. Thirumalai, "Hydration for a series of hydrocarbons," Proc. Natl. Acad. Sci. U. S. A. **95**, 8436 (1998).

154 S. V. Shevkunov and A. Vegiri, "Equilibrium structures of the N = 64 water cluster in the presence of external electric fields," J. Mol. Struct. THEOCHEM **574**, 27 (2001).

155 D. Rai, A. D. Kulkarni, S. P. Gejji and R. K. Pathak, "Water clusters (H2O)n, n=6-8, in external electric fields," J. Chem. Phys. **128**, 034310 (2008).

156 J. R. Errington and P. G. Debenedetti, "Relationship between structural order and the anomalies of liquid water," Nature **409**, 318 (2001).

157 E. Duboue, D. Laage and E. Normale, "Characterization of the Local Structure in Liquid Water by Various Order Parameters," J. Phys. Chem. A **119**, 8406 (2015).

158 Z. Yan, S. V. Buldyrev, P. Kumar, N. Giovambattista, P. G. Debenedetti and H. E. Stanley, "Structure of the first- and second-neighbor shells of simulated water: Quantitative relation to translational and orientational order," Phys. Rev. E - Stat. Nonlinear, Soft Matter Phys. **76**, 1 (2007).

159 C. D. Daub, K. Leung and A. Luzar, "Structure of aqueous solutions of monosodium glutamate," J. Phys. Chem. B **113**, 7687 (2009).

160 P. Mark and L. Nilsson, "Structure and dynamics of liquid water with different long-range interaction truncation and temperature control methods in molecular dynamics simulations," J. Comput. Chem. **23**, 1211 (2002).

161 J. KOLAFA and I. NEZBEDA, "Effect of short and long range forces on the structure of water. II. Orientational ordering and the dielectric constant," Mol. Phys. **98**, 1505 (2000).

162 I. M. Svishchev and P. G. Kusalik, "Structure in liquid water: A study of spatial distribution functions," J. Chem. Phys. **99**, 3049 (1993).

163 Z. Futera and N. J. English, "Electric-Field Effects on Adsorbed-Water Structural and Dynamical Properties at Rutile- and Anatase-TiO $_2$ Surfaces," J. Phys. Chem. C **120**, 19603 (2016).

164 M. Girardi and W. Figueiredo, "Three-dimensional square water in the presence of

an external electric field," J. Chem. Phys. **125**, 94508 (2006).

165 S. Sen, M. Boda, S. Venkat Lata, G. Naresh Patwari, V. S. Pande, Z. Kisiel and B. H. Pate, "Internal electric fields in small water clusters [($H_2O)_n$; n = 2–6]," Phys. Chem. Chem. Phys. **18**, 16730 (2016).

166 E. Duboue, D. Laage, E. Normale, E. Duboué-Dijon and D. Laage, "Characterization of the Local Structure in Liquid Water by Various Order Parameters," J. Phys. Chem. B **119**, 8406 (2015).

167 S. V. Shevkunov and A. Vegiri, "Electric field induced transitions in water clusters," J. Mol. Struct. THEOCHEM **593**, 19 (2002).

168 Z. Futera and N. J. English, "Electric-Field Effects on Adsorbed-Water Structural and Dynamical Properties at Rutile-and Anatase-TiO 2 Surfaces," J. Phys. Chem. C **120**, 19603 (2016).

169 Winarto, E. Yamamoto and K. Yasuoka, "Water Molecules in a Carbon Nanotube under an Applied Electric Field at Various Temperatures and Pressures," Water **9**, 473 (2017).

170 S. D. Fried and S. G. Boxer, "Measuring Electric Fields and Noncovalent Interactions Using the Vibrational Stark Effect," Acc. Chem. Res. **48**, 998 (2015).

171 F. Saija, F. Aliotta, M. E. Fontanella, M. Pochylski, G. Salvato, C. Vasi and R. C. Ponterio, "Communication: An extended model of liquid bridging," J. Chem. Phys. **133**, 081104 (2010).

172 R. Kumar, J. R. Schmidt and J. L. Skinner, "Hydrogen bonding definitions and dynamics in liquid water," J. Chem. Phys. **126**, 204107 (2007).

173 M. Chen, H.-Y. Ko, R. C. Remsing, M. F. Calegari Andrade, B. Santra, Z. Sun, A. Selloni, R. Car, M. L. Klein, J. P. Perdew and X. Wu, "Ab initio theory and modeling of water.," Proc. Natl. Acad. Sci. U. S. A. **114**, 10846 (2017).

174 G. Stirnemann, J. T. Hynes and D. Laage, "Water Hydrogen Bond Dynamics in Aqueous Solutions of Amphiphiles," J. Phys. Chem. B **114**, 3052 (2010).

175 C. Merlet, B. Rotenberg, P. a Madden and M. Salanne, "Computer simulations of ionic liquids at electrochemical interfaces.," Phys. Chem. Chem. Phys. **15**, 15781 (2013).

176 S. Wei, C. Zhong and H. Su-Yi, "Molecular dynamics simulation of liquid water under the influence of an external electric field," Mol. Simul. **31**, 555 (2005).

177 P. K. Mishra, O. Vendrell and R. Santra, "Subpicosecond energy transfer from a highly intense THz pulse to water: A computational study based on the TIP4P/2005 rigid-water-molecule model," **93**, 032124 (2016).

178 P. K. Mishra, O. Vendrell and R. Santra, "Ultrafast Energy Transfer to Liquid Water by Sub-Picosecond High-Intensity Terahertz Pulses: An Ab Initio Molecular Dynamics Study," Angew. Chemie Int. Ed. **52**, 13685 (2013).

179 R. Reale, N. J. English, P. Marracino, M. Liberti and F. Apollonio, "Molecular Physics: An International Journal at the Interface Between Chemistry and Physics Dipolar response and hydrogen-bond kinetics in liquid water in square-wave time-varying electric fields) Dipolar response and hydrogen-bond kinetics in liquid water," Mol. Phys. An Int. J. Interface Between Chem. Phys. **11214**, 1870 (2015).

180 S. Chowdhuri and A. Chandra, "Hydrogen bonds in aqueous electrolyte solutions: Statistics and dynamics based on both geometric and energetic criteria," Phys. Rev. E - Stat. Nonlinear, Soft Matter Phys. **66**, 1 (2002).

181 D. Vanzo, D. Bratko and A. Luzar, "Tunable Wetting of Surfaces with Ionic Functionalities," J. Phys. Chem. C **116**, 15467 (2012).

182 S. Floros, M. Liakopoulou-Kyriakides, K. Karatasos and G. E. Papadopoulos, "Frequency dependent non-thermal effects of oscillating electric fields in the microwave region on the properties of a solvated lysozyme system: A molecular dynamics study," PLoS One **12**, 0169505 January (2017).

183 M. G. Mazza, N. Giovambattista, H. E. Stanley and F. W. Starr, "Connection of translational and rotational dynamical heterogeneities with the breakdown of the Stokes-Einstein and Stokes-Einstein-Debye relations in water," Phys. Rev. E - Stat.

Nonlinear, Soft Matter Phys. **76**, 031203 (2007).

184 A. M. Cohen, *Numerical Methods for Laplace Transform Inversion*, Springer US, Boston, MA, 2007.

185 G. A. Cisneros, K. T. Wikfeldt, L. Ojamäe, J. Lu, Y. Xu, H. Torabifard, A. P. Bartók, G. Csányi, V. Molinero and F. Paesani, "Modeling Molecular Interactions in Water: From Pairwise to Many-Body Potential Energy Functions," Chem. Rev. **116**, 7501 (2016).

Appendices

Appendix 1. Tetrahedral order parameters

Table S. 1 The value of the tetrahedral first and second layer order parameter for some electric E_0 strengths and frequencies. Generally, there is no significant change in these values over the different external E-fields.

	DC	
	q	Q_6
Zero field	0.64	0.21
Static $E_0 = 0.1 \frac{V}{\text{Å}}$	0.64	0.21
Static $E_0 = 0.2 \frac{V}{\text{Å}}$	0.65	0.21

Appendix 2. The effect of thermostat

The non-equilibrium molecular dynamics simulation results presented in this thesis have been done using Nosé-Hoover thermostat[23] at $T = 300\ K$. Here we show the results of the most

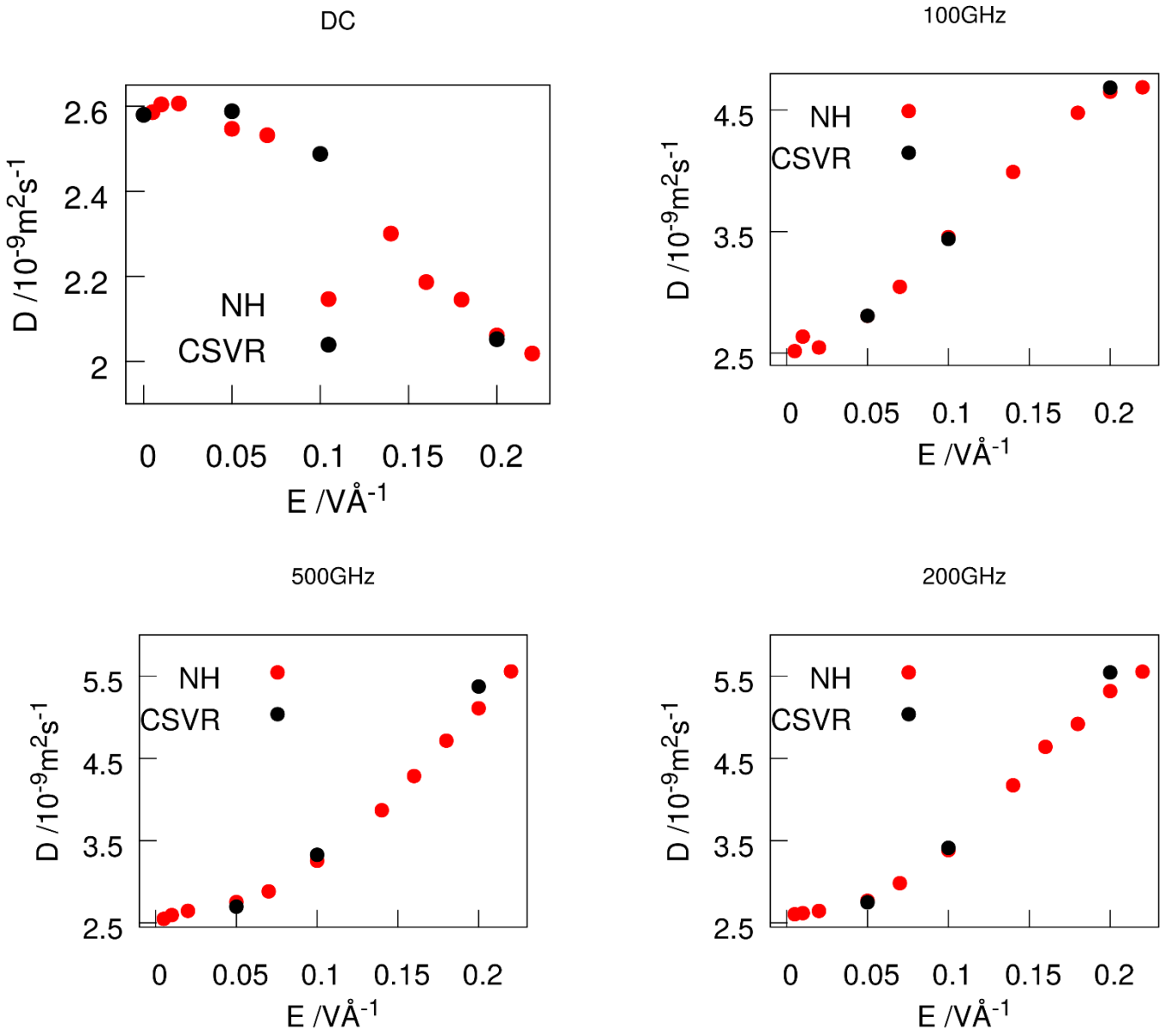

Figure S 1. Comparing the diffusion coefficient under static and alternating E-fields using Nosé-Hoover and CSVR thermostat. There is no difference in the results. For the detail of the CSVR simulation see the Laamps appendix.

important dynamical variables from the simulation using Velocity Rescaling (CSVR) hermostat.[26]

As we can see, the choice of thermostat does not affect the results.

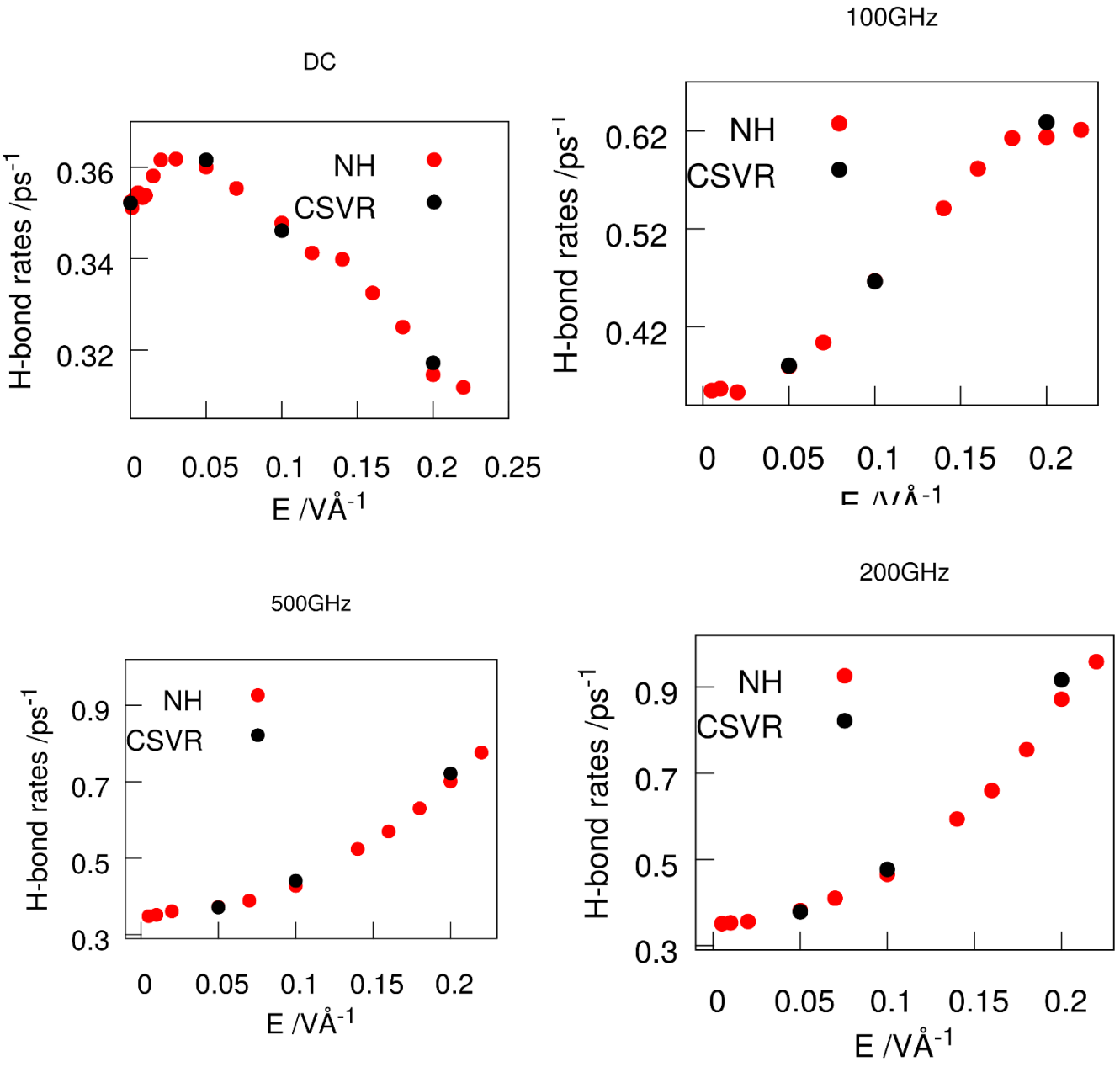

Figure S 2. The comparison of the H-bond dynamics rate using Luzar and Chandler model under different DC and AC E-fields using Nosé-Hoover and CSVR thermostat.

Appendix 3. Large jump trajectories

For calculating the dynamics of hydrogen bonds, we use correlation functions. But we can see the H-bond switching process from the probability distributions of angles and distances during H-bond switches. In the following plot, the color is the 3rd dimension indicating the probability. The x-axis is time and the y-axis are the distance or angle. The plots are not normalized and the number beside the color bars show how probable is the process in 300 picoseconds simulations. Laage and Hynes [45,61] use these correlation plots to show the mechanism of the H-bond jump.

Here we are looking at 3 variables from 500 fs before a switch to 500 fs after the switch. $O^* - O_a$ distance, $O^* - O_b$ distance and $\phi = \widehat{O_a O^* O_b}$ angle. If the bond formation is a re-bond, then $O_a = O_b$. These plots are called "*Heat map*" and the more probable points are *hotter* points.

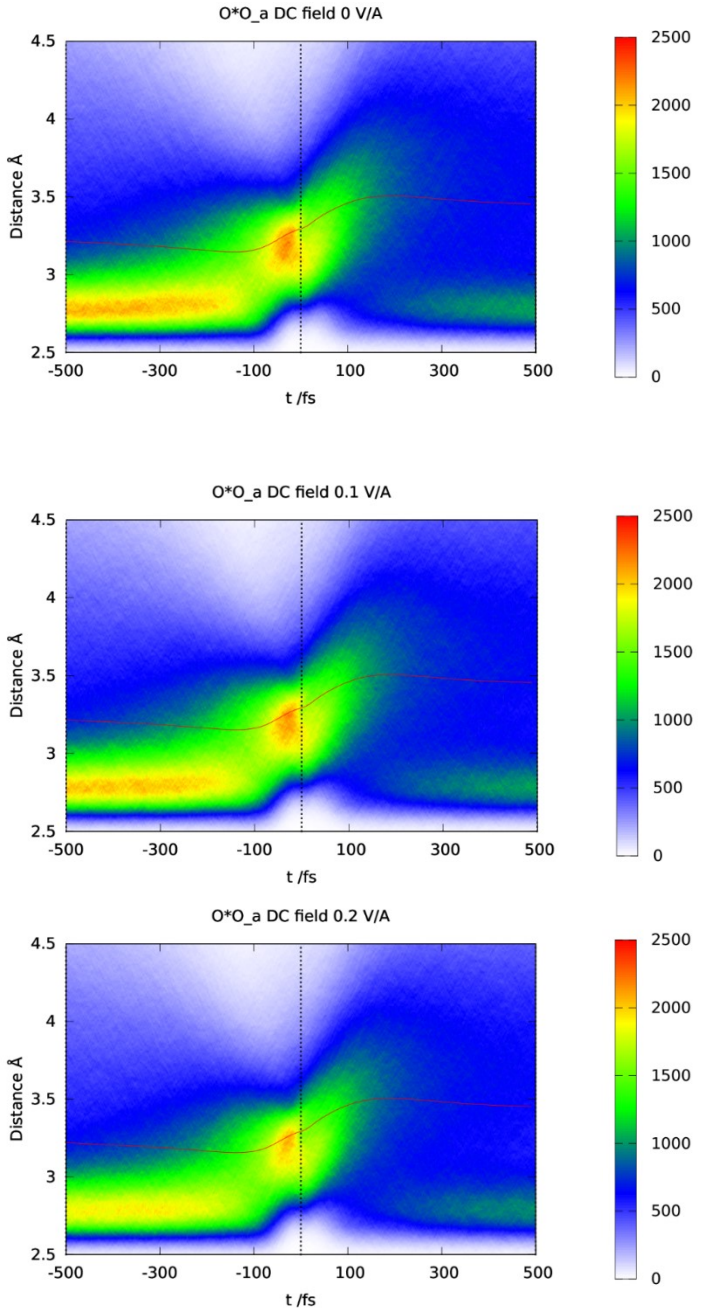

Figure S 3. The $O^* - O_a$ distance under zero field (top) under $0.1\ V\text{Å}^{-1}$ *static E-field (middle) and under* $0.2\ V\text{Å}^{-1}$ *at bottom. The H-bond jump mechanism does not change under static E-fields.*

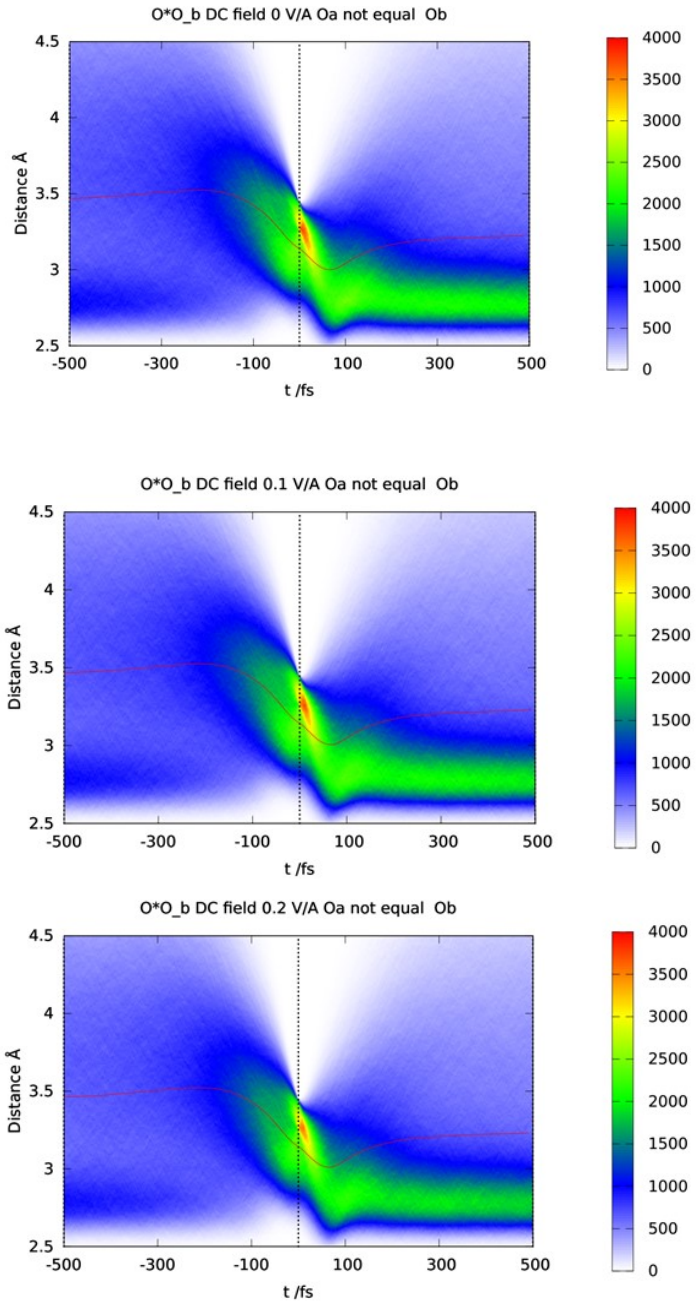

Figure S 4. The distribution of the $O^* - O_b$ distances during a switch. In such a switch, O_b enters the first shell and accepts the H-bond. Again, there is no clear different between the plots under the different static E-fields.

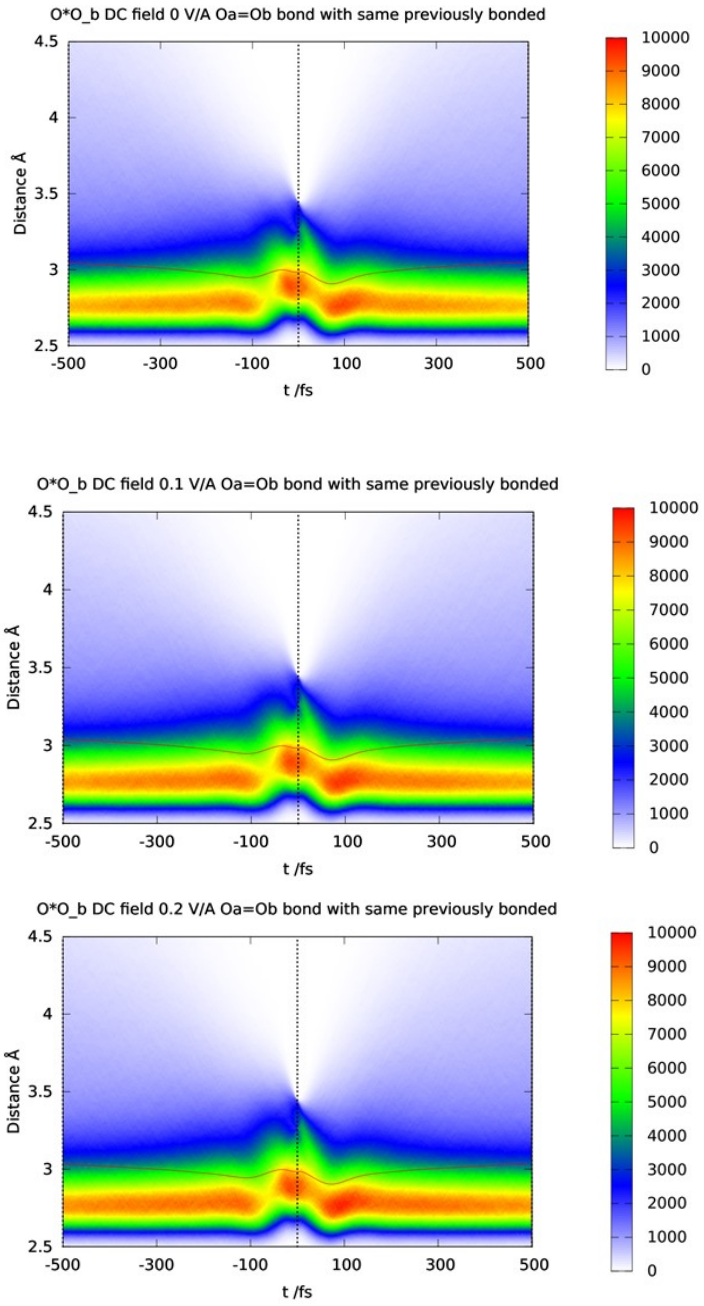

Figure S 5. The distribution of the $O^* - O_a$ distances when the bond reforms right away. This kind of bond H-bond breaks are usually due to thermal librations. As we showed in chapter 4, the static E-filed around $E = 0.2\, V\mathring{A}^{-1}$ are too weak to influence these kind of librations.

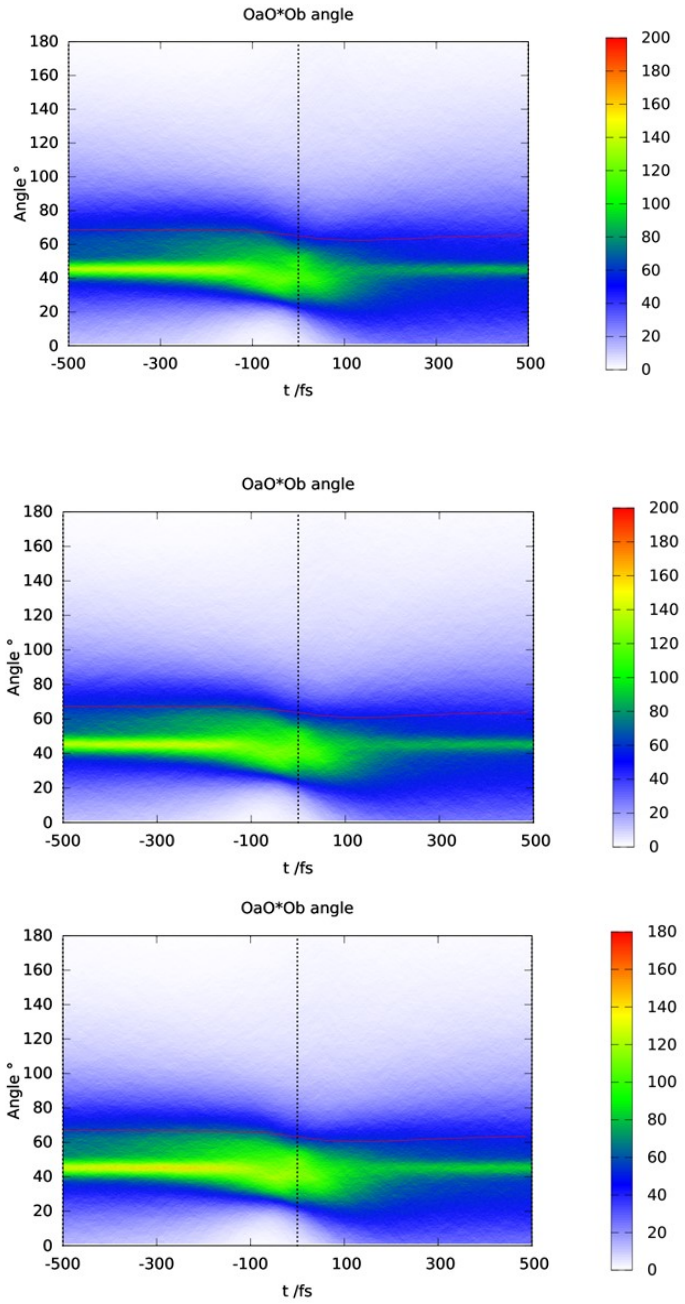

Figure S 6. The frame angle $\widehat{O_a O^* O_b}$ during a H-bond switch remains constant, and this does not change under static E-fields.

Appendix 4. The other-way bonding probability

Figure S 7 shows function $c"(t) = c(t) - c_t(t)$, the probability that a pair that where H-bonded by donating H^* to O_a at $t = 0$, re-form their bond in another way, for example switching the donor-acceptor roles.

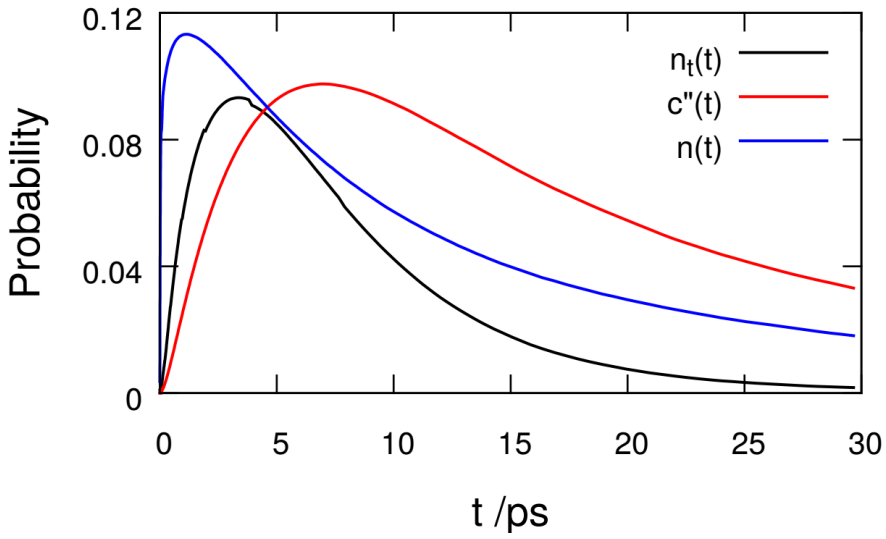

Figure S 7. The probability of other-way bonding.

Appendix 5. Accessing the validity of eq. 9

To get the analytic curve (red), the inverse Laplace transforms in eq. 10 and eq. 11 should be solved. They have been solved using Stehfest method,[184] the code for doing this calculation is included in the coding appendix.

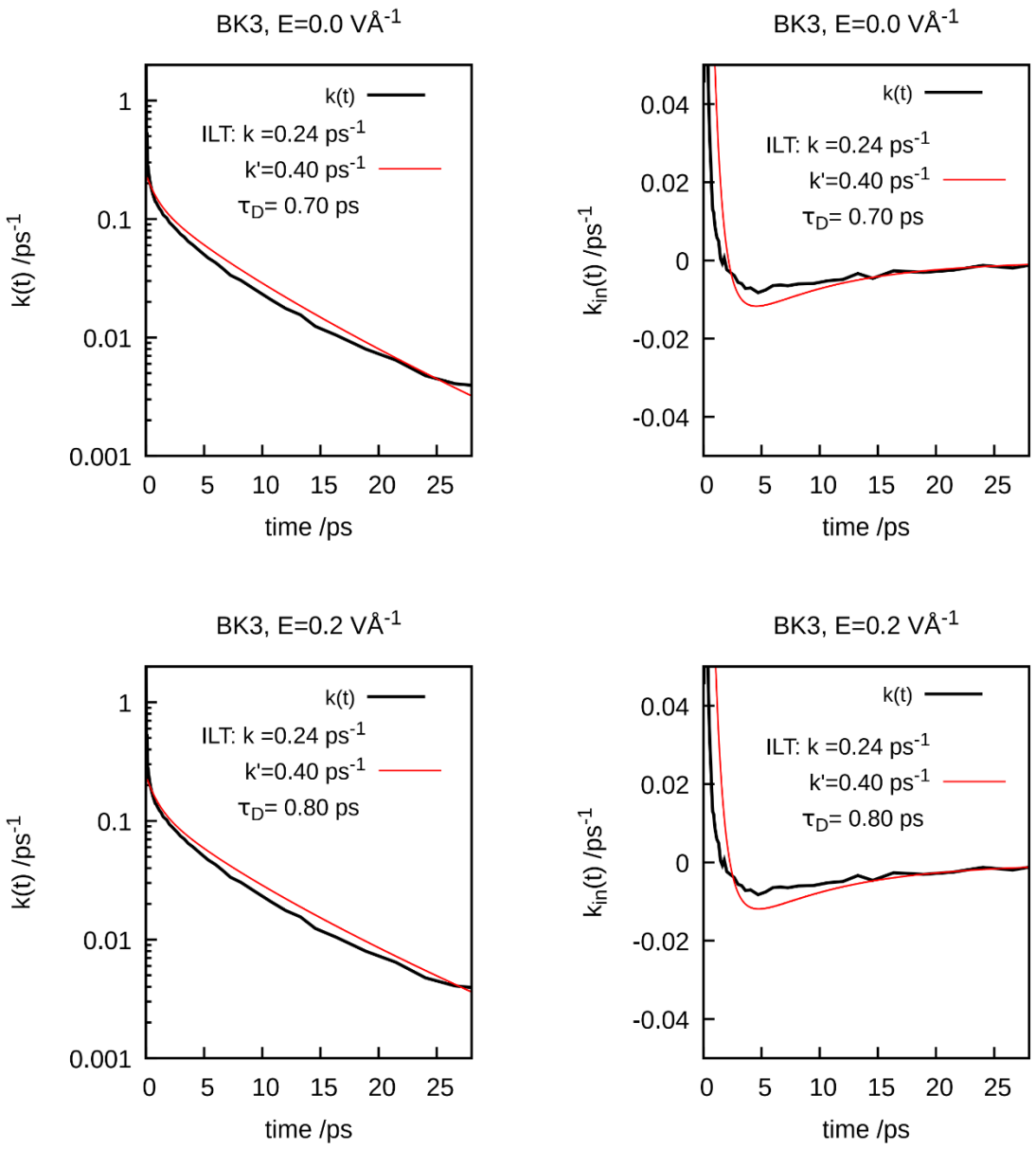

Figure S 8. The $k(t)$ and $k_{in}(t)$ functions for BK3 water and the best estimation of the diffusion time, $\tau_D = 0.7\ ps$ for zero field and $\tau_D = 0.8\ ps$ under $0.2\ V/\text{Å}$.

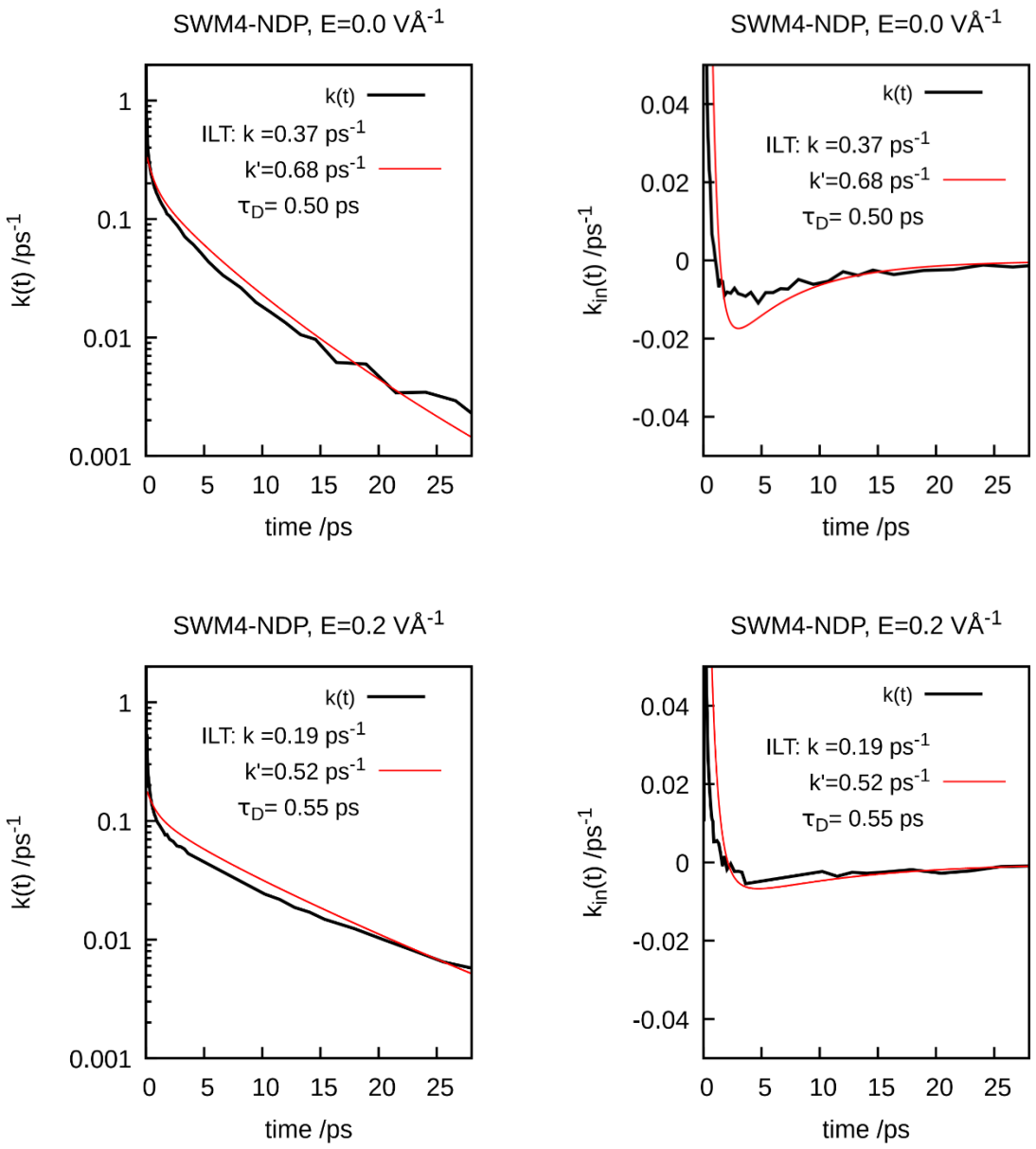

Figure S 9. The $k(t)$ and $k_{in}(t)$ functions for SWM4-NDP water and the best estimation of the diffusion time, $\tau_D = 0.5\ ps$ for zero field and $\tau_D = 0.5\ ps$ under $0.2\ V/\text{Å}$.

Appendix 6. The polarizable Water models

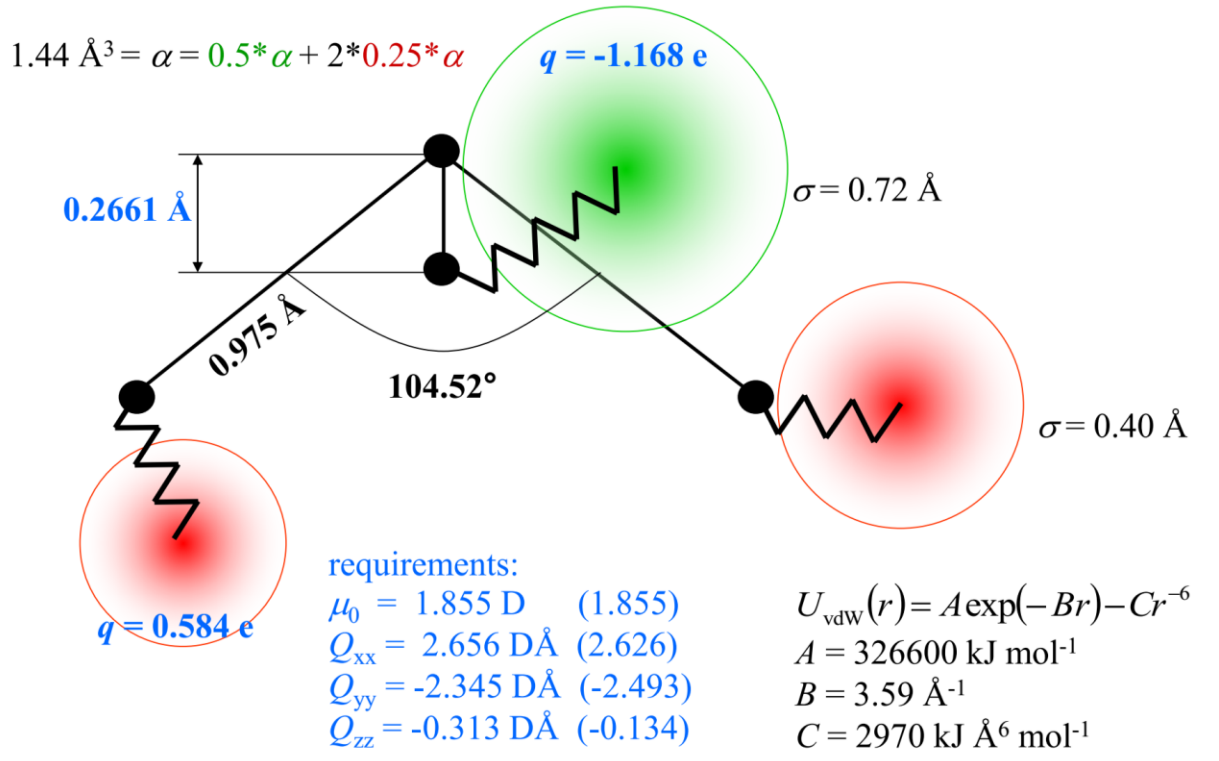

A. 1. Baranyai and Kiss introduced the BK3 water in 2014.[94] *The above picture is from their presentation that they kindly shared with us.*

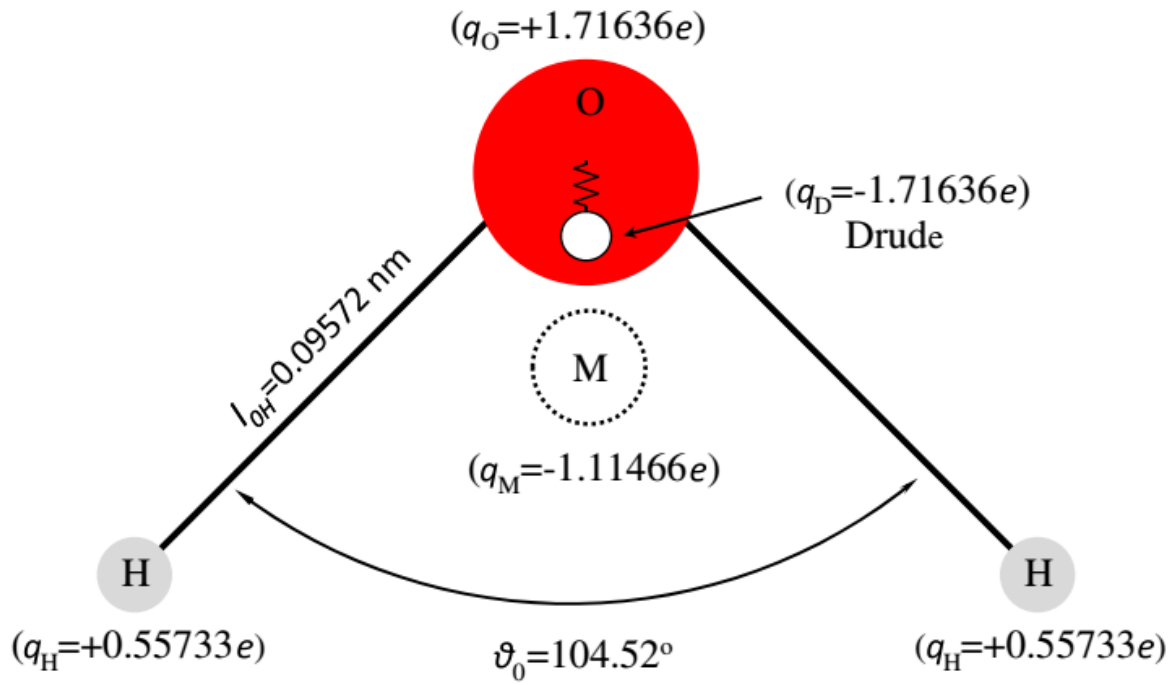

A. 2. The SWM4-NDP water model is a 5-particle water model with a Drude particle attached to the oxygen atom. The picture has taken from ref. [87]

Appendix 7. Buckingham and Lennard Jones potential

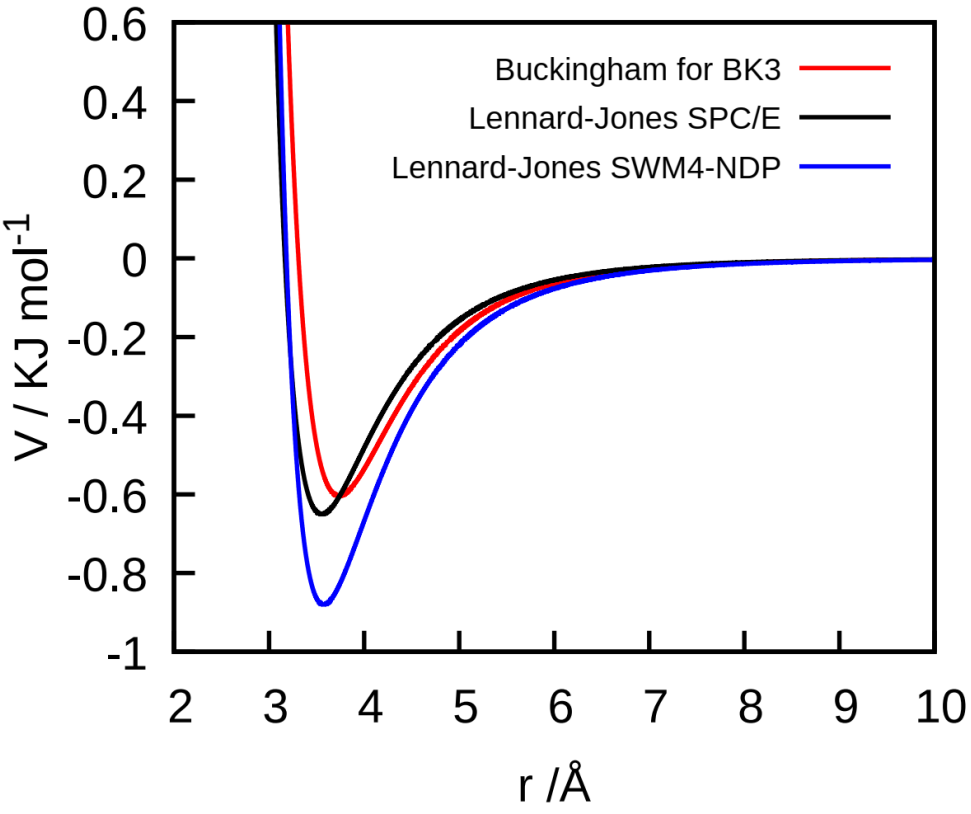

Figure 47. The Oxygen-Oxygen potential of Buckingham (with BK3 parameters), and Lennard Jones potential with SPC/E and SWM4-NDP parameters.

Vita

Education

Graduate Student of Computational Chemical Physics — **Aug 2013-Present**

Virginia Commonwealth University, Richmond, VA.

Data Science Specialization (Online certified course) — **November 2017-Present**

Johns Hopkins University

Toastmaster Communication and leadership development — **March 2017-Present**

M. Sc. in physics — ***2008-2011***

The University of Zanjan, Zanjan, Iran.

B. Sc. in physics — **2003-2007**

The University of Zanjan, Zanjan, Iran.

Work Experiences

- Research assistant at Virginia Commonwealth University. Simulations and analyze the simulation datasets by developing efficient post-processing programs. (Support: National Science Foundation)
- Teaching assistant at Virginia Commonwealth University, teaching general and physical chemistry.
- Participating in some Hackathon competitions: Developing an idea for an automated health system, developing an idea about for a modern date match system.
- Several volunteering jobs as scientific judge and assistant in Virginia high schools.
- Developing and maintaining web applications for small businesses. I have used HTML, CSS, JSP for front-end and java scripts for the back-end, and MySQL for the database.

Programming Skills

- Programming Language: **C / C++,** Objective C, **Visual Basic**, **Fortran**
- Developing skills under certified programs: **R**, **Python,** MySQL**, Java**, MATLAB, **Git**, Cloud computing
- Data analysis skills: Practical **Machine Learning**, Data cleaning, statistical inference, regression, and correlation models, Predictive modeling
- **Linux/Unix shell** scripting: Bash programming, **Awk**, **GNU Emacs**, Vim, Nano
- High-performance computing (HPC)
- Web programming: HTML, CSS, JSP, **Java Script**
- System administration: Hardware and Network Fixing
- Software Applications: Microsoft Word, Microsoft Access, Microsoft Excel, Microsoft Power point, Mathematica, Gnuplot, Visual Molecular dynamics (VMD), Adobe Photoshop, LATEX
- Molecular Dynamic packages: LAMMPS, GROMAC, and coding for Monte Carlo modeling

Publications:

- M. Shafiei, M. von Domaros, D. Bratko and A. Luzar, " Anisotropic Structure and Dynamics of Water under Static Electric Fields," J Chem. Phys. (2018), submitted.
- M. Shafiei, D. Bratko and A. Luzar, " Anisotropic Structure and Dynamics of Water under Static Electric Fields," (Under Preparation).
- M. Shafiei, D. Bratko and A. Luzar, "Studying the dynamics of water under alternating electric field," (Under Preparation).
- Foulaadvand, M. E.; Shafiei, M. One-dimensional Brownian motion in hard rods: The adiabatic piston problem. Europhys. Lett. 2013, 104, 30002.
- Monte Carlo Simulation of One-Dimensional Gas of Hard Needles. http://www.gammajournal.ir/indexen.htm

Presentations:

Poster Presentation

- Shafiei, M.; Bratko, D.; Luzar, A Unified Framework for Hydrogen Bond Dynamics in Water, Gordon Research Conference: Water and Aqueous solutions, July 22-27, 2018, Holderness, NH.

Contributed Talk

- Shafiei, M.; Bratko, D.; Luzar, Generalized Framework For Studying Hydrogen Bond Dynamics, Virginia Academy of Science, May 23-25, 2018, Longwood, VA.
- Shafiei, M.; Bratko, D.; Luzar, Water Hydrogen Bond Dynamics under Electric Field, American Physical Society meeting (Co, March 5-9th, 2018, Los Angeles, CA.
- Shafiei, M.; Bratko, D.; Luzar, A. Dynamics of water under an electric field, 4th Virginia Soft Matter Workshop, Oct 29th, 2016, Richmond, VA.
- Shafiei, M.; Bratko, D.; Luzar, A. Kinetics of Hydrogen Bond of Water and Application to a Water-Surface, Sep 4th, 2017, Harrisonburg, VA.